



Professor Leszek Filipczyński

Scientific biography is an accumulation of facts and titles, often so numerous, and so swiftly each other that it is not easy to understand, how a single individual might be able to initiate and perform so much work. Scientific profile should contain more than such a biography: apart from listing the achievements, titles, and awards, it should reflect individual features of a man, and first of all his virtues which should be regarded as a source of his scientific achievements. In the case of Professor Leszek Filipczyński — full member of the Polish Academy of Sciences — there is such a lot of both scientific and organizational achievements, that it is easy to guess what stands behind them: unusual mind, unusual industry, rare ease to contact people, and an exceptional organizational skills.

Leszek Filipczyński was born 23-th of December 1923 in Łódź. The outbreak of the war forces the 16 years old secondary-school pupil to undertake a manual work; he chose a profession of metalworker. Five years of occupation spent in a mechanical workshop developed certain attitude of the future scientist's mind: a sense of pragmatism and awareness of importance of experiment, which is to verify a theory. This attitude of Prof. Filipczyński is to be detected throughout all his further scientific activity; his every scientific discovery involved a definite application: elaborated research methods were always implemented in practice together with an instrumentation to their practical realization.

After the war, in 1945, L. Filipczyński began his study at a Faculty of Physics of the Łódź University. He continued his studies at the Gdańsk University during the years 1945-1948 (mechanics, electrotechnology), and completed in 1949 at the Warsaw Technical University, obtaining his master's degree in radiotechnical engineering.

He started his work before completing studies as an assistant at the Telecommunication Faculty of the Warsaw Technical University, at the Radiolocation Chair, and afterwards as a research worker at the State Institute of Telecommunication (1948-1949). Then L. Filipczyński became a close collaborator of Prof. Ignacy Malecki — the pioneer of acoustics in Poland. They organized together the Laboratory of Acoustics at the Central Institute of Technical Physics in Warsaw (1950-1951), which was in 1952 transformed into the Department for Vibrations Research, and in 1953 incorporated into the Institute of Fundamental Technological Research of the Polish Academy of Sciences. L. Filipczyński has been linked with this institute ever since till now; he held the positions of a head of the Laboratory of Passive Applications of Ultrasounds (1953-1969), a head of Ultrasonic Department, a deputy director for scientific problems (1969-1994), and a general director of the institute (1969-1974).

Organization of the ultrasonic technology in Poland, first for industry and afterwards, for medicine as well as designing new types of ultrasonic instrumentation, was harmonized with the scientific analysis of the foundations of this technique. The L. Filipczyński's research studies, being original, world-wide unique, and always performed at the highest scientific level, were the ground of his quick scientific career.

In 1955 he obtained a doctor's degree, the title of his thesis being: Electroacoustic transformation and radiation of acoustic waves for the purpose of ultrasonic defectoscopy (Prof. I. Malecki conferred the degree). In 1957 L. Filipczyński was given a title of an associate professor for his research publications on ultrasonic scattering in solids, in 1962 a professor, in 1969 a full professor and a corresponding member of the Polish Academy of Sciences (at the age of 46). Since 1976 professor L. Filipczyński is a full member of the Polish Academy of Sciences, and since 1993 also a member of the New York Academy of Sciences.

Prof. L. Filipczyński is an author, coauthor or editor of 12 monographs, and over 240 original publications and scientific reports, printed in Polish and foreign periodicals (among others: *Acustica*, *Ultrasound in Medicine and Biology*, *IEEE Transactions on Ultrasonics, Ferroelectrics and Frequency Control*, *Archives of Acoustics*, *Journal of Technical Physics*) and in *Conferences Proceedings*. These works concerned the following subjects:

1. Theory and experimental research of piezoelectric and magnetostrictive ultrasonic transducers.
2. Radiation of elastic waves into a solid medium, reflection of waves on inclusions, waves in spiral systems, ultrasonic focussed Gaussian beams.
3. Materials fatigue testing using ultrasonic frequencies.
4. Theoretical and experimental foundations of ultrasonic defectoscopy and determination of the strength of concrete by ultrasonic method.
5. Studies on electroacoustic parameters of ultrasonic transmitting-receiving systems.
6. Absolute methods of measuring of displacements, acoustic velocity and intensity of elastic waves of various types.
7. Visualization of internal organs by means of ultrasounds.
8. Echoencephalographic examination of the brain.
9. Ultrasonography and ultrasonic ophthalmoscopy.
10. Ultrasonography of the heart.
11. Ultrasonic methods of measuring of liquid flows and blood flow.
12. Detectability of pathological structures by means of ultrasonography (e.g. microcalcifications in female breasts, etc.).
13. Thermal effects generated by ultrasonic beams of low and extremely high pressures.
14. Investigation of ultrasonic shadow.
15. Generation and propagation as well as development of metrology of shock waves for lithotripsy (non-invasive disintegration of renal stones).

Beside the works listed above, which have been in line with the basic scientific activity in the field of ultrasonics and its applications. Prof. L. Filipczyński is an author of numerous designs of ultrasonic instrumentation, namely: ultrasonic defectoscopes and concretoscopes, ultrasonic spectroscopes, an unique ultrasonic device for testing fatigue of materials by means of ultrasonic flexural waves, ultrasonograph for visualization of abdominal cavity, ultrasonic ophthalmoscopes for examination of the eye, echoencephalograph for examination of the brain, ultrasonocardiograph for examination of the heart, ultrasonic detector of the pulse of the fetus and the state of the placenta, instrument for disintegration of kidney stones by shock waves lithotripsy.

The mentioned instruments, and also a number of measuring and diagnostic methods (applied in medicine), have been created on the ground of 62 patents of Prof. L. Filipczyński. These instruments, unique throughout Poland and the world, have been manufactured for the home industry and medicine by the enterprises: INCO, RADIOTECHNIKA, TECHPAN, SONOPAN. The users of the instruments were the following: metallurgy, aviation, mining and, first of all, numerous medical institutions, hospitals, clinics, and many others. All home manufacturers which produce ultrasonic diagnostic instrumentation for medicine have their roots in the activity of Prof. L. Filipczyński and his followers.

The initiating and creative contributions of Prof. L. Filipczyński, his scientific and organizational achievements were awarded many times; he obtained: (twice, in 1966 and 1978) the Collective Second Class State Prize, the Prize of the Chairman of the Committee for Science and Technology (1967, 1968), five times the Prizes of the Scientific Secretary of the Polish Academy of Sciences (1971, 1975, 1977, 1980, 1984), and the PAS department prizes (1977). He was also awarded several high state prizes, among others: the Commander's Cross, the Officer's Cross, the Cavalier's Cross of the Revival of Poland. He was also distinguished by the Nicolaus Copernicus Medal of the Polish Academy of Sciences, by Medal of the Mining and Metallurgy Academy in Cracow, and recently by the Medal of the Naval Forces of the Polish Republic.

The high scientific and organizational dignities achieved, and the necessary duties involved, have not lowered the scientific activity of Prof. L. Filipczyński. On the contrary, his talent and passion for science resulted in a dynamic idea of creating foundations of ultrasonic medical diagnosis. After a few years this difficult task has been completed, and its creator was a member-promotor and a member of the Technical Council of the International Society for Ultrasonic Diagnostics. He was honored during the International Congress for Acoustics in London in 1974 with the task of delivering the plenary lecture on the ultrasonic medical diagnosis.

The outstanding output of Prof. L. Filipczyński, his discovering achievements in application of ultrasonics to medicine have been once more appreciated in 1988, when he obtained in Washington the Diploma of Pioneer of Ultrasonics in Medicine, granted by the American Institute for Ultrasonic in Medicine.

Recognized by the world-wide scientific authorities as a pioneer in this branch, Prof. L. Filipczyński is also considered a „father” of the Polish School of Ultrasonic Medical Diagnosis’.

He promoted 10 doctors, his closest collaborators and continuators of his activity in Poland. A special emphasis should be placed upon the fact that Prof. L. Filipczyński, using his knowledge and authority, pushed forward in home medical environment a notable group of specialists physicians (including 3 professors, 4 associated professors, 10 doctors). Ultrasonic medical diagnosis became to grow as an avalanche; and Prof. L. Filipczyński's merits were also the organization of the First International Conference on Ultrasonics in Medicine and Biology UBIOMED-1 in Jabłonna (1972), continued afterwards in several countries of the Central Europe, co-organization of scientific societies — the Section of Ultrasonics in Biology and Medicine at the Polish Acoustical Society and the Polish Ultrasonographic Society.

Prof. L. Filipczyński is a Polish acoustician particularly estimated abroad. Apart from the above mentioned membership of the International Society for Ultrasonic Diagnosis, he was granted Honorary Medals of the Technical Universities in Prague and the University in Brno twice, a Honorary membership since 1972 of the American Institute for Ultrasonics in Medicine, the Yugoslavian Society for Ultrasonics in Medicine, and the German Society for Ultrasonics in Medicine. He is since 1974 a member of advisory editorial board of the periodical „Ultrasound in Medicine and Biology” (Pergamon Press) and was also a member of the Commission for Standardization of the International Electrotechnics Society. In years 1975–1979 he was a vice-chairman of the European Federation for Ultrasonics in Medicine, and also a member of the International Commission for Acoustics ICA (1974–1980).

He has been always active and full of initiatives, the duties he was performing in Poland might be an evidence of it: a member of the Polish Committee for Acoustics of the Polish Academy of Sciences, and its chairman since 1972, member-founder of Polish Acoustical Society, and its vice-chairman in years 1975–1978, actually its Honorary Member (since 1992), also a Honorary Member of the Polish Ultrasonographic Society (since 1992) a chairman of the Scientific Council of the Institute of Fundamental Technical Problems of the Polish Academy of Sciences in years 1989–1993, a chairman of the Scientific Council of the Institute for Biocybernetics and Biomedical Engineering of the Polish Academy of Sciences since 1982 till now. In former years a member of scientific councils of the Center for Medical Technology and the Tele-radiotechnical Institute.

The obligation of scientist is to bring up his deputies and successors. Prof. L. Filipczyński, since the beginning of the sixties, has been lecturing at the Warsaw Technical University, Department of Electroacoustics of the Faculty of Communication (later Electronics) the following subject: ultrasounds and, later on, at the Department of Fine Mechanics of the Warsaw Technical University, the subject: ultrasounds in medicine. He lectured also at the Doctor's Studies at the Institute of Fundamental Technical Problems of the Polish Academy of Sciences. He looks after the recruitment of talented people to his team, he is also exquisite in scientific co-operation, organizes and conducts seminars, confers and reviews scientific work from the branch of ultra-acoustics at the Institute of Fundamental

Technological Research of the Polish Academy of Sciences, and outside the Institute.

He is a man of high erudition and modesty, theorist and experimenter, exacting and just as a boss, cordial colleague and friend for many ones, respected by everyone who knows him, and respecting others.

Prof. L. Filipczyński beside his virtues, so typical for representatives of exact sciences, is a man of personal charm — he is a humanist, susceptible to beauty, connoisseur of arts, playing piano with deep feeling...

This article contains quotations from the publication of Prof. J. WEHR, Scientific personalities among the members of the Polish Academy of Science: Leszek Filipczyński, *Nauka Polska*, 2, 83–86 (1976).

*J. Etienne and J. Ranachowski*

### Doctors conferred by Prof. L. Filipczyński

1. Grażyna ŁYPACEWICZ, *Electroacoustic problems of ultrasonic transducers applied in medical diagnosis* (1970).
2. Bogumił PEŃSKO, *Ultrasonic method of fatigue testing of wires and ropes* (1972).
3. Jerzy KOPEĆ, *Elaboration of ultrasonic method of brain testing utilizing instrumentation with type B presentation* (1973).
4. Andrzej NOWICKI, *Ultrasonic Doppler impulse method and instrumentation for measurements of blood flows in cardiovascular system* (1976).
5. Tadeusz POWAŁOWSKI, *Measurements of flow of liquids by means of ultrasonic Doppler Continuous wave method* (1976).
6. Jerzy ETIENNE, *Selected problems of application of ultrasounds in obstetrics* (1977).
7. Anna MARKIEWICZ, *Analysis of impulse transmit-receiving ultrasonic systems for the purpose of medical diagnosis* (1978).
8. Tamara MARUK-KUJAWSKA, *Dynamic focussing of ultrasonic beam by means of annular transducers* (1980).
9. Maciej PIECHOCKI, *Ultrasonic Doppler methods of measuring of disturbed blood flows* (1983).
10. Jerzy LITNIEWSKI, *Signal from the acoustic microscope during work beyond the focus and its application to interpretation of biological images* (1990).

### List of publications

- [1] *Temperature elevation in focused Gaussian ultrasonic beams and the insonation time*, L. FILIPCZYŃSKI, T. KUJAWSKA and T. WÓJCIK, *J. Ultrasound Med. Biol.*, 19, 687–697 (1993).
- [2] *Shock wave pulse pressure after penetration of kidney tissue*, L. FILIPCZYŃSKI, J. ETIENNE and T. KUJAWSKA, *IEEE Transactions on Ultrasonics, Ferroelectrics and Frequency Control*, 1, 130–134 (1994).

- [3] *Zjawiska temperaturowe w ultrasonografii*, L. FILIPCZYŃSKI, *Ultrasonografia Polska*, 2, 13–19, (1992).
- [4] *An attempt to reconstruct the lithotripter shock wave pulse in kidney: Possible temperature effects*, L. FILIPCZYŃSKI, J. ETIENNE, and M. PIECHOCKI, *Ultrasound in Med. Biol.*, 18, 6/7, 569–577 (1992).
- [5] *Quantitative ultrasonography*, L. FILIPCZYŃSKI, *Archives of Acoustics*, 16, 207–228 (1991).
- [6] *Estimation of transient temperature elevation in lithotripsy and in ultrasonography*, L. FILIPCZYŃSKI and J. WÓJCIK, *Ultrasound in Med. Biol.*, 17, 715–71 (1991).
- [7] *The shadow behind rotational rigid and elastic bodies immersed in fluids — computed and measured*, L. FILIPCZYŃSKI, T. KUJAWSKA and T. WASZCZUK [in:] *Acoustic imaging* [Eds.] H. Emert and Haxjes Plenum Press, New York 1992, 127–131.
- [8] *Evaluation of calcification detectability in female breasts by ultrasound*, L. FILIPCZYŃSKI, T. KUJAWSKA and G. ŁYPACEWICZ, *Archives of Acoustics*, 15, 107–119 (1990) see also *Evaluation of calcification detectability in female breast by ultrasound*, [in:] *Breast echography* [Eds.] F. Dambrosio and E. Durante, Ferrara 1991, 177–183.
- [9] *The shadow behind a sphere immersed in water — measured estimated and computed*, L. FILIPCZYŃSKI, T. KUJAWSKA and T. WASZCZUK, *IEEE Transactions on Ultrasonics, Ferroelectrics and Frequency Control*, 38, 35–39 (1991).
- [10] *Capacitance hydrophone for pressure determination in lithotripsy*, L. FILIPCZYŃSKI, J. ETIENNE, J. *Ultrasound Med. Biol.*, 16, 157–165 (1990).
- [11] *Ultradźwiękowe metody wizualizacji w medycynie*, L. FILIPCZYŃSKI, [in:] *Biopomiary* [Eds.] L. Filipczyński and W. Torbicz, WKŁ, Warszawa 1990, 96–114.
- [12] *Estimation of the temperature increase in the focus of a lithotripter for the case of high rate administration*, L. FILIPCZYŃSKI and M. PIECHOCKI, *Ultrasound Med. Biol.*, 16, 149–156 and 727 (1990).
- [13] *Ein Hydrophon für Druckmessungen in der Lithotripsie*, L. FILIPCZYŃSKI and J. ETIENNE, *Ultraschallmesstechnik in Forschung und Praxis* [Red.] H. Hein and R. Millner, M. Luther Universität Halle—Wittenberg, Halle Saale 1990, 17–20.
- [14] *Deviation of the acoustic pressure to particle velocity ratio from the value in liquids and solids at high pressures*, L. FILIPCZYŃSKI and A. GRABOWSKA, *Archives of Acoustics*, 14, 173–179 (1989).
- [15] *Acoustical shadow of a sphere immersed in water. II.* L. FILIPCZYŃSKI and T. KUJAWSKA, *Archives of Acoustics*, 14, 183–192 (1989).
- [16] *Acoustical shadow of a sphere immersed in water. I.* L. FILIPCZYŃSKI and T. KUJAWSKA, *Archives of Acoustics*, 14, 29–43 (1989).
- [17] *An experimental lithotripsy system for the study of shock wave effects*, L. FILIPCZYŃSKI, J. ETIENNE, A. GRABOWSKA, T. WASZCZUK, H. KOWALSKA, M. GRZYŃSKI and J. STANISLAWSKI, *Archives of Acoustics*, 14, 11–27 (1989).
- [18] *The reflection of a Gaussian pulse of a plane ultrasonic wave from rigid and elastic spheres in water*, L. FILIPCZYŃSKI and T. KUJAWSKA, *Archives of Acoustics*, 12, 113–128 (1987).
- [19] *Ultrasound and medicine*, L. FILIPCZYŃSKI and H. KOWALSKI [in:] *Acoustics. Education and development* [Eds.] A. ŚLIWIŃSKI and G. BUDZYŃSKI, World Scientific, Singapore, New Jersey 1987, 85–92.
- [20] *Generacja ciepła pod wpływem płaskich fal ultradźwiękowych w lepkosprężystym ciele Voigta*, L. FILIPCZYŃSKI, *Archiwum Akustyki*, 22, 273–306 (1987).
- [21] *Angioultrasonografia — metoda badania tętnic pozaczaszkowych*, M. BARAŃSKA-GIERUSZAK, J. ETIENNE, L. FILIPCZYŃSKI, R. GOŁĄBEK, B. KARWARSKI, H. NIELUBOWICZOWA, A. NOWICKI, T. POWAŁOWSKI, T. SECOMSKI and A. WLECIAŁ, *Neurologia i Neurochirurgia Polska*, 40, 297–302 (1986).
- [22] *Absorption of longitudinal and shear waves and generation of heat in soft tissues*, L. FILIPCZYŃSKI, *Ultrasound Med. Biol.*, 12, 223–238 (1986).
- [23] *Detectability of blood vessels by means of the ultrasonic echo method using a focused ultrasonic beam*, L. FILIPCZYŃSKI, *Archives of Acoustics*, 7, 1 253–270 (1982) see also *Detectability of blood vessels with ultrasonic echo method: Physical considerations*, L. FILIPCZYŃSKI, *Excerpta Medica* [Eds.] A. Kurjak and A. Kratochwil, Amsterdam 81–85, 1981.

- [24] *Estimation of the collateral circulation C. C. I. on the lower extremities*, J. WESOŁOWSKI, A. NOWICKI, B. TOPOLSKA, T. PALKO, G. PAWLICKI, L. FILIPCZYŃSKI, Archives of Acoustics, **9**, 191–198 (1984) see also Polski Przegląd Chirurgiczny, **55**, 105–108 (1983).
- [25] *Ultrasonic gray Doppler angiography*, T. POWAŁOWSKI, J. ETIENNE, L. FILIPCZYŃSKI, A. NOWICKI, M. PIECHOCKI, W. SECOMSKI, A. WLECIAŁ, M. BARAŃSKA, Archives of Acoustics, **9**, 131–136 (1984).
- [26] *Ultrasonic characterization of tissues in cardiology*, L. FILIPCZYŃSKI, Archives of Acoustics, **8**, 83–94 (1983).
- [27] *Detectability of gas bubbles in blood by the ultrasonic method*, L. FILIPCZYŃSKI, Archives of Acoustics, **8**, 11–29 (1983) see also Innovation et Technologie en Biologie et Medicine, **5**, 67–76 (1984).
- [28] *Application of the stationary echo cancellation technique SEC in ultrasonic Doppler measurements of blood flow in children's heart*, L. FILIPCZYŃSKI, A. NOWICKI, A. CHRÓŚCICKI, Archives of Acoustics, **7**, 247–253 (1982).
- [29] *Transducers and sound fields*, L. FILIPCZYŃSKI [in:] Ultrasound interactions in biology and medicine, [Eds.] R. Millner, H. Rosenfeld, U. Cobet, Plenum Press, New York, 7–17, 1983.
- [30] *Detectability of small blood vessels and flat boundaries of soft tissues in the ultrasonic pulse echo method*, L. FILIPCZYŃSKI, Archives of Acoustics, **6**, 45–56 (1981).
- [31] *Absolute measurement methods and possibilities of thermographics estimation of the ultrasonic dose in vivo*, L. FILIPCZYŃSKI [in:] Investigative ultrasonology, [Eds.] C. Hill, C. Alvisi, Pitmann Medical, Kent 1980, 127–131.
- [32] *Diagnostyka tętniaków rzekomych przy pomocy ultradźwięków*, J. WESOŁOWSKI, M. KLUKOWSKI, G. ŁYPACEWICZ, B. MALIŃSKI, H. KOWALSKI, L. FILIPCZYŃSKI, H. RYKOWSKI, Polski Przegląd Chirurgiczny, **52**, 701–705 (1980).
- [33] *Ultrasonic wave propagation along the surface of a rod immersed in a liquid*, L. FILIPCZYŃSKI, Archives of Acoustics, **4**, 271–286 (1979) see also Proc. 9th ICA Congr. on Acoustics, Madrid 1977, paper K70.
- [34] *Methods of measuring the performance of ultrasonic pulse—echo diagnostic equipment*, K. BRENDEL, L. FILIPCZYŃSKI et al., Ultrasound in Med. Biol., **2**, 342–350 (1976).
- [35] *Measurement of the temperature increase generated in soft tissues by ultrasonic diagnostic Doppler equipment*, L. FILIPCZYŃSKI, Ultrasound in Med. Biol., **4**, 151–155 (1978).
- [36] *Zdrowotne aspekty zastosowań ultradźwięków w świetle stanowiska Światowej Organizacji Zdrowia*, Archiwum Akustyki, **13**, 245–251 (1978).
- [37] *Ultrasonic method and apparatus for fatigue testing of steel wires*, B. PEŃSKO, L. FILIPCZYŃSKI, Proc. 2nd Congress of the Federation of Acoustical Societies of Europe FASE—78 Warszawa 1978, vol. I, 253–256.
- [38] *Temperature effects in soft tissues estimated and measured*, L. FILIPCZYŃSKI, ditto vol. II, 23–26.
- [39] *Badania doświadczalne i teoretyczne efektu temperaturowego powstającego pod wpływem fal ultradźwiękowych generowanych w tkankach miękkich za pomocą dopplerowskiej aparatury diagnostycznej*, L. FILIPCZYŃSKI, Archiwum Akustyki, **13**, 215–222 (1978).
- [40] *Thermal effects in soft tissues developed under the influence of focused ultrasonic fields of long duration*, L. FILIPCZYŃSKI, Archives of Acoustics, **2**, 297–303 (1977).
- [41] *Thermal effects in soft tissues of short duration*, L. FILIPCZYŃSKI, Archives of Acoustics, **1**, 309–321 (1976).
- [42] *Attempts at the ultrasonic visualization of the heart in real time*, L. FILIPCZYŃSKI and J. SAŁKOWSKI, Archives of Acoustics, **2**, 61–66 (1977).
- [43] *Wyznaczenie natężenia w ogniskowanej wiązce ultradźwiękowej za pomocą metody elektrodynamicznej i pojemnościowej w zastosowaniu do automatycznej wizualizacji struktur oka*, L. FILIPCZYŃSKI, G. ŁYPACEWICZ, J. SAŁKOWSKI and T. WASZCZUK, Archiwum Akustyki, **11**, 189–198 (1976).
- [44] *Lokalizacja łożyska metodą dopplerowską z zastosowaniem dwóch głowic ultradźwiękowych*, W. BARDOWSKI, J. ETIENNE, L. FILIPCZYŃSKI, J. GRONIEWSKI, H. KLAWE and J. KRETOWICZ, Ginekologia Polska, **46**, 1067–1073 (1975) see also Proc. FASE—78 vol. II [Eds.] L. Filipczyński and J. Zieniuk Warszawa 1978, 89–92.



- [45] *Quantitative transcutaneous measurements of blood flow in carotid artery by means of pulse and continuous wave Doppler methods*, K. BORODZIŃSKI, L. FILIPCZYŃSKI, A. NOWICKI and T. POWAŁOWSKI, *Ultrasound in Med. Biol.*, **2**, 189–193 (1976).
- [46] *Automatic eye visualization and ultrasonic intensity determination in focused beams by means of electrodynamic and capacitance methods*, L. FILIPCZYŃSKI, G. ŁYPACEWICZ, J. SĄLKOWSKI and T. WASZCZUK [in:] *Ultrasonics in Medicine* [Ed.] E. Katzner et al., Excerpta Medica, Amsterdam, Oxford 1975, 123–134.
- [47] *Intensity determination of ultrasonic beams used in ultrasonography in the case of gravid uterus*, J. ETIENNE, L. FILIPCZYŃSKI, A. FIREK, J. GRONIEWSKI, J. KRETOWICZ, G. ŁYPACEWICZ and J. SĄLKOWSKI, *Ultrasound in Med. Biol.*, **2**, 119–122 (1978).
- [48] *Transienta, equivalent circuits and negative capacitance of piezoelectric transducers with thickness vibrations*, L. FILIPCZYŃSKI, *Journal of Technical Physics*, **16**, 121–135 (1975).
- [49] *Bezkontaktowa metoda pomiaru mocy w falowodzie ultradźwiękowym w czasie rzeczywistym*, L. FILIPCZYŃSKI and Z. TOCZYŃSKI, *Archiwum Akustyki*, **10**, 257–277 (1975).
- [50] *Ultrasonograf UG-4 do wizualizacji narządów jamy brzusznej i jego zastosowanie kliniczne*, L. FILIPCZYŃSKI, J. GRONIEWSKI, G. ŁYPACEWICZ, J. SĄLKOWSKI and T. WASZCZUK, *Archiwum Akustyki*, **10**, 171–190 (1975) see also *Ginekologia Polska*, **46**, 397 (1975).
- [51] *Intensity determination of ultrasonic focused beams by means of electrodynamic and capacitance methods*, L. FILIPCZYŃSKI, G. ŁYPACEWICZ and J. SĄLKOWSKI, *Proc. Vibr. Probl.*, **15**, 297–305 (1974); see also *Proc. Colloq. Ultras. Bioeffects and Dosimetry*, London 1974, *Ultrasound in Med. Biol.*, **1**, 475 (1975).
- [52] *Metoda pomiaru ogólnej czułości aparatury ultradźwiękowej wykorzystującej zjawisko Dopplera*, K. BORODZIŃSKI, L. FILIPCZYŃSKI and T. POWAŁOWSKI, *Archiwum Akustyki*, **10**, 65–75 (1975) see also *Proc. X. Intern. Conf. Med. Biol. Eng. Dresden* paper 21–1 (1973).
- [53] *Ultrasonic medical diagnostic methods*, L. FILIPCZYŃSKI, 8th Intern. Congress on Acoustics, London 1974, Invited plenary paper, [in:] *Acoustics 1974* [Ed.] R. Stephens Chapman Hill, London 1975, 71, 85.
- [54] *Ultrasonograf UO-3 do wizualizacji struktur oka i jego zastosowanie kliniczne*, L. FILIPCZYŃSKI, D. KOMITOWSKI, G. ŁYPACEWICZ, B. ROŚCISZEWSKA and J. SĄLKOWSKI, *Archiwum Akustyki*, **8**, 265 (1973).
- [55] *Application of ultrasound to fatigue testing of steel wires and cables*, B. PEŃSKO, D. WISZNIOWSKI, L. FILIPCZYŃSKI and Z. KAWECKI, *Proc. Vibr. Probl.*, **14**, 285–304 (1973).
- [56] *Intensity determination of ultrasonic pulses by means of a capacitance transducer*, Workshop Proc. on Interaction of ultrasound and biological tissues, [Eds.] J. Reid, M. Sikov, US Dept. of Health, Education and Welfare, Bureau of Radiological Health, Rockville 1972, 171.
- [57] *Diagnostyczna przydatność echoencefalografii A na podstawie analizy badań wykonanych u 2000 osób*, T. BACIA, A. BIELAWSKI, L. FILIPCZYŃSKI, J. KOPEĆ, W. MAZUROWSKI, J. MROZIAK, L. STĘPIEŃ, Z. SZLAMIŃSKI, *Polski Tygodnik Lekarski*, **27**, 589–592 (1972).
- [58] *Theoretical study and experiments on spherical focusing transducers with Gaussian surface velocity distribution*, L. FILIPCZYŃSKI, J. ETIENNE, *Acustica*, **28**, 121–128 (1973) and *Archiwum Akustyki*, **8**, 341–360 (1973).
- [59] *Zastosowanie ultradźwięków do badania wytrzymałości zmęczeniowej drutów stalowych i lin*, B. PEŃSKO, L. FILIPCZYŃSKI, D. WISZNIOWSKI and Z. KAWECKI, *Arch. Inżyn. Łąd.*, **19**, 713–730 (1973).
- [60] *Ogólna czułość ultradźwiękowej aparatury impulsowej i jej znaczenie w diagnostyce chorób oczu*, L. FILIPCZYŃSKI and G. ŁYPACEWICZ, *Archiwum Akustyki*, **9**, 67–84 (1974).
- [61] *Badanie wpływu ultradźwięków promieniowanych przez detektor na chromosomy człowieka w hodowli limfocytów*, L. FILIPCZYŃSKI, J. KRETOWICZ, A. NOWICKI, T. POWAŁOWSKI and J. STARZYŃSKA, *Archiwum Akustyki*, **8**, 247–264 (1973).
- [62] *Ultrasonic intensity in the imaging of eye structures*, L. FILIPCZYŃSKI, G. ŁYPACEWICZ, D. KOMITOWSKI, B. ROŚCISZEWSKA, J. SĄLKOWSKI, *Proc. Vibr. Probl.*, **13**, 1, 15–25 (1972) see also *Ultrasonic intensity levels in imaging of eye structures and their influence on eye tissues*, *Proc. Intern. Congr. SIDUO-IV* Ed. J. Pojol Paris 1971, 17–23.
- [63] *Dosage problem, acoustical output and overall sensitivity of ultrasonic diagnostic methods*, L. FILIPCZYŃSKI, *Proc. Intern. Congr. on Acoustics*, Budapest 1971 paper 20R31.

- [64] *Metoda i pomiary drgań koncentora ultradźwiękowego*, L. FILIPCZYŃSKI and B. LEŚNIAK, *Archiwum Akustyki*, **3**, 307–317 (1970).
- [65] *Ultradźwiękowa metoda badania tętna na zasadzie zjawiska Dopplera*, J. ETIENNE, L. FILIPCZYŃSKI, A. NOWICKI, T. POWAŁOWSKI, *Archiwum Akustyki*, **6**, 213–222 (1971) see also *Problemy Techniki w Medycynie*, **2**, 4, 289–299 (1971).
- [66] *Measurements of the clamped capacitance  $C_0$  and the electromechanical coupling coefficient  $K_t$  of ceramic transducers under mechanical load*, G. ŁYPACEWICZ and L. FILIPCZYŃSKI, *Acustica*, **25**, 1, 64–68 (1971) and *Proc. Vibr. Probl.*, **11**, 319–330 (1970).
- [67] *Measurement method and experimental study of ceramic transducer vibrations*, G. ŁYPACEWICZ and L. FILIPCZYŃSKI, *Acustica*, **25**, 1, 64–68 (1971) and *Proc. Vibr. Probl.*, **11**, 319–33 (1970).
- [68] *Compound and rapid scan ultrasonic imaging of eye structures ophthalmic ultrasound*, L. FILIPCZYŃSKI, *Proceeding of the Fourth International Congress of Ultrasonography in Ophthalmology*, Philadelphia 1968, [Ed.] R. Sarin, C. V. Mosby Comp. Saint Luis 1969, 207–212.
- [69] *Dependence between the  $Q$ -value of piezoelectric transducer loaded acoustically and the electromechanical coupling coefficient  $k$* , L. FILIPCZYŃSKI and G. ŁYPACEWICZ, *Proc. Vibr. Probl.*, **10**, 2, 213–229 (1969).
- [70] *Absolute measurements of particle velocity, displacements or intensity of ultrasonic pulses in liquids and solids*, L. FILIPCZYŃSKI, *Acustica*, **21**, 3, 173–170 (1969).
- [71] *The near field distribution on the axis of a vibrating piston*, L. FILIPCZYŃSKI, 6th Intern. Congress on Acoustics, Tokyo 1968, paper L-3-2, 68–72 see also *Archiwum Akustyki*, **3**, 73–90 (1968).
- [72] *Visualization of the inside of the abdomen by means of ultrasonics and two methods of measuring ultrasonic doses*, L. FILIPCZYŃSKI and J. GRONIEWSKI, *Digest of the VII Intern. Conf. Medical and Biological Engineering*, Stockholm 1967, 320.
- [73] *Zastosowanie ultradźwięków metody echa w diagnostyce laryngologicznej u dzieci*, H. BRZEZIŃSKA, L. FILIPCZYŃSKI and G. ŁYPACEWICZ, *Archiwum Akustyki*, **3**, 4, 323–334 (1969).
- [74] *Ultradźwiękowe metody badania czynności serca w położnictwie i kardiologii*, J. ETIENNE, L. FILIPCZYŃSKI, K. ILMURZYŃSKA and J. SALKOWSKI, *Archiwum Akustyki*, **5**, 113–128 (1970).
- [75] *Znaczenie echoencefalografu w diagnostyce klinicznej*, T. BACIA, L. FILIPCZYŃSKI, J. KOPEĆ, W. MAZUROWSKI and Z. SZLAMIŃSKI, *Neurologia i Neurochirurgia Polska*, **18**, 203–209 (1968).
- [76] *Przydatność badań ultradźwiękowych dla rozpoznawania życia płodu*, L. FILIPCZYŃSKI, J. GRONIEWSKI, J. KRETOWICZ, G. ŁYPACEWICZ, J. ROSZKOWSKI, A. WICHRZYCKI, *Ginekologia Polska*, **39**, 3, 339–341 (1968).
- [77] *Ultrasonic problems of the diagnostic equipment for eye examination*, L. FILIPCZYŃSKI, J. ETIENNE, G. ŁYPACEWICZ, B. ROŚCISZEWSKA, II Symposium Internationale de Diagnostica Ultrasonica in Ophthalmologia, Brno 1967, *Acta Facultatis Medicae Universitatis Brunensis*, Brno 1968, 27–33.
- [78] *The absolute method of intensity measurements of liquid borne ultrasonic pulses with the electrodynamic transducer*, *Proc. Vibr. Probl.*, **8**, 21–26 (1967).
- [79] *Visualizing internal structures of the eye by means of ultrasonics*, L. FILIPCZYŃSKI, J. ETIENNE, G. ŁYPACEWICZ, J. SALKOWSKI, *Proc. Vibr. Probl.*, **8**, 357–368 (1967).
- [80] *Badanie wytrzymałości zmęczeniowej metodą ultradźwiękową*, L. FILIPCZYŃSKI, E. LUTY, J. ETIENNE, *Przegl. Mech.*, **25**, 257–259, 1966.
- [81] *Dwie bezwzględne metody pomiarów natężenia impulsów ultradźwiękowych w cieczach za pomocą przetwornika elektrodynamicznego oraz przetwornika pojemnościowego*, L. FILIPCZYŃSKI, *Archiwum Akustyki*, **3**, 2, 161–176 (1967).
- [82] *Visualizing the inside of the abdomen by means of ultrasonics*, L. FILIPCZYŃSKI, J. ETIENNE and G. ŁYPACEWICZ, *Proc. Vibr. Probl.*, **7**, 211–220 (1966).
- [83] *Elektroakustyczne parametry ultradźwiękowych układów nadawczo-odbiorczych*, L. FILIPCZYŃSKI, *Archiwum Akustyki*, **1**, 77–90 (1965) see also in *Wissenschaftliche Zeitschrift Humboldt Univ. Universität Berlin, Math. – Nat. R.*, **14**, 63–66 (1965).
- [84] *Measuring pulse intensity of ultrasonic longitudinal and transverse waves in solids*, L. FILIPCZYŃSKI, *Proc. Vibr. Probl.*, **7**, 31–46 (1966) see also *Method for intensity measurements of ultrasonic transverse and longitudinal waves in pulses*, L. FILIPCZYŃSKI, Paper D11 of the V Intern. Conf. on Acoustics, Liège 1965, 1–4.

- [85] *Prototyp urządzenia ultradźwiękowego do badania szyn w torach*, L. FILIPCZYŃSKI and Z. PAWŁOWSKI, *Zeszyty Problemowe Nauka Polska*, **26**, 471–474 (1965).
- [86] *Defektoskop ultradźwiękowy do badania spoin typu DS-1*, L. FILIPCZYŃSKI, ditto 449–459.
- [87] *Ultradźwiękowa impulsowa metoda badania drutów ferromagnetycznych przy wykorzystaniu ich własności magnetostrykcyjnych*, L. FILIPCZYŃSKI, ditto, 261–273.
- [88] *Konstrukcja defektoskopu ultradźwiękowego DI-12*, L. FILIPCZYŃSKI, ditto, 460–473.
- [89] *Measurements of longitudinal and transverse waves radiated by a compressional source into elastic semi-space*, L. FILIPCZYŃSKI, *Proc. Vibr. Probl.*, **5**, 89–93 (1964).
- [90] *Measurement method and apparatus for testing the fatigue and internal losses in metals with ultrasonic frequencies*, L. FILIPCZYŃSKI, J. ETIENNE, *Proc. Conf. on Acoustics of Solid Media* Warsaw, PWN, Warszawa 1964, 49–56.
- [91] *Generation of transverse waves in solids by means of compressional sources*, L. FILIPCZYŃSKI, ditto, 37–48.
- [92] *Ultraschallapparatur und Messungen der inneren Dämpfung und der Dauerfestigkeit bei Schwingungen von grossen Amplituden*, L. FILIPCZYŃSKI, III Intern. Congress on Material Testing, Budapest 1964 vol. II, 93–98, vol. III, 295–300.
- [93] *Measurements of mode conversion of ultrasonic waves on a solid–solid boundary*, L. FILIPCZYŃSKI, *Proc. Vibr. Probl.*, **4**, 255–263 (1963).
- [94] *Spektroskop ultradźwiękowy SU-1 i jego zastosowanie do pomiaru grubości*, L. FILIPCZYŃSKI and W. ROWICKI, *Pomiary, Automatyka, Kontrola*, **9**, 357–359 (1963).
- [95] *Measurements of internal losses in materials at high amplitude vibrations and ultrasonic frequencies*, L. FILIPCZYŃSKI and LIN DZON-MOU, *Proc. Vibr. Probl.*, **4**, 155–174 (1963) see also *Badanie zmęczenia materiałów przy częstotliwościach ultradźwiękowych*, LIN DZON-MOU, L. FILIPCZYŃSKI, K. KRZYCZKA and Z. PAWŁOWSKI, *Materiały II Konferencji Wytrzymałościowej SIMP WAT*, Warszawa 1961, 243–244.
- [96] *Propagation of ultrasonic waves in spirals*, L. FILIPCZYŃSKI, *Proc. Vibr. Probl.*, **3**, 241–251 (1962).
- [97] *Scattering of a plane longitudinal wave on a free surface of a disc in solid medium*, L. FILIPCZYŃSKI, *Proc. Vibr. Probl.*, **2**, 41–56 (1961).
- [98] *Wpływ sprzegającej warstewki cieczy na własności przetwornika kwarcowego o cięciu X obciążonego osrodkiem stałym*, L. FILIPCZYŃSKI, *Poznańskie Towarzystwo Przyjaciół Nauk Prace Komisji Matem. Przyrodn.*, **8**, 89–107 (1961).
- [99] *Electrical equivalent circuit of the piezoelectric transducer*, L. FILIPCZYŃSKI, *Proc. Symposium on Electroacoustic Transducer* Krynica 1958, PWN, Warszawa 1961, 75–84.
- [100] *Transients and the equivalent circuit of the magnetostrictive transducer*, L. FILIPCZYŃSKI, ditto, 61–74.
- [101] *Parameters of flaw detectability by ultrasonics*, L. FILIPCZYŃSKI, *Proc. Third Intern. Conf. on Nondestructive Testing*, Tokyo 1961, Panpacific Press 1961, 630.
- [102] *Transients and the equivalent electrical circuit of the piezoelectric transducer*, L. FILIPCZYŃSKI, *Acustica*, **10**, 149–154 (1960).
- [103] *Mechanism of vibrations in the magnetostrictive transducer*, L. FILIPCZYŃSKI, *Proc. Vibr. Probl.*, **1**, 15028 (1959).
- [104] *The development of ultrasonic methods for material testing in Poland*, L. FILIPCZYŃSKI and I. MAŁECKI, *Nondestructive Testing*, **5**, 276–280 (1959).
- [105] *Ultrazvukovej impulsnyj metod kontrola kačestva betona [in Russ]*. L. FILIPCZYŃSKI and A. SAWCZUK, *Beton i żelazobeton*, **2**, 45–52 (1958).
- [106] *Aparatura i technika pomiarów ultradźwiękowych w Polsce*, L. FILIPCZYŃSKI and Z. PAWŁOWSKI, *Pomiary, Automatyka, Kontrola*, **4**, 321–324 (1958) see also *Feingeratetechnik*, **7**, 295–298.
- [107] *Properties of the X-cut quartz transducer loaded with a solid medium*, L. FILIPCZYŃSKI, *Proc. II Conf. on Ultrasonics* PAN Warsaw 1956, PWN, Warszawa 1957, 35–47.
- [108] *Ultrasonic concrete tester BI-2*, L. FILIPCZYŃSKI and I. GRZENKOWICZ, ditto, 251–252.
- [109] *The reflection of plane elastic waves from a cylinder with a free surface*, L. FILIPCZYŃSKI, ditto 21–27.
- [110] *Miniaturized ultrasonic flaw detector DI-9*. A. CHINDELEWICZ, L. FILIPCZYŃSKI, ditto, 249.
- [111] *Radiation of acoustic waves for pulse ultrasonic flaw detection purposes*, L. FILIPCZYŃSKI, ditto, 249.

- [112] *Konstrukcja defektoskopu ultradźwiękowego DI-6*, L. FILIPCZYŃSKI, *Przegląd Telekomunikacyjny*, **29**, 298–302 (1956).
- [113] *Analiza wykrywalności wad przy użyciu defektoskopii ultradźwiękowej*, L. FILIPCZYŃSKI, *Mat. Konf. Tech. Ultradzw. PAN Warszawa 1953*, PWN, Warszawa 1955, 22–30.
- [114] *Defektoskopia ultradźwiękowa*, L. FILIPCZYŃSKI, *Mat. Zjazdu Młodej Kadry Politechniki Warszawskiej*, Warszawa X. 1953, *Elektryka*, **8**, 43–57 (1955).
- [115] *Analiza przebiegów elektromechanicznych w przetworniku kwarcowym*, L. FILIPCZYŃSKI, *Mat. I Konf. Techniki Ultradźwiękowej PAN, Warszawa IX 1953*, PWN, Warszawa 1955, 13–21.
- [116] *Defektoskop ultradźwiękowy DI-4*, L. FILIPCZYŃSKI, *Przegląd Telekomunikacyjny*, **28**, 155–159 (1955).
- [117] *Pochłaniacze przestrzenne — teoria ich działania i wyniki badań doświadczalnych*, I. MAŁECKI and L. FILIPCZYŃSKI, *Prace Centralnego Instytutu Ochrony Pracy*, **2/7**, 1–13 (1953).
- [118] *Falowod akustyczny*, L. FILIPCZYŃSKI, *Kinotechnik*, **43**, 824–826, (1952).
- [119] *Badania warunków akustycznych w przemyśle włókienniczym*, L. FILIPCZYŃSKI and T. JANISZEWSKI, *Prace Centralnego Instytutu Ochrony Pracy*, **1**, 2, 1–5 (1951).
- [120] *Pomiary współczynników pochłaniania przy użyciu akustycznej linii długiej*, I. MAŁECKI and L. FILIPCZYŃSKI, *Przegląd Telekomunikacyjny*, **4**, 113–116 (1951).

### Monographs

- [1] *Application of ultrasound in biomeasurements, in diagnosis and therapy*, L. FILIPCZYŃSKI [Red.] International Center of Biocybernetics, Warszawa 1972, 352 pp.
- [2] *Biopomiary* [Biomeasurements, [in Polish], L. FILIPCZYŃSKI and W. TORBICZ [Red.] Wydawnictwa Komunikacji i Łączności, Warszawa 1990, 602 pp.
- [3] *Przepływ krwi — hemodynamika i ultradźwiękowe dopplerowskie metody pomiarowe* [Blood flow — hemodynamics and ultrasonic Doppler measurement methods [in Polish], L. FILIPCZYŃSKI, R. HERCZYŃSKI, A. NOWICKI and T. POWAŁOWSKI, PWN, Warszawa—Poznań 1980, 163 pp.
- [4] *Diagnostyka ultradźwiękowa w położnictwie i chorobach kobiecych* [Ultrasonic diagnostic in obstetrics and in gynecology, [in Polish], L. FILIPCZYŃSKI and I. ROSZKOWSKI [Red.] Państwowe Zakłady Wydawnictw Lekarskich, Warszawa 1977, 189 pp.
- [5] *Ultradźwiękowe metody diagnostyczne* [Ultrasonic diagnostic methods in Polish], L. FILIPCZYŃSKI [in:] *Elektronika medyczna*, J. Keller [Red.] part 6 pp. 102–106, Wydawnictwa Komunikacji i Łączności, Warszawa 1972.
- [6] *Ultrasonic in biology and medicine*, L. FILIPCZYŃSKI [Ed.], PWN, Warszawa 1972, 274 pp.
- [7] *Ultrasonic methods of testing materials*, L. FILIPCZYŃSKI, Z. PAWŁOWSKI and J. WEHR, Butterworth, London 1966.
- [8] *Proc. of the Conference on Acoustics of Solid Media*, L. FILIPCZYŃSKI [Ed.], PWN, Warszawa 1966.
- [9] *Ultradźwiękowe metody badań materiałów* [Ultrasonic methods of testing materials], [in Polish], L. FILIPCZYŃSKI, Z. PAWŁOWSKI and J. WEHR, Wyd. II WNT, Warszawa 1963; Wyd. I, WNT, Warszawa 1959, 295 pp.
- [10] *Wytwarzanie i odbiór fal ultradźwiękowych za pomocą przetwornika kwarcowego o cięciu X* [Generation and reception of ultrasonic waves by means of the X-cut quartz transducer, [in Polish], L. FILIPCZYŃSKI, PWN, Warszawa 1960, 64 pp.
- [11] *Defektoskopia ultradźwiękowa* [Ultrasonic defectoscopy], [in Polish], L. FILIPCZYŃSKI, Z. PAWŁOWSKI and J. WEHR, Wyd. skryptowe SIMP—NOT Warszawa 1957.
- [12] *Technika nagrywania i odtwarzania dźwięków* [Technics of sound recording and reproducing], Pr. zb. pod. red. I. Maleckiego i L. Filipczyńskiego — rozdz. 6, 8, 9, Państwowe Wydawnictwa Techniczne, Warszawa 1953, 487 pp.

Moreover, prof. L. Filipczyński is the author or coauthor of 126 foreign and Polish reports in Conference Proceedings.

## HIGH-FREQUENCY DOPPLER ULTRASOUND FLOWMETER

A. NOWICKI, W. SECOMSKI, P. KARŁOWICZ AND G. ŁYPACEWICZ

Ultrasonic Department  
Institute of Fundamental Technological Research  
Polish Academy of Sciences  
(00-049 Warszawa, Świątokrzyska 21)

This paper discusses a new Doppler device for measuring blood flow in small vessels. The ultrasound frequency applied is 20 MHz. Two different ultrasound probes were designed with transducer diameters of 0.9 mm and 1.6 mm. The transducers were located at the point of a catheter. As measured at 1.5 mm depth, the lateral resolutions were 1 mm and 1.7 mm, respectively. The flowmeter is very sensitive. Compared with standard flowmeters (from 2 to 8 MHz), signals from subcutaneous vessels are greater by 10-20 dB.

### 1. Introduction

The ultrasound Doppler measurement of the blood flow rate in small vessels is an important clinical issue both in the evaluation and diagnosis of the Raynaud disease as well as in the course of intraoperative vessel identification, e.g., during neurological operations and plastic surgery applied to hands and other organs. Because of the required high lateral resolution, the ultrasound beam should be narrow. The flows under study are often very slow; this, in turn, affects the choice of the ultrasound frequency, one which is several times higher than the one commonly used in standard flowmeters for the diagnosis of large peripheral vessels. Usually, flow rate measurements are taken for large peripheral vessels using 2-8 MHz frequencies.

HARTLEY and COLE [5], and the Green *et al.* [4] applied a pulsed Doppler method at 20 MHz for the intraoperative estimation of blood flow in small vessels. CATHIGNOL *et al.* [3] developed a device working at a similar frequency, but one with more limited measuring volume. PYNE [12] presented the results of blood flow rate in skin, an organ which is part of the thermoregulation system. In his research, Payne evaluated the usefulness of heat conductivity, xenon clearance, a Doppler laser flowmeter and the ultrasound Doppler working at 15 MHz and 30 MHz [11]. However promising, the results of the Doppler measurements showed that the

spectra of Doppler signals measured in small arterioles fall much below 50 Hz, making it difficult to process and, as a result, to evaluate them quantitatively. BERSON *et al.* [2] greatly enhanced the frequency used, up to as much as 113 MHz, expanding the spectra measured up to about 1 kHz, but limiting the probing depth down to that of several hundred microns.

## 2. Method and Apparatus

### 2.1. Frequency selection

The ultrasound reflected from moving red cells returns to the ultrasonic transducer at a frequency which varies depending on the transmitted wave frequency. The frequency difference is expressed by the formula

$$f_d = 2f_T \frac{V}{c} \cos \theta \quad (1)$$

where  $f_d$  is the Doppler frequency,  $f_T$  is the transmitted wave frequency,  $v$  is the ultrasound propagation in blood and  $\theta$  is the angle between the ultrasonic wave propagation direction and the blood flow direction.

The selection of the optimum ultrasonic frequency is a compromise between attenuation by the medium being investigated and the wave energy being scattered by red cells. MC LEOD [8] gave a dependence describing the signal/noise ratio (SNR) as a function of scattering (an increase in signal with the fourth power of frequency), attenuation (an exponential signal drop with increasing frequency) and electronic noise which grows approximately linearly with increasing frequency.

$$\frac{S}{N} \div \frac{f_0^4}{f_0 d^2} e^{-2\alpha f_0 d} \quad (2)$$

The optimum frequency  $f_{opt}$  (maximum SNR) can be calculated by differentiating expression (2) over frequency and zeroing the result

$$f_{opt} = \frac{3}{2\alpha d} \quad (3)$$

If attenuation  $\alpha$  is denoted as  $k$ , in dB/MHz/cm, expression (3) becomes

$$f_{opt} = \frac{30 \log e}{k d} \quad (4)$$

The mean damping in soft tissue is about 1 dB/MHz/cm and, therefore,  $f_{opt} = 15/d$  MHz. The experimental results [1, 3] indicate that in modern low-noise apparatus  $f_{opt}$  can be even twice as high. The ultrasonic frequency as determined from formula (4) falls between 15 MHz and 30 MHz for the wave penetration depth down to 1 cm.

## 2.2. Ultrasonic probe

As an effect of the technological limitations of polishing very thin piezoelectric (PZT 5) ceramic plates, the frequency of 20 MHz was chosen. At this frequency, the resonance thickness is about 0.1 mm. Attempts to produce thinner plates proved to be hardly repeatable.

Because of the intraoperative flow measurements in small vessels the probe should be as small as possible. In the C.W. method, the probe consists of two transducers, the transmitting and receiving ones, each having its own coaxial wiring to connect the transducer with the transmit-receive system. In the pulsed method, the ultrasonic probe has only one transmit-receive transducer connected with the transmitter and receiver equipped with the same wiring. It makes it possible to reduce greatly the external dimensions of the probe or catheter.

HARTLEY and COLE [5] describe a pulsed Doppler 20 MHz system designed for intraoperative blood flow rate monitoring in dogs' coronary vessels. The transducer was fixed to a narrow and thin band wound round a vessel.

The basic problem which emerges as an intraoperative 20 MHz probe is built is the preparation of the transducer. The piezoelectric ceramics PZT-5A, which is universally used in medical diagnosis has good efficiency, and is readily available and cheap. It is

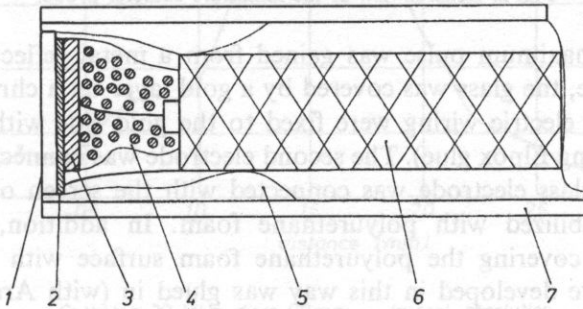


Fig. 1. Design of the tiny 20 MHz ultrasonic probe. 1) glass plate, 2) conducting glue layer, 3) ceramic transducer, 4) polyurethane foam, 5) glue, 6) coaxial cable, 7) pvc catheter.

necessary, however, to select the ceramics carefully, for at the required frequency of 20 MHz, its resonance thickness is lower than 100  $\mu\text{m}$  and the grain thickness and brittleness of the ceramic sinter will begin to play an essential role. In successive operations, it is well-advised to eliminate the ceramics in which faults occur. What is particularly significant are the faults, revealed in the course of polishing, which can cause short circuits between electrodes, by filling the space with conducting glue. In the first instance, these transducers were polished to appropriate thickness using methods applied in optical glass processing. The result is an element which maintains polarization and has an electrode on one side. It was easiest to reduce the transducer diameter by gradual edge crushing until the desired dimensions were attained — 1.6 mm or 0.9 mm. The transducer was placed on a BK 7, 0.2 mm thick glass plate, which was a substrate for the very delicate ceramic element. To improve the acoustic probe-water impedance matching, the glass plate was

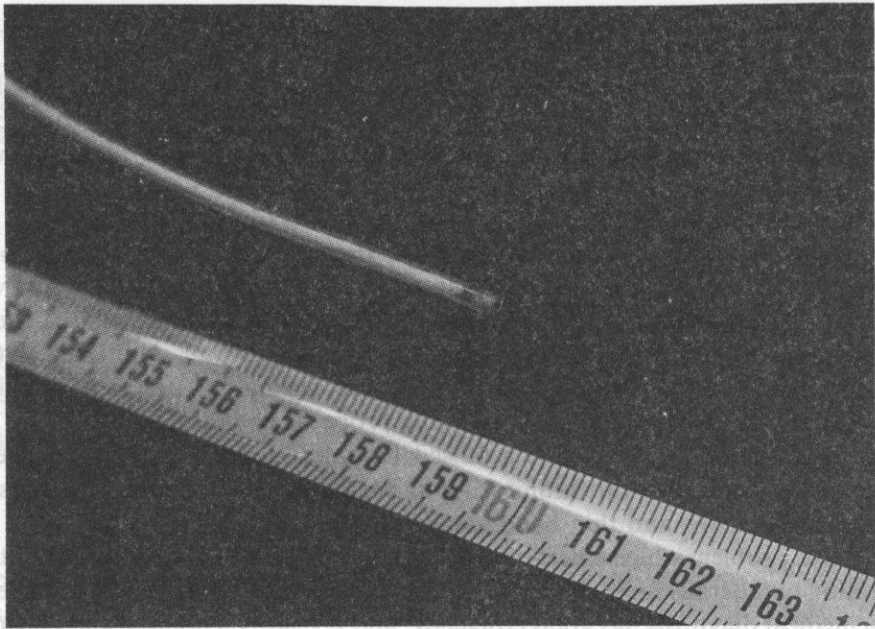


Fig. 2. General view of the miniature catheter probe.

polished until a maximum pulse was gained from a metal reflector submerged in water. On one side, the glass was covered by a gold layer on a chromium substrate. A transducer and electric wiring were fixed to the gold side without an electrode (with the conducting Elpox glue). The second electrode was connected with a coaxial  $50\ \Omega$  cable. The glass electrode was connected with the screen of this cable. This structure was stabilized with polyurethane foam. In addition, the screen was supplemented by covering the polyurethane foam surface with conducting glue. Then, the structure developed in this way was glued in (with Araldit resin) inside a 1.6 m long PVC catheter, with an external diameter of 1.6 mm or 2.5 mm, depending on the transducer diameter. Over the section inside the catheter, a special concentric  $50\ \Omega$  cable (Filotex Alcatel) was applied. At the site of connection with a standard RG 174 cable a parallel inductance was applied to compensate for the capacity of the transducer and cable. The probe and device were connected by a cable 1.95 m long.

The probe impedance was measured using a Network Analyzer HP 3577A bridge, comparing the measurement data with the impedance of a model whose parameters were changed so as to generate as similar curves as possible [6]. Figure 3 shows the modelling results. The differences between the measured and calculated model curves are caused by difficulties in defining the load on the back surface of the transducer and the thickness of the glass plate. A change in the layer thickness by several percent causes a very significant impedance change; and in the case of a layer with variable thickness, as a result of manual polishing, the resulting error cannot be calculated.



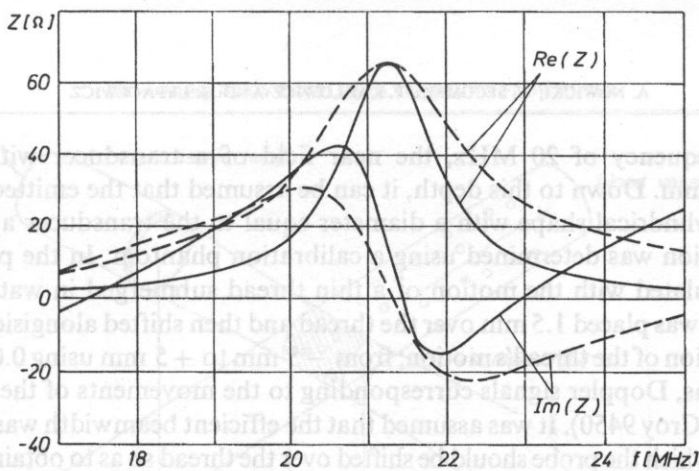


Fig. 3. Real and imaginary parts of the probe impedance measured using the HP 3577A bridge — solid lines; and those calculated for the model — dashed lines.

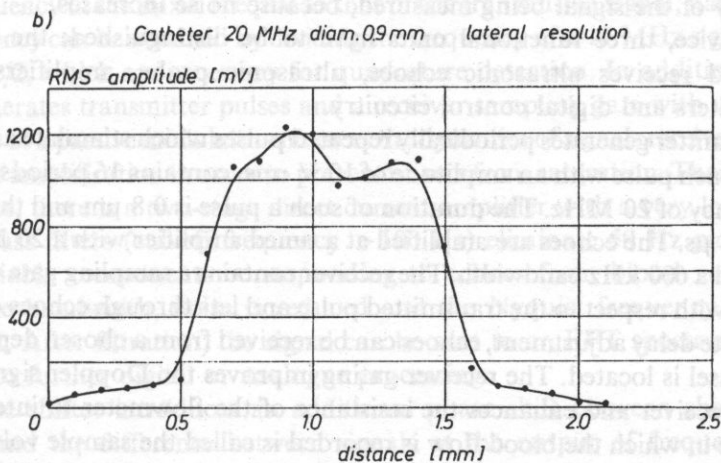
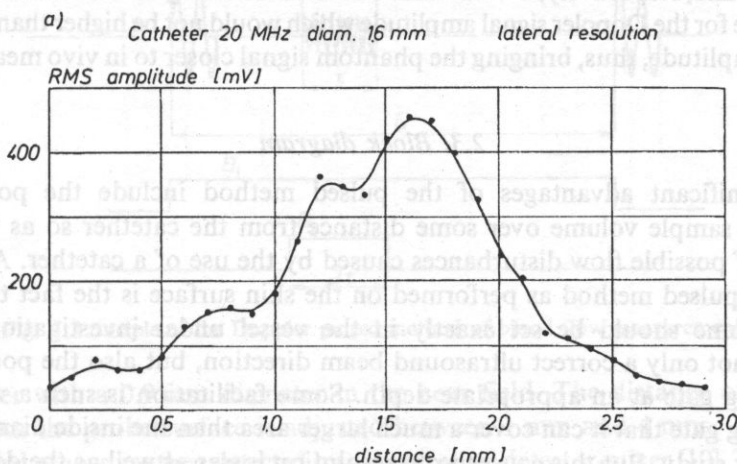


Fig. 4. Ultrasonic beam width (6 dB) measured using a thread phantom, a) transducer  $\Phi=1.6$  mm, b) transducer  $\Phi=0.9$  mm.

At the frequency of 20 MHz, the near field of a transducer with a 1.6 mm diameter is 8 mm. Down to this depth, it can be assumed that the emitted ultrasound beam has a cylindrical shape with a diameter equal to the transducer aperture. The lateral resolution was determined using a calibration phantom. In the phantom, the flow was simulated with the motion of a thin thread submerged in water.

The probe was placed 1.5 mm over the thread and then shifted alongside in keeping with the direction of the thread's motion; from  $-5$  mm to  $+5$  mm using 0.05 mm steps. At all positions, Doppler signals corresponding to the movements of the thread were registered (Le Croy 9450). It was assumed that the efficient beam width was equal to the section along which the probe should be shifted over the thread so as to obtain a half of the maximum Doppler signal amplitude. As expected, the measured width (6 dB) was equal to the transducer aperture, that is 1.7 mm and 1 mm for a transducer with a diameter  $\Phi = 1.6$  mm and, respectively,  $\Phi = 0.9$  mm. The transmitter signal was decreased as much as to provide for the Doppler signal amplitude which would not be higher than 30 dB than the noise amplitude, thus, bringing the phantom signal closer to in vivo measurements.

### 2.3. Block diagram

The significant advantages of the pulsed method include the possibility of moving the sample volume over some distance from the catheter so as to decrease the effect of possible flow disturbances caused by the use of a catheter. A disadvantage of the pulsed method as performed on the skin surface is the fact that a small sample volume should be set exactly in the vessel under investigation. What it requires is not only a correct ultrasound beam direction, but also the positioning of the sampling gate at an appropriate depth. Some facilitation is such a widening of the sampling gate that it can cover a much larger area than the inside diameter of the vessel under study. But this causes axial resolution losses as well as the deterioration of the quality of the signal being measured, because noise increases.

In the device, three functional units have to be distinguished: the part which transmits and receives ultrasonic echoes, ultrasonic probe, amplifiers and low-frequency filters and digital control circuitry.

The transmitter generates periodically repeated pulses which stimulate an ultrasonic transducer. Each pulse with an amplitude of 10 V rms. contains 16 periods of sinusoid at the frequency of 20 MHz. The duration of such a pulse is 0.8  $\mu$ s and the repetition period is 12.8  $\mu$ s. The echoes are amplified at a tuned amplifier with a 20 MHz center frequency and a 600 kHz bandwidth. The receiver contains a sampling gate with a delay which varies with respect to the transmitted pulse and lets through echoes over 1.6  $\mu$ s. Due to the gate delay adjustment, echoes can be received from a chosen depth at which the blood vessel is located. The receiver gating improves the Doppler signal-to-noise ratio of the receiver and enhances the resistance of the flowmeter to interference.

The space in which the blood flow is recorded is called the sample volume, and is cylindrical in shape. For a pulse of 0.8  $\mu$ s duration, the cylinder height is about 0.5 mm. Its diameter depends on the ultrasound beam width, and is 1 mm for

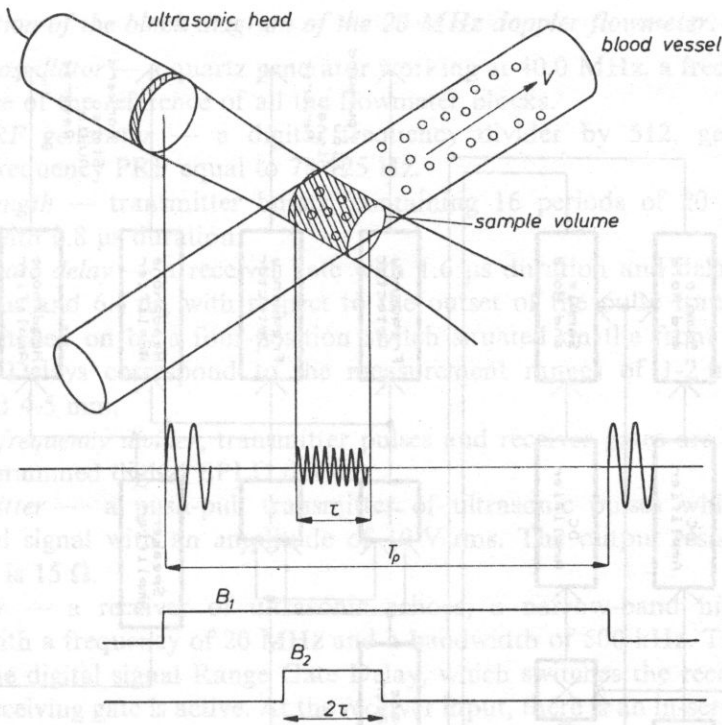


Fig. 5. Principle of the Doppler pulsed method of blood flow measurements.

a transducer with a 0.9 mm diameter in the near field. The distance of the sample volume from the probe surface is adjusted between 1 mm and 4 mm.

Amplified echoes are then detected by a quadrature detector-mixer [10]. The reference signal frequency in the mixer is equal to that of the transmitted signal, namely 20 MHz. This frequency can be obtained by dividing the frequency of a 40 MHz signals, shifted in phase by  $\pi/2$ , which are necessary for quadrature detection. In addition, this digital system generates transmitter pulses and a receiver sampling gate with variable delay.

The use of a passive modulator enhances the dynamics of signals received, but restricts the receiver amplification in order to prevent mixers from saturation. Therefore, directly after mixers, there is a two-stage direct current amplifier with a very low noise level.

High-pass filters (cut-off frequency  $> 100$  Hz) eliminate 50 Hz pick-up and the slowly variable components corresponding to echoes from blood vessel walls. By limiting the bandwidth, noise is reduced and the Nyquist frequency (39.6 kHz) is filtered out. After filtration, the signal can be sent to an FFT spectrum analyser or subjected to further digital or analogue processing.

A phase shifter introduces an additional phase shift between channels by  $\pi/2$ . The sum and the difference between signals at the output of frequency detectors correspond to flows towards and away from the ultrasonic probe. These signals are also connected to a stereophonic earphone amplifier and a loudspeaker amplifier.

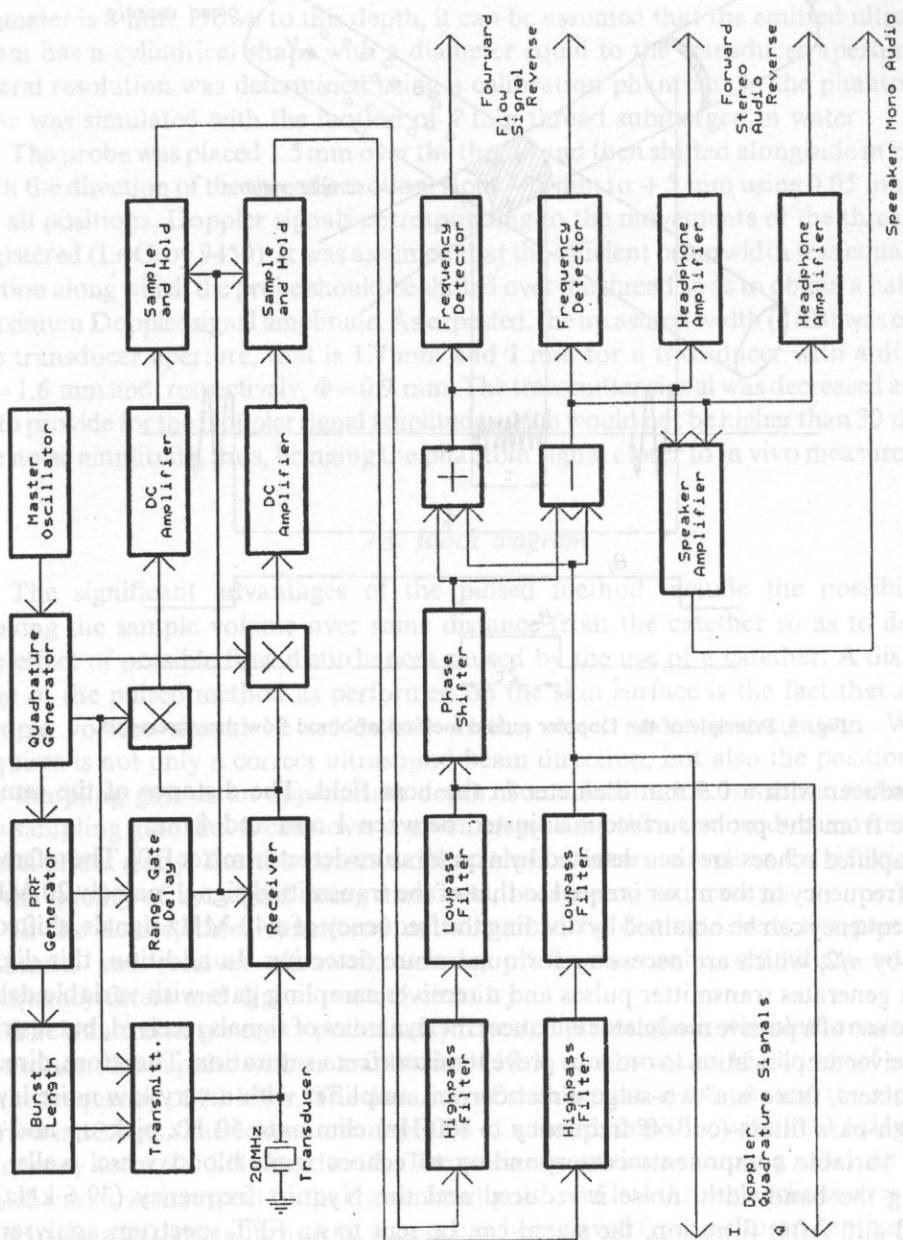


Fig. 6. Block diagram of the flowmeter.

*Description of the block diagram of the 20 MHz doppler flowmeter.*

*Master oscillator* — a quartz generator working at 40.0 MHz, a frequency which is the source of the reference of all the flowmeter blocks.

The *PRF generator* — a digital frequency divider by 512, generating the repetition frequency PRF equal to 78 125 Hz.

*Burst length* — transmitter bursts, containing 16 periods of 20 MHz carrier frequency with 0.8  $\mu$ s duration.

*Range gate delay* — a receiver gate with 1.6  $\mu$ s duration and delays of 1.6  $\mu$ s, 3.2  $\mu$ s, 4.8  $\mu$ s and 6.4  $\mu$ s, with respect to the outset of the pulse transmitted. The delay is switched on by a four-position switch situated on the front panel of the flowmeter. Delays correspond to the measurement ranges of 1-2 mm, 2-3 mm, 3-4 mm and 4-5 mm.

*Digital frequency divider*, transmitter pulses and receiver gates are implemented in one programmed digital EPLD device.

*Transmitter* — a push-pull transmitter of ultrasonic pulses which generates a sinusoidal signal with an amplitude of 10 V rms. The output resistance of the transmitter is 15  $\Omega$ .

*Receiver* — a receiver of ultrasonic echoes, a narrow-band high-frequency amplifier with a frequency of 20 MHz and a bandwidth of 500 kHz. The receiver is gated by the digital signal Range Gate Delay, which switches the receiver on only when the receiving gate is active. At the receiver input, there is an in-series resonance circuit with a diode limiter, which enhances the receiver sensitivity and separates the receiver from the transmitter during the transmission. The receiver consists of a two-gate MOSFET transistor and a monolithic buffer amplifier.

*Quadrature generator* — two digital frequency dividers by 2, controlled by a 40 MHz clock with inverse bias. As an effect, at their output there are 20 MHz signals with their phase shifted by  $\pi/2$ , which provides for quadrature detection.

*DC amplifier* — a post-detection signal is amplified by a two-stage amplifier with a low noise level and full amplification of 27 dB.

*High-pass filter* — a first order high-pass filter which eliminates the D.C. component of the signal as well as the slowly variable components originating from blood vessel motions. The cut-off frequency of the filter is 80 Hz.

*Low-pass filter* — a Bessel fourth-order low-pass filter which eliminates the repetition frequency and prevents aliasing. The cut-off frequency of the filter is 16 kHz.

*Phase shifter* — a five-stage phase shifter which ensures the phase difference between channels I and Q equal to  $\pi/2$  with an accuracy of 0.5% over the frequency range of 150 Hz-15 kHz.

*Frequency detector* — a zero crossing integrated detector, its output voltage is in direct proportion to the second moment of the input signal spectrum.

*Headphone amplifier* — a stereophonic headphone amplifier which makes it possible to hear separately flows towards and away from the probe.

### 3. Evaluation of the size of the signal scattered in blood

An attempt will now be made to estimate the effect of the sampling gate duration on the signal-to-noise ratio of the Doppler signal. If an ultrasonic wave is incident on a single blood cell, which is small compared with the wavelength, the scattered wave propagates in all directions as a spherical wave. A blood cell has the shape of a disk with an average thickness of  $2.5 \mu\text{m}$  and a diameter of  $8 \mu\text{m}$ . The average erythrocyte volume is about  $90 \mu\text{m}^3$ . A sphere of this size would have a radius equal to  $2.78 \mu\text{m}$ .

The strength of the scattered wave can be calculated from the product of the effective scattering surface  $\delta$  and the incident wave intensity.

$$I_{\delta} = \left( \frac{P_t A}{x^2 \lambda^2} \right) \left( \frac{\delta}{4\pi x^2} \right) e^{-4\alpha x}, \quad (5)$$

where  $P_t$  is the transmitted signal power,  $\alpha$  is the wave attenuation coefficient in the medium and  $A$  is the transducer surface area.

The first term is responsible for the intensity of the wave incident on a blood cell with the scattering surface  $\delta$ , located at the distance  $x$  from the transducer. The second term accounts for the spherical wave propagation.

The determination of the power scattered by a large number of blood cells requires some discussion. The scattering cross section of a particle with dimensions much smaller than the wavelength can be determined from the expression given by MORSE and INGARD [9]

$$\delta = \frac{4\pi k^4 a^6}{9} \left[ \left( \frac{\kappa_k - \kappa}{\kappa} \right)^2 + \frac{1}{3} \left( \frac{3\rho_k - \rho}{2\rho_k + \rho} \right)^2 \right], \quad (6)$$

where  $k=2\pi/\lambda$  is the wave number,  $a$  is the blood cell radius,  $\kappa_k$  is the adiabatic compressibility coefficient of the blood cell equal to  $34.1 \times 10^{-13} \text{ m}^2/\text{dyne}$ ,  $\kappa$  is the adiabatic compressibility coefficient of plasma equal to  $40.9 \times 10^{-13} \text{ m}^2/\text{dyne}$ ,  $\rho_k$  is the blood cell density equal to  $1.092 \times 10^3 \text{ kg/m}^3$  and  $\rho$  is the plasma density equal to  $1.021 \times 10^3 \text{ kg/m}^3$  [13].

At 20 MHz, the scattering cross section  $\delta$  (20 MHz) of one blood cell is equal to  $9.24 \times 10^{-16} \text{ m}^2$ . 1% HMTC is equivalent to  $1.07 \times 10^{14}$  blood cells in  $1 \text{ m}^3$ , hence the scattering coefficient  $\eta$  (HMTC=40%,  $f=20 \text{ MHz}$ ) is  $\eta = \delta(20 \text{ MHz}) \times 1.07 \times 40 = 3.96 \text{ m}^{-1}$ . Since for normal hematocrit (HMTC from 40% to 45%) the average distance between two blood cells is about 10% of their diameter; with such packing the blood cells cannot be considered independent scattering sources. SHUNG *et al.* [13] showed that the scattering coefficient  $\eta$  grows linearly with increasing hematocrit only up to HMTC of 8%, and then an increase in  $\eta$  is slower, to reach a plateau for HMTC of 24-30%, and then to drop. From the scattering coefficients determined by SHUNG *et al.*, over the frequency range of 5 to 15 MHz, the value of  $\eta$  was approximated at 20 MHz, to obtain  $\eta = 1.32 \text{ m}^{-1}$ , three times

lower than the value derived from formula (6). Since our purpose is only to estimate approximately the power scattered by blood cells, although some potentially large error can be made, it is justifiable to adopt the latter value in further calculations.

As a further step, the total intensity of the scattered signal can be determined as

$$I_r = \frac{P_t A^2}{x^4 \lambda^2 4\pi} \cdot \frac{c\tau}{2} \eta e^{-4\alpha x}. \quad (7)$$

In formula (7), the total radiation power,  $P_t$ , is unknown. The accuracy of measurements of the ultrasonic field distribution and the calculations of the power radiated as made on this basis depend on the dimensions of the active measuring component of the hydrophone. The available hydrophones include an active measuring component equal to about 0.5 mm, which is exceedingly large for transducer measurements taken in this case. Therefore, the scattering intensity was estimated only theoretically. The following calculation procedure was followed. On the basis of the measured impedance of the two probes, the coefficient of electromechanical coupling  $k_t=0.5$  and the dielectric constant  $\epsilon=900$  were determined. These data were introduced to the equivalent model of piezoelectric transducer, acc. to MASON [7]; the acoustic pressures and powers as well as the intensities of the radiated wave and of the wave reflected from an ideal reflector at a distance of 1.5 mm from the transducer were calculated. The average skin absorption,  $\alpha=2.3$  dB/cm/MHz was adopted. When expressed in nepers, the total attenuation, after covering a distance twice as long as 1.5 mm, is 0.08 N/MHz. The calculated results are shown in Table 1.

**Table 1.** The calculated values of pressure, intensity, transmitted and received power and the receiving voltages at the transducer for two different 20 MHz piezoelectric transducers

Transducer		
	$F=0.9$ mm	$F=1.6$ mm
Transmission voltage [ $V_{pp}$ ]	30	30
Radiated acoustic pressure [ $N/m^2$ ]	$0.79 \times 10^6$	$0.46 \times 10^6$
Received acoustic pressure [ $N/m^2$ ]	$0.15 \times 10^6$	$0.89 \times 10^6$
Transmitted wave intensity [ $W/m^2$ ]	$0.21 \times 10^6$	$0.72 \times 10^6$
Received wave intensity [ $W/m^2$ ]	$0.74 \times 10^4$	$0.26 \times 10^4$
Radiated acoustic power $P_t$ [W]	0.13	0.14
Received voltage [ $V_{pp}$ ]	0.865	0.854

For comparison, echoes from an ideal reflector were measured for the amplitude of the transmitted pulse, as in the simulation  $V_{pp}=30$  V. The amplitude of an echo from an ideal reflector submerged in water was  $1.5 V_{pp}$  (for the transducer with  $\Phi=0.9$  mm). Taking into account the skin attenuation, instead of one in water, the echo in question would amount to  $0.4 V_{pp}$ , slightly twice lower than the modelled one. Bearing in mind the fact that the model considered only the impedance of the transmitter and receiver, the twofold difference between the calculated and measured values can be accepted. In the scattering calculation, it was assumed that if the voltage  $0.865 V_{pp}$  corresponds to the radiated power of 0.13 W, then the radiated power of 0.028 W corresponds to the voltage of  $0.4 V_{pp}$ . Respectively, the intensity of the scattered wave received is  $0.16$  W/cm<sup>2</sup>.

By substituting  $\tau=0.8 \times 10^{-6}$  s,  $\alpha=2.3$  dB/cm/MHz,  $\eta=1.32$  m<sup>-1</sup>, the transducer surface area  $A=6.36 \times 10^{-7}$  m<sup>2</sup> (for a transducer with  $\Phi=0.9$  mm) and  $x=1.5$  mm, the intensity of the scattered wave  $I_r=1.05 \times 10^{-4}$  W/cm<sup>2</sup>, which is about 1520 times lower than that of a wave reflected from an ideal reflector. The voltage generated by the scattered wave would be almost 40 times lower, that is,  $10$  mV<sub>pp</sub>.

In the pseudo-continuous mode, that is, without sample and hold gate, the noise signal detected in a time equal to the repetition period  $T_p$  is added to the Doppler signal from the vessel under study. In this case, the sampling gate is on throughout the time between successive transmitted pulses. During the repetition period  $T_p=12.8$   $\mu$ s the ultrasonic wave will travel, from here and back, a distance of 19.2 mm, corresponding to the penetration depth of 9.6 mm. The duration of the transmitted pulse  $\tau$  is 0.8  $\mu$ s.

Let the vessel under study be 0.75 mm wide and located at a distance of 1.5 mm from the probe. The ultrasonic pulse travels a distance from the anterior wall to the posterior wall of the vessel and back (when neglecting the angle between the beam and the vessel) over 1  $\mu$ s. The duration of a signal scattered by a blood cell is then 0.078 of the repetition period  $T_p$ . In studies on small vessels, it is well-advised for the sampling gate to account for the whole vessel. Accounting for small displacements of a vessel in the course of measurements, in practical applications, the length of the sampling gate is slightly longer so that it can begin before and end after the wave has crossed a vessel. The length of the sample gate in the present system is 1.6  $\mu$ s (0.125  $T_p$ ).

As estimated, the intensity of the wave scattered by blood cells is  $1.05 \times 10^{-4}$  W/cm<sup>2</sup> and, respectively, the voltage at the transducer is  $U_r=10$  mV<sub>pp</sub>. When referred to its input, the effective voltage of the receiver noise is 6.6  $\mu$ V rms. (18  $\mu$ V<sub>pp</sub>). The input signal is the sum of the Doppler component which corresponds to scattering and noise,  $U_{in}=U_{dop}+U_{noise}$ , with voltages equal respectively to 10 mV and 18  $\mu$ V.



$$U_{\text{dop}} = \begin{cases} 10 \text{ mV} & \text{for } 2/10 T < t < 3/10 T \\ 0 \text{ V} & \text{for } t < 2/10 T, t > 3/10 T \end{cases} \quad (8)$$

These values correspond to those measured in a blood cell with an 0.5 mm diameter, located 1 mm under the skin surface.  $U_{\text{noise}} = 18.5 \mu\text{V}$  between the end of one transmitted pulse and the beginning of another, that is, practically, over the time  $T_p$ .

The Doppler component at the output of the integrating gate is equal to

$$\overline{U_{\text{dop}}} = \frac{1}{\frac{2}{16}T} \int_{\frac{2}{16}T}^{\frac{3}{16}T} 10 \text{ mV} dt = 5 \text{ mV} \quad (9)$$

on the other hand, the averaged noise voltage is

$$\overline{U_{\text{noise}}} = \frac{1}{\frac{2}{16}T} \int_{\frac{2}{16}T}^{\frac{4}{16}T} 18.5 \mu\text{V} dt = 18.5 \mu\text{V} \quad (10)$$

The signal-to-noise ratio, SNR, for such a signal is

$$\text{SNR} = 10 \log \frac{U_{\text{dop}}^2}{U_{\text{noise}}^2} = 48 \text{ dB}$$

The correct Doppler frequency measurement by the zero-crossing method (ZCC) requires SNR which is greater than 10 dB (a Doppler component three times greater than noise). The FFT spectrum analysis makes it possible to carry out measurements for smaller signal,  $\text{SNR} > 6\text{dB}$ , that is, when Doppler signal is twice as big as noise. The device is sufficiently sensitive even in the continuous mode, that is, when the sampling gate is open throughout the repetition period. In the continuous mode, without a sampling gate (or when it is open throughout the repetition time), the Doppler signal voltage is much lower (by a factor of five, in this case), because it is averaged over the time  $T_p$ , whereas the noise component remains at the same level. Even in this case, SNR is very high and exceeds 30 dB. In the continuous mode, it is much easier to locate a vessel. Figure 7 shows examples of Doppler signals recorded in the continuous mode from the digital artery, the radial artery and the upper palm vein. Therefore, e.g., the voltage of the signal scattered in a vein was about  $2.7 \text{ mV}_{\text{pp}}$ . With the sample and hold gate this voltage would increase by a factor of 5 up to 13 mV, the value being very close to  $10 \text{ mV}_{\text{pp}}$  theoretically calculated.

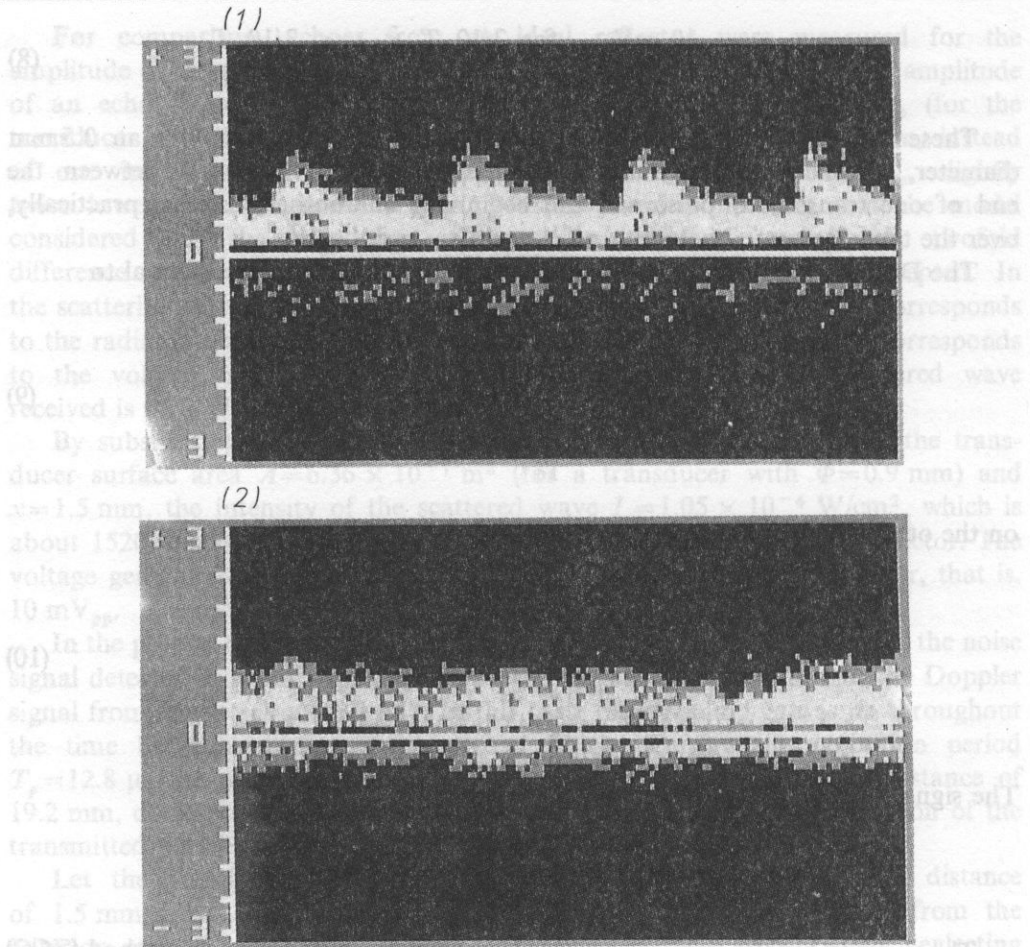


Fig. 7. Spectra of Doppler blood flow signals recorded subcutaneously at 1) digital artery at 2.5 mm depth, 2) hand vein at 2 mm depth.

#### 4. Conclusions

Laboratory measurements confirmed the theoretically predicted, much larger amplitudes of Doppler signals compared with standard flowmeters working over the frequency range from 2 MHz. Special attention was paid to the design of the probe in order to achieve good lateral resolution. The total loss in the reflection of the radiated wave from an ideal reflector was lower than 26 dB.

The preliminary results of blood flow measurements in small vessels proved to be very promising. The high transversal and longitudinal resolution made it possible to locate and distinguish vessels under study, opening up a new application range of the Doppler technique in the intra- and post-operative control of the correctness of

vessel reconstructive surgery and the patency of the very narrow vessels sewn together in plastic surgery as well as in the course of and after bone replant operations in order to control the effect of perforators. Some other potential applications include the diagnosis of damaged flow in small hand vessels and intraoperative blood flow control in cranial vessels in the course of neurological operations.

## References

- [1] D.W. BAKER, F.K. FORSTER and R.E. DAIGLE, *Doppler principle and technique*, in: *Ultrasound, its application in medicine and biology*, [Ed.] F.J. Fry Chapter 3, 161–287, Elsevier Sc. Publ. Company, New York 1978.
- [2] M. BERSON, F. PATAT, Z.Q. WANG, D. BASSE and L. POURCELOT, *Very high frequency pulsed Doppler apparatus*, *Ultrasound in Med. and Biol.*, **15**, 2, 121–131 (1989).
- [3] D. CATHIGNOL, J.Z. CHAPELON, J.L. MESTAS and C. FURCADE, *Description et application d'un velocimetre ultrasonore Doppler pour les petits vaisseaux*, *Med. and Biol. Eng.*, **21**, 358–364 (1983).
- [4] E.R. GREENE, W.F. BLAIR and C. HARTLEY, *Noninvasive pulsed Doppler blood velocity measurements and calculated flow in human digital arteries*, *ISA Trans.*, **20**, 2, 15–24 (1981).
- [5] C.J. HARTLEY and J.S. COLE, *An ultrasonic pulsed Doppler system for measuring blood flow in small vessels*, *Journal of Applied Physiology*, **37**, 4, 626–629 (1974).
- [6] G. ŁYPACEWICZ and E. DURIASZ, *Design of ultrasonic probes for medical diagnostics*, *Archives of Acoustics*, **15**, 3–4 (1990).
- [7] W.P. MASON, *Physical acoustics*, vol. 1, Part A, Academic Press, New York 1964.
- [8] F.d. MC LEOD, *Multichannel pulsed Doppler techniques*, *Cardiovascular Res.*, **4**, 428 (1972).
- [9] P.M. MORSE and K.U. INGARD, *Theoretical acoustics*, McGraw Hill, New York 1968.
- [10] A. NOWICKI, *Doppler Echography* (in Polish — Echografia dopplerowska), Polish Scientific Publishers PWN, Warszawa 1989.
- [11] P.A. PAINE, S.M. JAWAD and R.Y. FADDOUL, *A high frequency ultrasound pulsed Doppler system for the measurement of skin blood flow*, 4th Int. Symp. Bioeng. Skin, Besançon, France, Sept. 1983.
- [12] P.A. PAINE, *Measurement of skin blood flow*, *Electronics and Power*, March 30, 219–221 (1984).
- [13] K.K. SHUNG, A. RUBENS and J.M. REID, *Scattering of ultrasound by blood*, *IEEE Trans. Biomed. Eng. BME-24*, **4**, 325–331 (1977).

## 1. Introduction

The evaluation of the elasticity of arteries was based on the examination of changes in the transversal dimensions of the vessel which are caused by blood pressure variations. It involves differently defined coefficients which are often applied in references to characterize the elastic properties of arterial walls. E.g., they include:

1) the elastic modulus  $E_v$ , as described by Petrášová in 1960 [14]:

$$E_v = \frac{\Delta P \cdot D_d}{\Delta D} \quad (1.1)$$

where  $\Delta D/D_d$  is a relative increase in the vessel diameter as a function of the blood pressure growth  $\Delta P$ .

## NONINVASIVE EVALUATION OF THE ELASTICITY OF COMMON CAROTID ARTERY WALL

T. POWAŁOWSKI AND Z. TRAWIŃSKI

Ultrasonic Department  
Institute of Fundamentals Technological Research  
Polish Academy of Sciences  
(00-049 Warszawa, Świętokrzyska 21)

The elasticity of common carotid arteries was examined on the basis of noninvasive ultrasonic measurements of the diameter of the carotid artery and the systolic and diastolic pressures as determined by a cuff on the brachial artery. The measurements were performed for a group of 20 males, aged from 27 to 45 years. The examines were fighter plane pilots. The examinations were carried out for different systolic and diastolic pressures which were recorded along with measurements of the diameter of the carotid artery during rest, following an exercise test. This paper presents the results of measurements of the maximum and minimum diameters of the common carotid artery for different systolic and diastolic pressures in the brachial artery. Good coincidence was gained between the experimental results and the logarithmic function as described by POWAŁOWSKI. The coefficient of the determination  $R^2$  fell between 0.993 and 0.999. On the basis of the results of the measurements of the artery diameter and the blood pressure, the values of coefficients describing the elastic properties of the common carotid arteries were defined. The investigated coefficients included: the elastic modulus  $E_p$ , the arterial distensibility coefficient  $DC$ , the cross-sectional compliance  $CC$  and the logarithmic stiffness coefficient  $\alpha$ .

### KEY WORDS:

Arterial wall elasticity, carotid artery, ultrasound

### 1. Introduction

The evaluation of the elasticity of arteries was based on the examination of changes in the transversal dimensions of the vessel which are caused by blood pressure variations. It involves differently defined coefficients which are often applied in references to characterise the elastic properties of arterial walls. E.g., they include:

1) the elastic modulus  $E_p$  as described by PETERSON in 1960 [14]:

$$E_p = \frac{\Delta P}{\Delta D} \frac{Dd}{D}, \quad (1.1)$$

where  $\Delta D/Dd$  is a relative increase in the vessel diameter as a function of the blood pressure growth  $\Delta P$ ;

2) the arterial distensibility coefficient  $DC$  and the cross-sectional compliance  $CC$  as applied in 1986 by RENEMAN *et al.* in carotid wall studies [19, 20]:

$$DC = \frac{2 \Delta D / Dd}{\Delta P}, \quad (1.2)$$

$$CC = \frac{\pi \Delta D Dd}{2 \Delta P}. \quad (1.3)$$

Experimental studies performed on large arterial vessels (the aorta, the carotid artery, and the femoral artery) by BERGEL [3], LOON [9], SIMON [22] and HAYASHI [6] demonstrated that there is a nonlinear dependence between the change in the transversal artery dimensions and that in the blood pressure. This means that the coefficients described by formulae (1.1)–(1.3) depend on the blood pressure, making it difficult to comparatively evaluate the arterial wall elasticity studies performed on their basis.

So far there has been no unambiguous agreement on the form of the analytical dependence between the blood pressure and the change in the transversal arterial dimensions. Most of the functions proposed in the references are empirical in nature. They include the functions described by LOON [9], HAYASHI [6], STETTLER [23], MEISTER [11], LANGEWOUTERST [8] and POWAŁOWSKI [15, 16, 17]. Out of these functions, it is only the one proposed by POWAŁOWSKI that can be determined via noninvasive measurements of systolic and diastolic blood pressures and the maximum and minimum vessel diameters. It has the following form:

$$D^2(P) = Dd^2 \left[ 1 + \frac{1}{\alpha} \ln \frac{P}{Pd} \right], \quad (1.4)$$

where  $\alpha$  is defined as the logarithmic coefficient of arterial wall stiffness, in the following form:

$$\alpha = \frac{Dd^2}{Ds^2 - Dd^2} \ln \left( \frac{Ps}{Pd} \right), \quad (1.5)$$

where  $Ds$  and  $Dd$  are vessel diameters for the systolic pressure  $Ps$  and the diastolic pressure  $Pd$ , respectively.

The coefficient  $\alpha$  proposed by POWAŁOWSKI is an attempt to take into account the effect of the blood pressure on the stiffness coefficient in comparative examinations.

The coefficients described by formulae (1.1)–(1.3) and (1.5) are applied in evaluating the elasticity of arterial walls in noninvasive studies [1, 17, 19, 20]. In these studies, the ultrasonic method is used to determine the maximum and minimum arterial diameters. Cuff-measured systolic and diastolic pressures are subordinated to the above values. As the common carotid arteries are examined, the blood pressure is measured with a cuff on the brachial artery of a patient in a lying position.

The purpose of the work is to examine ultrasonically the dependence between the maximum and minimum diameters of the common carotid artery and the blood pressure in the brachial artery as well as to analyse the coefficients  $E_p$ ,  $DC$ ,  $CC$  and  $\alpha$  for different blood pressures.

## 2. The results of research and discussion

The examinations were carried out on the common carotid arteries of a group of 20 men, aged from 27 to 45. The patients were fighter plane pilots. (The study was performed at the Military Institute of Aviation Medicine in Warsaw).

The examinations were performed using the measuring system, called the Vascular Echo Doppler, elaborated by the present authors. Its block diagram is shown in fig. 1. The equipment consisted of a pulsed ultrasound system tracking displacements of carotid artery walls. The accuracy of arterial wall displacement identification was  $7 \mu\text{m}$ . The internal artery diameter was determined on the basis of digital measurements of the time between selected echo slopes detected from the internal layer of the arterial wall [5, 18].

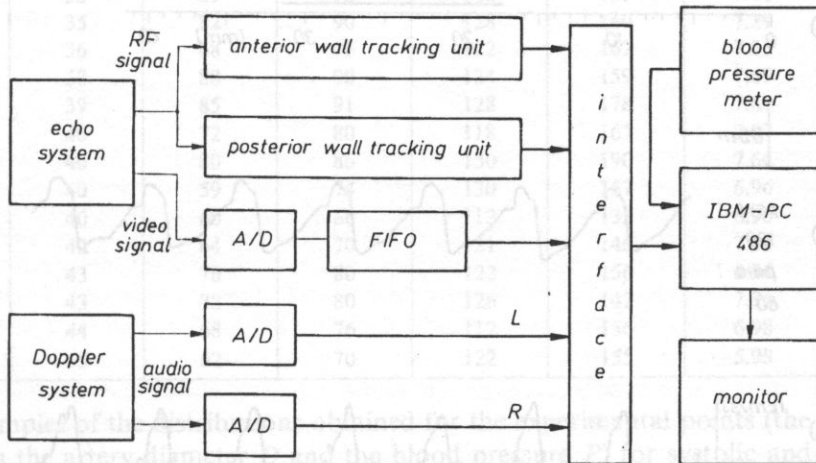


Fig. 1. A block diagram of the measuring system: A/D — an analog-to-digital converter; FIFO — memory (First Input, First Output) applied for collecting echo image data.

The frequency of the transmitted ultrasound was 6.75 MHz. The ultrasound was focused at the 1–3 cm depth from the surface of the skin. The width of the ultrasound beam at the focus was 1 mm (defined for the sound pressure of  $-20$  dB compared with the maximum value on the beam axis). The width of the transmitted pulsed ultrasound was  $0.3 \mu\text{s}$  (2 cycles of a high-frequency transmitter), representing its length of 0.45 mm in tissue. As an effect, it was possible to gain single echoes from the external and internal surfaces of the walls of the common carotid artery under study.

To facilitate the location of the artery under study in the course of the measurements, the pulse probe was mechanically coupled with that of a c.w. Doppler flowmeter. The pulse probe was set perpendicular to the artery, assuming as the measure of perpendicular position the gaining of the maximum amplitude of echoes from the blood vessel walls.

In the course of the evaluation, the measured data were displayed on the screen of an IBM PC connected on-line with an ultrasound system and memorized by this computer (Fig. 2). Along with the ultrasonically measured data, the values of the systolic and diastolic pressures which were cuff-measured were entered into the computer's memory.

The measurements were performed on a lying patient before and after exercise. The exercise examinations were carried out on a cyclometer. Directly following the exercise, the high blood pressure gradually dropped during rest, to reach after 8–10 minutes the pressure measured before the exercise test.

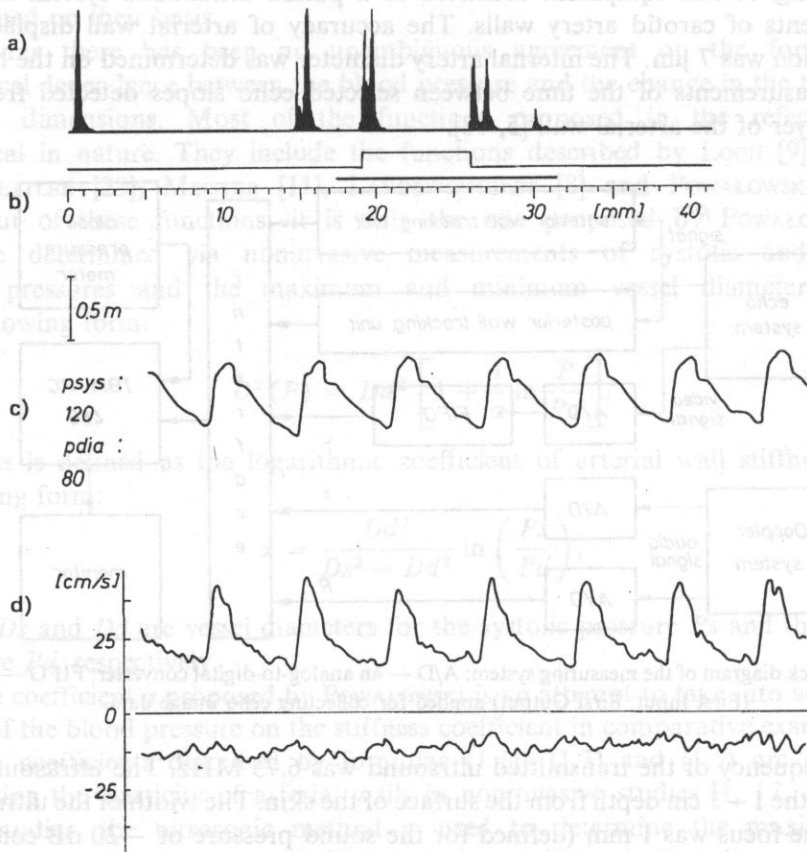


Fig. 2. The data presented in the course of the measurement on the monitor of an IBM PC: a) echoes from the walls of the common carotid artery, b) internal artery diameter, c) artery diameter variations (scale 0.5 mm), d) blood flow velocity; psys and pdia are the systolic and diastolic blood pressures (mm Hg) in the brachial artery.

The pressure was measured every minute. The pressures between the successive measuring points were calculated using linear interpolation. The intervals of systolic and diastolic pressures measured for particular examines are shown in Table 1. Changes in the systolic pressure were greater than those in the diastolic pressure, falling between 14 mmHg and 60 mmHg.

**Table 1.** The results of measurements of the systolic  $P_s$  and the diastolic  $P_d$  brachial blood pressures and the diameter  $D$  of the common carotid arteries in patients:  $R^2$  — the coefficient of determination calculated for the evaluation of the degree of approximation of the results of experimental research using the logarithmic function  $D(P)$  (formula (1.4))  $D \text{ min}_a$  — the mean value of the minimum diameter

No.	Age [years]	$P_d$ [mm Hg]		$P_s$ [mm Hg]		$D \text{ min}_a$ [mm]	$R^2$
		min	max	min	max		
1	27	75	80	125	150	7.59	0.999
2	28	84	90	141	164	6.44	0.997
3	30	69	71	118	146	7.19	0.999
4	32	58	64	128	152	6.35	0.998
5	33	68	78	120	156	6.98	0.997
6	33	60	69	122	136	5.73	0.998
7	35	69	72	118	139	7.60	0.999
8	35	82	90	128	160	7.29	0.999
9	36	68	76	122	162	7.25	0.998
10	38	88	90	134	159	7.69	0.999
11	39	85	91	128	178	7.69	0.999
12	40	72	80	118	167	7.07	0.998
13	40	80	86	130	190	7.64	0.999
14	40	59	74	130	157	6.96	0.993
15	40	60	66	112	133	6.90	0.998
16	42	64	70	121	146	7.01	0.998
17	43	76	80	122	156	6.36	0.998
18	43	78	80	126	142	7.96	0.998
19	44	68	76	112	156	6.98	0.996
20	45	62	70	122	155	5.98	0.998

Examples of the distributions obtained for the experimental points (the relations between the artery diameter  $D$  and the blood pressure  $P$ ) for systolic and diastolic pressures are shown in Fig. 3.

The distribution of the experimental points was described using the logarithmic function  $D(P)$  as obtained from formula (1.4). The coefficient of determination  $R^2$  for the group of the people examined fell within the interval between 0.993 and 0.999 (see Table 1). The scatter of the majority of the experimental points round the theoretical curve fell in the interval of values corresponding to error of roughly  $\pm 14 \mu\text{m}$  as the change in the vascular diameter was measured.

The high coincidence between the results of the studies and the logarithmic function as described by POWAŁOWSKI indicates that the latter function can be adopted as the basis for the evaluation of the elasticity of common carotid arteries performed



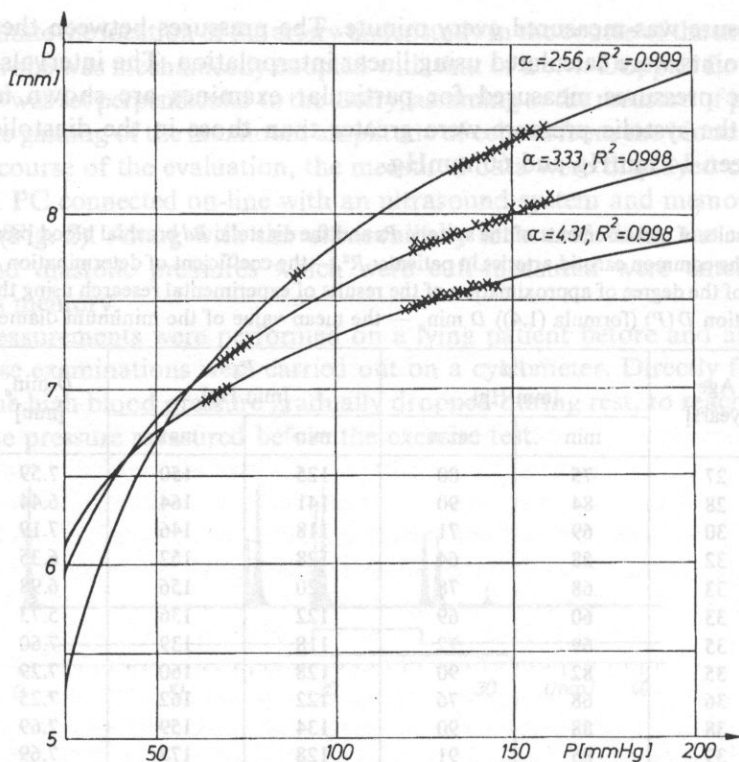


Fig. 3. The results of measurements of the dependence between the diameter  $D$  of the common carotid artery and the blood pressure  $P$  in the brachial artery for three patients numbered 9, 10 and 16 (compare Tables 1 and 2). The maximum and minimum carotid diameters were subordinated respectively to the systolic and diastolic pressures. The solid line represents the logarithmic function  $D(P)$  determined from formula (1.4). The figure shows the mean values of the stiffness coefficients  $\alpha$  (formula (1.5)) calculated for patients as well as the coefficient of determination  $R^2$  calculated for the evaluation of the degree of approximation of the experimental research results as a function of the logarithmic function  $D(P)$ .

on the basis of measurements of the maximum and minimum diameters of the carotid artery and the systolic and diastolic pressures as measured in the brachial artery.

The logarithmic function  $D^2(P)$  is an empirical one, which, as its author [17] showed, corresponds with good accuracy ( $R^2=0.9868$ ) to the results of examinations performed directly in the carotid artery over the pressure range from 25 mmHg to 200 mmHg.

Assuming for the common carotid artery the values of the systolic and diastolic pressures determined in the brachial artery, it is necessary to discuss this type of comparative evaluation. The pressure wave which propagates along the vascular system changes its shape. As Mc DONALD [10] noticed, in moving from the aorta towards the lower-lying peripheral vessels, the systolic pressure is observed to increase as the diastolic and mean pressures drop slightly. There have been, e.g.,

attempts to explain this phenomenon with the effect of summation of the progressive and reflected pressure waves. Thus, the question arises whether a similar phenomenon takes place in the case of vessels in the upper part of the body and what are the possible blood pressure differences between the aorta and the brachial artery. The common carotid artery is very close to the aortic arch, and it can be assumed that the blood pressure difference between these vascular points can be neglected.

In 1955, in examining the blood pressure when using a catheter simultaneously in the brachial artery and the aortic arch, KROEKER [7] observed that for the same heart work cycle the systolic pressure in the brachial artery was 9% greater, and the diastolic pressure was 4% lower than the analogous pressures in the aorta. Some doubts have on the other hand been raised by the fact that when measuring in a similar way the blood pressures in the radial and femoral arteries this author obtained for all of the three arteries almost the same blood pressure differences between them and the aortic arch. Referring, in turn, to the experimental work performed by ARNDT [2], RILEY [21] noted that the pressure difference between the common carotid artery and the brachial artery can be neglected. A very significant argument for this view is provided by the research results presented in 1982 by BOROW [4]. They apply to comparative evaluation between the blood pressure in the brachial artery determined noninvasively by the oscillometric method (the automatic cuff method) and the blood pressure measured using a catheter in the ascending aorta. These studies, carried out on a group of 30 persons aged from 30 to 83 years, indicated that for a lying patient the differences in the systolic and diastolic pressures between the aorta and the brachial artery are 1% and 1.7% (the mean value), respectively, so they can be neglected in practice.

In the light of the research mentioned, it should be said that the method applied for the evaluation of the systolic and diastolic pressures in the common carotid artery as based on measurements of these pressures in the brachial artery should not introduce significant error into the noninvasive examination of the elasticity of the carotid arteries.

On the basis of the studies performed, in keeping with formulae (1.1)–(1.3) and (1.5), the values of the coefficients  $E_p$ ,  $DC$ ,  $CC$  and  $\alpha$  were determined. The mean values of the coefficients and the relative changes in their values are shown in Table 2. These results indicate that the relative changes in the value of the coefficient  $\alpha$  are several times smaller than the changes in the values of the other coefficients. Figs. 4–7 represent the relative (with respect to the mean value) values of particular coefficients as a function of the systolic pressure. They indicate that the value of the coefficient  $\alpha$  does not depend significantly on the systolic pressure but the pressure has a distinct impact on the values of the coefficients  $E_p$ ,  $DC$  and  $CC$ . The coefficient  $E_p$  increases, whereas the coefficients  $DC$  and  $CC$  decrease as a function of the systolic pressure.

The effect of the diastolic pressure on the values of the coefficients under study which describe the elastic properties of arteries is difficult to identify in an experimental way, because the diastolic pressure changes in the patients examined were slight. Assuming as the starting point of discussion the previously considered

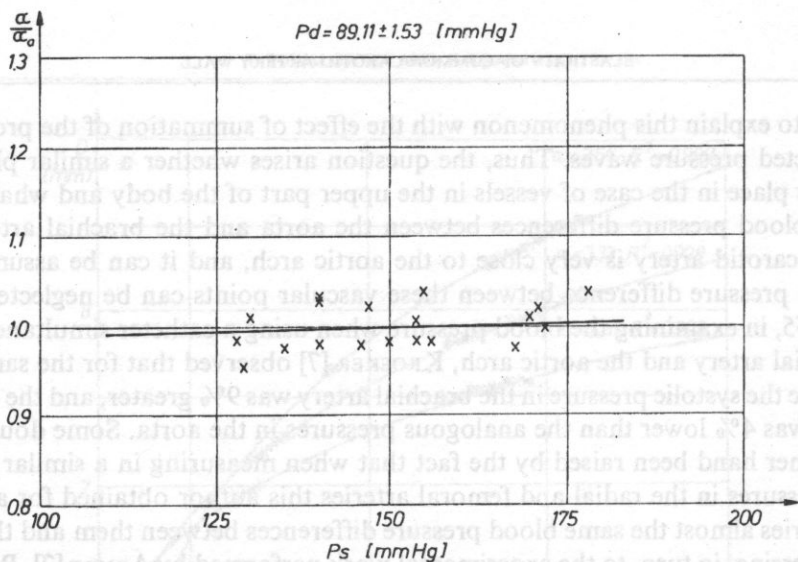


Fig. 4. The relative (with respect to the mean value of  $\alpha_a$ ) value of the logarithmic stiffness coefficient  $\alpha$  as a function of variations in the systolic pressure  $P_s$  as calculated from examinations of a 39-year-old man (no. 11, see Tables 1 and 2). The correlation coefficient is 0.167.

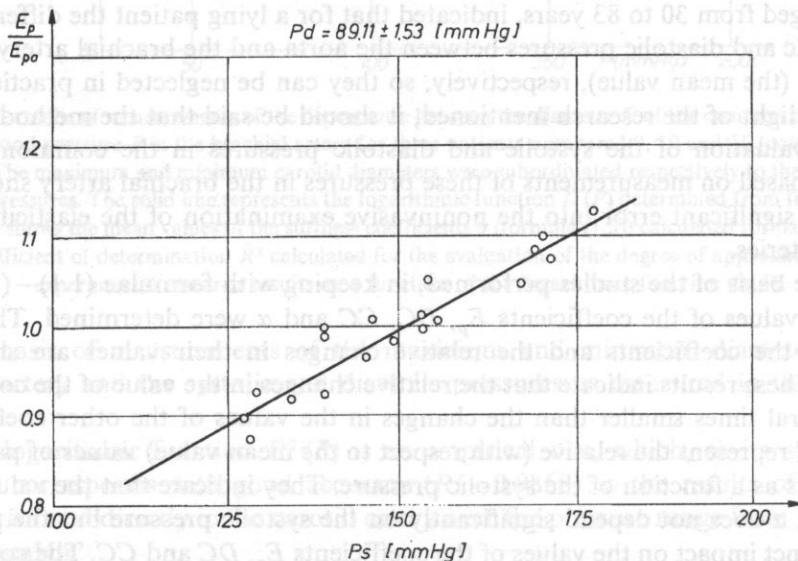


Fig. 5. The relative (with respect to the mean value of  $E_{pa}$ ) value of the elastic module  $E_p$  as a function of variations in the systolic pressure  $P_s$  calculated on the basis of examinations performed on a 39-year-old man (No. 11, see Tables 1 and 2). The correlation coefficient is 0.946.

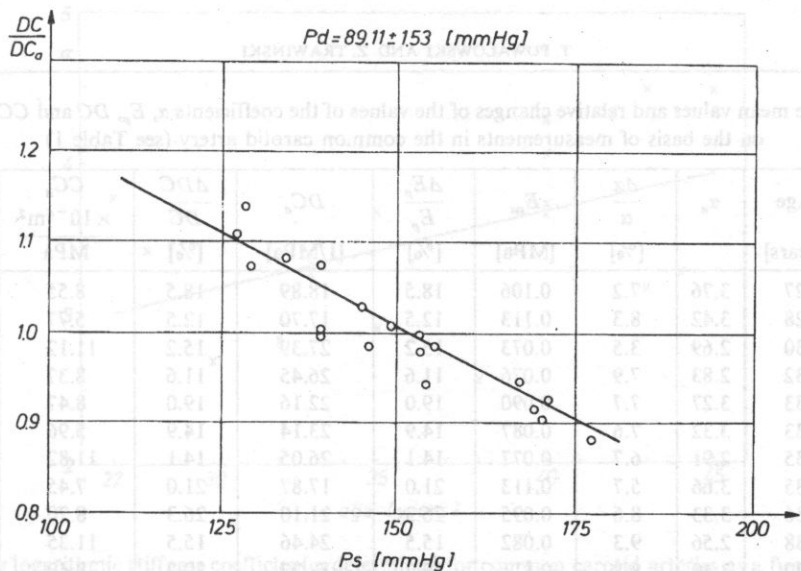


Fig. 6. The relative (with respect to the mean value of  $DC_0$ ) value of the arterial distensibility coefficient  $DC$  as a function of variations in the systolic pressure  $P_s$  calculated from examinations of a 39-year-old man (No. 11, see Tables 1 and 2). The correlation coefficient is  $-0.937$ .

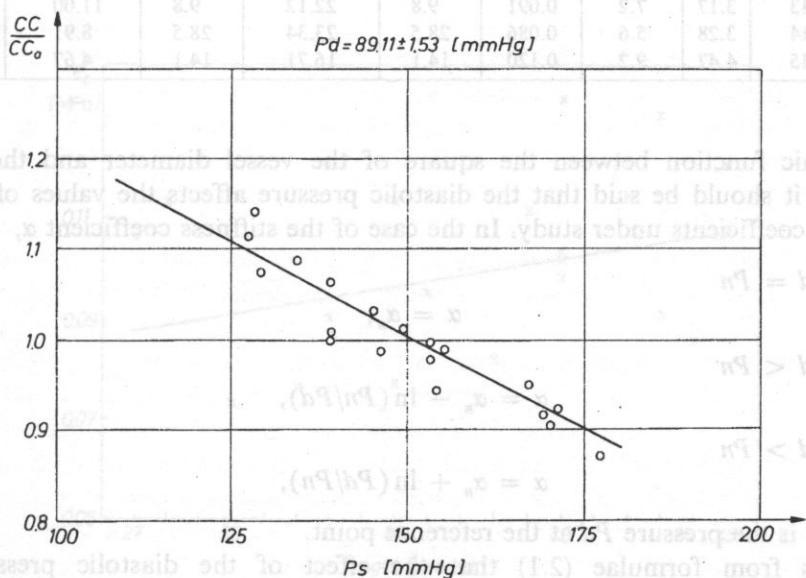


Fig. 7. The relative (with respect to the mean value of  $CC_0$ ) cross-sectional compliance  $CC$  as a function of variations in the systolic pressure  $P_s$  calculated on the basis of examinations performed on a 39-year-old man (No. 11, see Tables 1 and 2). The correlation coefficient is  $-0.944$ .

**Table 2.** The mean values and relative changes of the values of the coefficients  $\alpha$ ,  $E_p$ ,  $DC$  and  $CC$  calculated on the basis of measurements in the common carotid artery (see Table 1)

No.	Age [years]	$\alpha_a$	$\frac{\Delta\alpha}{\alpha}$ [%]	$E_{pa}$ [MPa]	$\frac{\Delta E_p}{E_p}$ [%]	$DC_a$ [1/MPa]	$\frac{\Delta DC}{DC}$ [%]	$CC_a$ $\times 10^{-4} \text{m}^2$ MPa	$\frac{\Delta CC}{CC}$ [%]
1	27	3.76	7.2	0.106	18.5	18.89	18.5	8.55	17.3
2	28	3.42	8.3	0.113	12.5	17.70	12.5	5.77	12.0
3	30	2.69	3.5	0.073	15.2	27.39	15.2	11.12	15.8
4	32	2.83	7.9	0.076	11.6	26.45	11.6	8.37	13.2
5	33	3.27	7.7	0.090	19.0	22.16	19.0	8.47	18.8
6	33	3.32	7.6	0.087	14.9	23.14	14.9	5.96	11.5
7	35	2.91	6.7	0.077	14.1	26.05	14.1	11.82	14.4
8	35	3.66	5.7	0.113	21.0	17.87	21.0	7.45	18.1
9	36	3.33	8.6	0.095	26.3	21.10	26.3	8.70	25.8
10	38	2.56	9.3	0.082	15.5	24.46	15.5	11.35	15.5
11	39	3.40	8.8	0.111	29.2	18.27	29.2	8.49	31.3
12	40	3.66	7.4	0.102	30.6	19.68	30.6	7.72	27.4
13	40	4.27	7.7	0.133	32.6	15.15	32.6	6.93	32.6
14	40	3.71	9.7	0.103	12.3	19.42	12.3	7.40	19.1
15	40	4.05	7.7	0.098	17.6	20.39	17.6	7.63	15.5
16	42	4.31	10.0	0.114	18.6	17.60	18.6	6.80	20.5
17	43	4.48	9.3	0.130	15.4	15.44	15.4	4.90	16.7
18	43	3.17	7.2	0.091	9.8	22.12	9.8	11.00	10.9
19	44	3.28	5.6	0.086	28.5	23.34	28.5	8.91	23.5
20	45	4.47	9.2	0.120	14.1	16.71	14.1	4.67	16.4

logarithmic function between the square of the vessel diameter and the blood pressure, it should be said that the diastolic pressure affects the values of all the elasticity coefficients under study. In the case of the stiffness coefficient  $\alpha$ ,

$$\text{for } Pd = Pn$$

$$\alpha = \alpha_n, \quad (2.1)_1$$

$$\text{for } Pd < Pn$$

$$\alpha = \alpha_n - \ln(Pn/Pd), \quad (2.1)_2$$

$$\text{for } Pd > Pn$$

$$\alpha = \alpha_n + \ln(Pd/Pn), \quad (2.1)_3$$

where  $Pn$  is the pressure  $Pd$  at the reference point.

It results from formulae (2.1) that the effect of the diastolic pressure on the value of the coefficient grows smaller when the value of the coefficient  $\alpha$  increases.

The evaluation of the effect of the blood pressure on the values of the particular elasticity coefficients is significant in comparative studies. An example of such studies in the references is the search for a correlation between the arterial elasticity and the age of patients [1, 12, 13, 17, 19, 20].

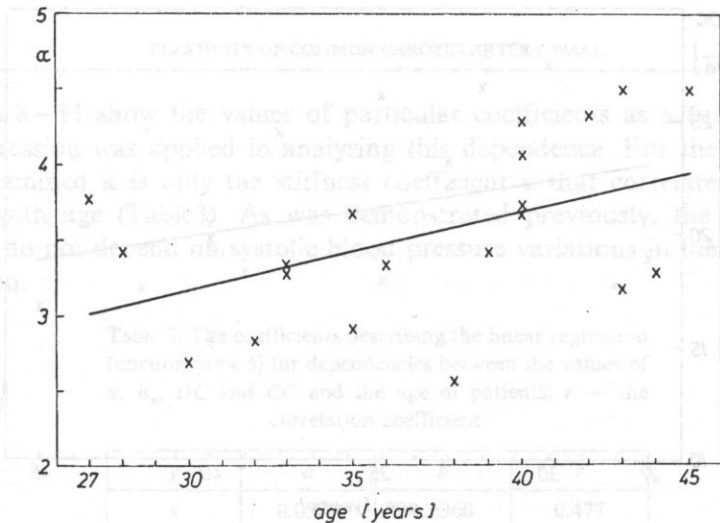


Fig. 8. The logarithmic stiffness coefficient  $\alpha$  determined for common carotid arteries as a function of the age of patients. The solid line represents the linear regression function (Table 3).

### 3. Conclusions

It is difficult to verify the noninvasive method for the evaluation of the elasticity of common carotid arteries because of the many factors which affect the ultimate result of measurements of the elasticity coefficients. They include: a) the function between the blood pressure and a change in the transversal cross-sections of the common carotid artery; b) the relation between the systolic and diastolic pressures in the common carotid artery and the brachial artery; c) the accuracy of the brachial blood pressure measurement using cuff; d) the accuracy of acoustic artery diameter measurements using ultrasound. Instead of an analysis of particularly factors the authors proposed a comprehensive approach. It consisted in ultrasonic measurements of the diameter of the common carotid artery for different blood pressures and in investigating the relation between the diameter of the common carotid artery and the blood pressure measured in the brachial artery.

The results of the measurements and calculations indicate that:

- 1) The distribution of points; the artery diameter - the blood pressure could be represented with high accuracy by the proposed logarithmic function described by formula (1.4). The scatter of data points around the theoretical curve fell in the range of 0.001 to 0.002 between  $R^2 = 0.93$  and  $0.999$  (Table 1). The scatter of most experimental points around the theoretical curve fell in the range of 0.001 to 0.002 between  $R^2 = 0.93$  and  $0.999$  (Table 1).

Fig. 9. The elastic modulus  $E_p$  determined for common carotid arteries as a function of the age of patients. The solid line represents the linear regression function (Table 3).

- 2) The effect of the systolic pressure on the value of the logarithmic stiffness coefficient  $\alpha$  (formula (1.5)) can be neglected. The calculations were carried out for a group of 20 persons for whom the systolic pressures fell between 112 mmHg and 190 mmHg, and the systolic pressure variations came between 14 mmHg and

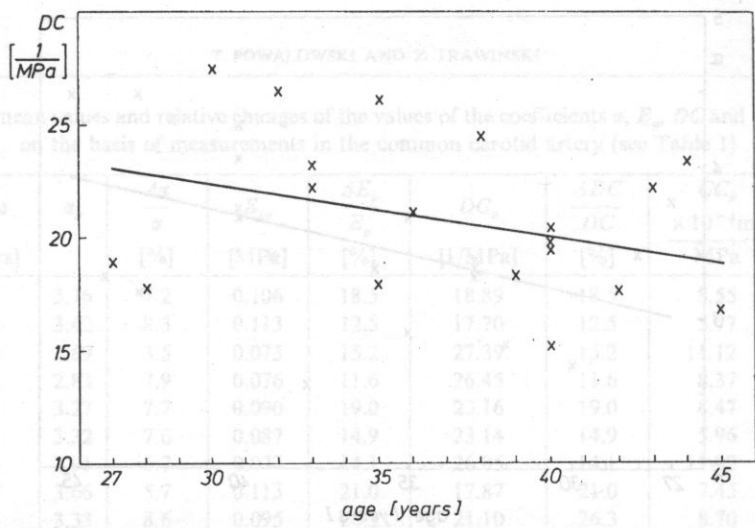


Fig. 10. The arterial distensibility coefficient  $DC$  determined for common carotid arteries as a function of the age of patients. The solid line represents the linear regression function (Table 3).

No.	Age (years)	$P_d$ (Pa)	$P_s$ (MPa)	$P_m$ (Pa)	$DC$ (1/MPa)	$DC$ (1/MPa)	$CC$ ( $\times 10^{-4} m^2/MPa$ )	$CC$ (%)
1	27	2.7	0.106	18.5	18.59	18.5	17.3	17.3
2	28	2.8	0.113	13.5	17.70	12.5	12.0	12.0
3	30	3.0	0.073	15.3	27.39	13.2	15.8	15.8
4	32	2.8	0.076	11.6	26.43	11.6	13.2	13.2
5	33	3.2	0.090	19.0	23.16	19.0	16.8	16.8
6	33	3.3	0.087	14.9	23.18	14.9	11.5	11.5
7	35	3.5	0.113	17.7	21.0	17.7	14.4	14.4
8	35	3.5	0.095	19.0	26.3	19.0	18.1	18.1
9	36	3.3	0.095	19.0	26.3	19.0	25.8	25.8
10	36	3.3	0.095	19.0	26.3	19.0	18.1	18.1
11	37	3.7	0.113	17.7	21.0	17.7	17.4	17.4
12	37	3.7	0.113	17.7	21.0	17.7	32.6	32.6
13	40	4.0	0.133	32.6	15.15	32.6	6.93	32.6
14	40	3.71	0.103	13.3	19.4	13.3	2.40	19.4
15	40	4.05	0.092	17.6	20.59	17.6	7.63	15.3
16	42	4.31	0.114	18.6	17.90	18.6	6.80	26.5
17	43	4.42	0.130	15.4	15.44	15.4	4.90	16.7
18	43	3.17	0.091	9.8	23.12	9.8	1.00	10.9
19	44	3.28	0.086	28.3	21.34	28.3	2.51	23.5
20	45	4.5	0.120	14.4	14.4	14.4	16.4	16.4

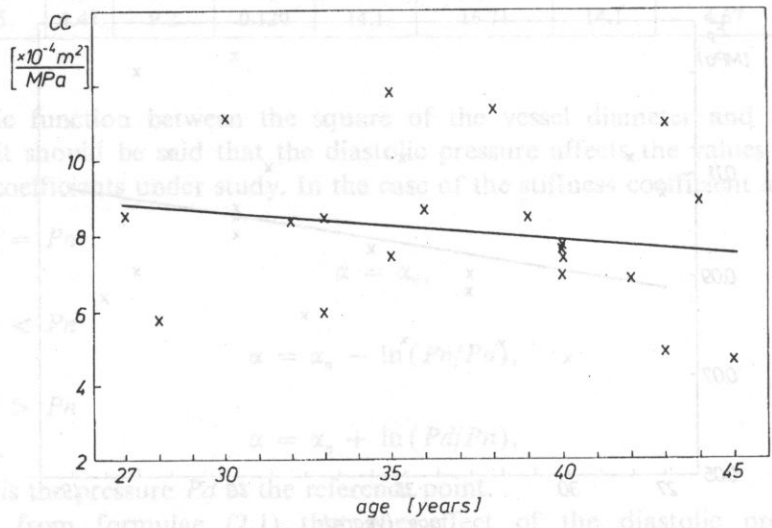


Fig. 11. The cross-sectional compliance  $CC$  determined for common carotid arteries as a function of the age of patients. The solid line represents the linear regression function (Table 3).

logarithmic function between the square of the vessel diameter and the blood pressure, it may be said that the diastolic pressure affects the values of all the elasticity coefficients under study. In the case of the stiffness coefficient  $DC$  for  $P_d = P_s$  (2.1), for  $P_d < P_s$  (2.1),  $\alpha = \alpha_0 - \ln(P_d/P_s)$ , (2.1), for  $P_d > P_s$  (2.1),  $\alpha = \alpha_0 + \ln(P_d/P_s)$ , (2.1), where  $P_d$  is the pressure  $P_d$  at the reference point of the diastolic pressure on It results from formulae (2.1) the effect of the diastolic pressure on

The evaluation of the effect of the blood pressure on the values of the particular elasticity coefficients is significant in comparative studies. An example of such studies in the references is the search for a correlation between the arterial elasticity and the age of patients [1, 12, 13, 17, 19, 20].

Figures 8–11 show the values of particular coefficients as a function of age. Linear regression was applied in analysing this dependence. For the group of the persons examined it is only the stiffness coefficient  $\alpha$  that correlates significantly ( $p < 0.05$ ) with age (Table 3). As was demonstrated previously, the value of this coefficient do not depend on systolic blood pressure variations in the course of the examination.

**Table 3.** The coefficients describing the linear regression function ( $ax+b$ ) for dependencies between the values of  $\alpha$ ,  $E_p$ ,  $DC$  and  $CC$  and the age of patients;  $r$  — the correlation coefficient

$y$	$a$	$b$	$r$
$\alpha$	0.0509	1.6360	0.477
$E_p$	0.0011	0.0579	0.347
$DC$	-0.2360	29.4335	-0.348
$CC$	-0.0730	10.8113	-0.191

### 3. Conclusions

It is difficult to verify the noninvasive method for the evaluation of the elasticity of common carotid arteries because of the many factors which affect the ultimate result of measurements of the elasticity coefficients. They include: a) the function between the blood pressure and a change in the transversal dimensions of the common carotid artery; b) the relation between the systolic and diastolic pressures in the common carotid artery and the brachial artery; c) the accuracy of the brachial blood pressure measurement using cuff; d) the accuracy of acrotid artery diameter measurements using ultrasound. Instead of an analysis of particular factors the authors proposed a comprehensive evaluation. It consisted in ultrasonic measurements of the diameter of the common carotid artery for different blood pressures and in investigating the relation between the diameter of the common carotid artery and the blood pressure measured in the brachial artery.

The results of the measurements and calculations indicate that;

1) The distribution of points: the artery diameter - the blood pressure could be represented with high accuracy by the proposed logarithmic function described by formula (1.4). The coefficient of determination  $R^2$  varied between 0.993 and 0.999 (Table 1). The scatter of most experimental points round the theoretical curve fell in the interval of values corresponding to an error of roughly  $\pm 14 \mu\text{m}$  in the measurement of vessel diameter changes.

2) The effect of the systolic pressure on the value of the logarithmic stiffness coefficient  $\alpha$  (formula (1.5)) can be neglected. The calculations were carried out for a group of 20 persons for whom the systolic pressures fell between 112 mmHg and 190 mmHg, and the systolic pressure variations came between 14 mmHg and



60 mmHg (Table 1). The relative changes in the value of the coefficient  $\alpha$  as a function of the systolic pressure in patients never exceeded 10% (Table 2 and fig. 4).

3) The logarithmic stiffness coefficient  $\alpha$  is a more objective indicator of the mechanical properties of the wall of the common carotid artery than the parameters used so far, including the elastic modulus  $E_p$ , the arterial distensibility coefficient  $DC$  or the compliance  $CC$ . Its value does not change significantly as a function of the systolic pressure when the value of the coefficient  $E_p$  grows as a function of the systolic pressure and the values of the coefficients  $DC$  and  $CC$  decrease as a function of that pressure (Figs. 4–7). The relative changes in the values of the coefficients  $E_p$ ,  $DC$  and  $CC$  as a function of variations in the systolic pressure were from 1.2 to 5.1 times larger than the changes of the value of the logarithmic stiffness coefficient  $\alpha$ .

### References

- [1] G. ACARO, S. LAURENT, G. JONDEAU, A.P. HOEKS, M.E. SAFAR, *Stiffness of the common carotid artery in treated hypertensive patients*, Journal of Hypertension, **9**, 947–954 (1991).
- [2] J.O. ARNDT, J. KLAUSKE, I. MERSCH, *The diameter of the intact carotid artery in man and its change with pulse pressure*, Pflügers Arch. ges. Physiol., **301**, 230–240 (1968).
- [3] D.H. BERGEL, *The static elastic properties of the arterial wall*, J. Physiol., **156**, 445–457 (1961).
- [4] K.M. BOROW, J.W. NEWBURGER, *Noninvasive estimation of central aortic pressure using the oscillometric method for analyzing systemic artery pulsatile blood flow: Comparative study of indirect systolic, diastolic and mean brachial artery pressure with simultaneous direct ascending aortic pressure measurements*, Amer. Heart J. **103**, 879–886 (1982).
- [5] D.H. GROVES, T. POWALOWSKI, D.H. WHITE, *A digital technique for tracking moving interfaces*, Ultrasound in Med. and Biol., **8**, 2, 185–190 (1982).
- [6] K. HAYASHI, H. HANDA, S. NAGASAWA, A. OKUMURA, K. MORITAKE, *Stiffness and elastic behaviour of human intracranial and extracranial arteries*, J. Biomechanics, **13**, 2, 175–184 (1980).
- [7] E.J. KROEKER, E.H. WOOD, *Comparison of simultaneously record central and peripheral arterial pressure pulses during rest, exercise and tilted position in man*, Circulation Research, vol. III, 1955.
- [8] G.J. LANGEWOUTERS, K.H. WESSELING, W.J. GOEDHARD, *The static elastic properties of 45 human thoracic and 20 abdominal aortas in vitro and the parameters of a new model*, J. of Biomechanics, **17**, 6, 425–435 (1984).
- [9] P. LOON, W. KLIP, E. BRADLEY, *Length-force and volume-pressure relationships of arteries*, Biomechanics, **14**, 181–201 (1977).
- [10] D.A. Mc DONALD, *Blood flow in arteries*, Edward Arnold Ltd., London, 1960.
- [11] J.J. MEISTER, *Mesure par echographie doppler et modelisation theorique de leffet de troubles cardiaques sur la pression et le debit arteriels*, Thesis, EPFL, Lausanne, 1983.
- [12] T. VAN MERODE, P.J.J. HICK, A.P.G. HOEKS, K.H. RAHN, R.S. RENEMAN, *Carotid artery wall properties in normotensive and borderline hypertensive subjects of various ages*. Ultrasound in Med. & Biol., **14**, 7, 563–569 (1988).
- [13] T. VAN MERODE, P.J.J. HICK, A.P.G. HOEKS, F.A.M. SMEETS and R.S. RENEMAN, *Differences in carotid artery wall properties between presumed-healthy men and women*, Ultrasound in Med. and Biol. **14**, 7, 571–574 (1988).
- [14] L. PETERSON, R. JENSEN, J. PARNEL, *Mechanical properties of arteries in vivo*, Circulation Res., **8**, 622–639 (1960).

- [15] T. POWALOWSKI, B. PEŃSKO, *Noninvasive ultrasonic method of pressure and flow measurements for estimation of hemodynamical properties of cerebrovascular system*, Archives of Acoustics, **10**, 3, 303–314 (1985).
- [16] T. POWALOWSKI, B. PEŃSKO, *Elasticite d'artere carotide de sujets normaux et pathologiques*, Colloque sur les Ultra-sons et Acoustique Physique, 63–73, Paris 1987.
- [17] T. POWALOWSKI, B. PEŃSKO, *A noninvasive ultrasonic method for the elasticity evaluation of the carotid arteries and its application in the diagnosis of the cerebro-vascular system*, Archives of Acoustics, **13**, 1–2, 109–126 (1988).
- [18] T. POWALOWSKI, *Ultrasonic system for noninvasive measurement of hemodynamic parameters of human arterial-vascular system*, Archives of Acoustics, **13**, 1–2, 89–108 (1988).
- [19] R.S. RENEMAN, T. VAN MERODE, P. HICK, A.P.G. HOEKS, *Cardiovascular Applications of Multi-Gate Pulsed Doppler Systems*, Ultrasound in Med. & Biol. **5**, 1, 357–370 (1986).
- [20] R. RENEMAN, t. MERODE, P. HICK, A. MUYTJENS, A. HOEKS, *Age related changes in carotid artery wall properties in men*, Ultrasound in Med. and Biol., **12**, 6, 465–471 (1986).
- [21] W.A. RILEY, R.W. BARNES, H.M. SCHEY, *An approach to the noninvasive periodic assessment of arterial elasticity in the young*, Preventive Medicine **13**, 169–184 (1984).
- [22] B. SIMON, A. KOBAYASHI, D. STRANDNESS, C. WIEDERHIELM, *Large deformation analysis of the arterial cross section*, J. of Basic Eng. 93D, 2 (1971).
- [23] J. STETTLER, P. NIEDERER, M. ANLIKER, *Theoretical analysis of arterial hemodynamics including the influence of bifurcations*, Annals of Biomedical Engineering, **9**, 145–164 (1981).

## 1 Introduction

The design principles of transducers with matching layers was described in the previous paper [5]. In this work the influence of electrical parameters: compensating inductances, a coaxial cable, wire connectors, a parallel resistance and input impedances of a transmitter and a receiver on the reflected pulse is discussed.

Calculations are carried out, modified Mason's model described in [4] being assumed (Fig. 1). Because in this paper only the PZT ceramic transducers are discussed, the mechanical and dielectrical losses can be neglected. All quantities are relative (dimensionless).

• frequency  $x = \pi f / f_0$

• mechanical impedance of the investigated medium  $R_0 = R_0 / R_0$

• mechanical impedances of the matching layers  $R_{01} = R_1 / R_0$

$R_{02} = R_2 / R_0$

## INFLUENCE OF THE ELECTRICAL PARAMETERS ON THE ULTRASONIC PROBE IMPEDANCE AND THE REFLECTED PULSES

G. ŁYPACEWICZ

Ultrasonic Department, Institute of Fundamental Technological  
Research, Polish Academy of Sciences  
(00-049 Warszawa, Świętokrzyska 21)

Basing on the modified Mason's equivalent circuit of an ultrasonic transmitting-receiving probe [3], [4] the influence of compensating inductances, a coaxial cable, wire conductors and parallel resistance on the probe impedance and the reflected pulses is discussed.

The influence of the wire conductors connecting a transducer with a coil or a coaxial connector for large diameters (i.e. 20 mm) and high frequencies (i.e. 10 MHz) on the probe impedance should be taken into account.

The influence of the coaxial cable on the probe impedance and the reflected pulses depends on the electrical impedance of a probe.

The compensating circuit containing three inductances — two in series and one parallel is discussed.

The influence of the parallel resistance on the reflected pulse is shown and compared with the influence of transducer backing.

It was shown that the length of transmitting burst should be chosen depending on the frequency band-width of the probe.

### 1. Introduction

The design principles of transducers with matching layers was described in the previous paper [5]. In this work the influence of electrical parameters: compensating inductances, a coaxial cable, wire connectors, a parallel resistance and input impedances of a transmitter and a receiver on the reflected pulse is discussed.

Calculations are carried out, modified Mason's model described in [4] being assumed (Fig. 1). Because in this paper only the PZT ceramic transducers are discussed, the mechanical and dielectrical losses can be neglected. All quantities are **relative** (dimensionless).

- frequency  $x = \Pi f / f_m$ ,
- mechanical impedance of the investigated medium  $R_b = R_B / R_p$ ,
- mechanical impedances of the matching layers  $R_{01} = R_1 / R_p$ ,  
 $R_{02} = R_2 / R_p$ ,

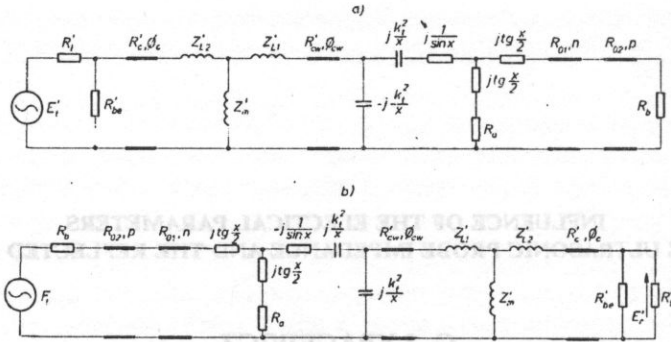


Fig. 1. Equivalent circuit of the transmitting (a) and receiving (b) probe circuit (parameters described in the paper).

- electrical impedance of the transmitter  $R_t' = R_t / Z_E$ ,
- electrical impedance of the receiver  $R_r' = R_r / Z_E$ ,
- characteristic resistances of the cables:
  - $R_c' = R_c / Z_E$  (coaxial cable),
  - $R_{cw}' = R_{cw} / Z_E$  (wire connectors),
- impedance of the parallel resistance  $R_{be}' = R_{be} / Z_E$ ,
- reactance of the inductances  $Z_m' = k_x^2 x / \Pi^2 m^2$  (parallel)
  - $Z_{L1}' = k_x^2 x L_1^2 / \Pi^2$
  - $Z_{L2}' = k_x^2 x L_2^2 / \Pi^2$  (in series),
- thickness of the matching layers  $n = d_{01} / \lambda_{e01}$ ,  
 $p = d_{02} / \lambda_{e02}$ ,
- length of the cables  $\Phi_{cw} = l_{cw} / \lambda_{et}$ ,  
 $\Phi_c = l_c / \lambda_{et}$
- voltage of the transmitter output  $E_t' = E_t / N$ ,
- amplitude of the pulse reflected from an ideal reflector  
 $E_r' = E_r / E_t$ ,
- mechanical force in the investigated medium  $F_t$ ,
- transmitting-receiving transfer function  $H$  (assuming the pulse reflection from the ideal reflector).

Here:

$Z_E = 1 / \text{Real}[Y_p(f_e)]$  — the electrical probe impedance.

$N^2 = 2k^2 f_m C_0 R_p$  — turns ratio of the electromechanical transformer  $E_t$  — voltage of the transmitter (on the electrical side of the electromechanical transformer),  $f_m$  — mechanical resonance frequency,  $f_e$  — electrical resonance frequency (for  $f_e$  the imaginary part of mechanical impedance of a loaded transducer is equal to 0 [4]),  $A$  — transducer area,  $R_p = A\rho_p c_p$ ,  $R_B = A\rho_b c_b$ ,  $R_A = A\rho_a c_a$ ,  $R_{01} = A\rho_{01} c_{01}$ ,  $R_{02} = A\rho_{02} c_{02}$  — mechanical impedances of the transducer, investigated medium, back loading and two matching layers, respectively,  $\lambda_{e01}$ ,  $\lambda_{e02}$  — acoustic wavelengths in the matching layers,  $d_{01}$ ,  $d_{02}$  — thickness of the matching layers,  $C_0$  — clamped capacitance of the transducer,  $m$ ,  $L_1$ ,  $L_2$  — parameters of inductances:

parallel and in series,  $k_t$  — electromechanical coupling coefficient for the thickness vibration,  $Y_p(f_e)$  — electrical admittance of the probe (without inductances and cables),  $R_{cw}$ ,  $R_c$  — characteristic resistances of the wire connectors and the coaxial cable,  $R_{be}$  — parallel resistance,  $\lambda_{emcw}$ ,  $\lambda_{emc}$  — electromagnetic wavelengths in the wire connectors and in the coaxial cable,  $l_{cw}$ ,  $l_c$  — length of the wire connectors and the coaxial cable.

As one can see all quantities describing the probe are dimensionless — the frequency is related to mechanical resonance frequency, the mechanical impedances are related to the transducer mechanical impedance, the electrical impedances are related to the electrical impedance of the probe for the electrical resonance frequency (calculated for the probe without cables and inductances), the thicknesses of matching layers are related to the acoustical wavelength, the lengths of cables are related to the electromagnetic wavelength and the reflected pulse amplitude is related to the transmitting pulse amplitude.

## 2. Coaxial cable, wire connectors

For the ultrasonic medical diagnosis transducers of 3–50 mm diameter operating at 2–20 MHz are used. The probe impedance (defined as  $Z_E = 1/\text{Real}[Y_p(f_e)]$ ) depends on the transducer dimensions (the thickness and the diameter), on the piezoelectric material parameters (see Table 1), on the acoustic load of the transducer (an investigated medium, a back loading, matching layers) (Figs. 2, 3) and on the compensating circuit (see Sec. 3).

Table 1.

Piezoelectric material	Density $\times 10^3 \text{kg/m}^3$	Acoustic impedance $\times 10^6 \text{kg/m}^2 \text{s}$	Relative dielectric constant $\epsilon_r$	Electromech. coupling coefficient $k_t$
quartz	2.65	15.1	4.6	0.09
PZT 5A	7.75	33.7	830	0.49
BaTiO <sub>3</sub>	5.7	31.2	1260	0.38
LiNbO <sub>3</sub>	4.65	34.2	30	0.49

Ultrasonic probes for the medical diagnostic application are made usually of the PZT material. As it is shown in Fig. 3, electrical impedances of the probe of a large diameter and a high frequency are equal to single ohms. In these cases, although the cable length is much smaller than the electromagnetic wavelength the influence of the cable on the impedance and transfer function of transmitting-receiving circuit is great, and therefore the cable should be taken into account and be treated as a long line.

Let us consider the influence of the cable, at different ratios of the cable characteristic resistance to the probe electrical impedance  $Z_E$ , on the probe admit-

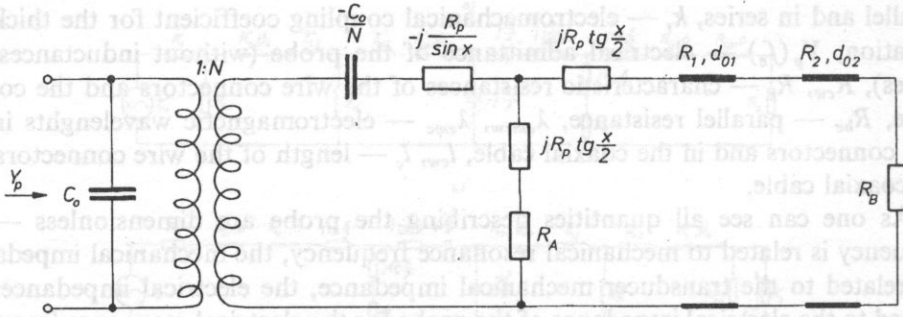


Fig. 2 Equivalent circuit of a transducer loaded acoustically through matching layers with an investigated medium impedance  $R_B = A\rho_b c_b$  and with a back load  $R_A = A\rho_a c_a$ .

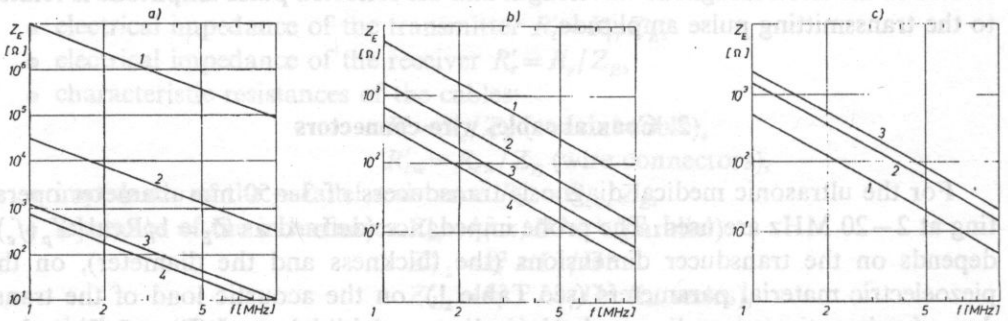


Fig. 3 Electric impedances  $Z_E$  of piezoelectric transducers calculated according to a circuit in Fig. 2 in the frequency function  $\rho_b c_b = 1.5 \cdot 10^6 \text{ kg/m}^2\text{s}$ ,  $\rho_a c_a = 3.2 \cdot 10^6 \text{ kg/m}^2\text{s}$ , a transducer piezoelectric material — PZT 5A (excluding 3a), a transducer diameter equal to 10 mm (excluding 3b), one matching layer —  $d_{01} = \lambda_{e01}/4$ ,  $\rho_{01} c_{01}$  (and  $\rho_{02} c_{02}$  — in Fig. 3c) calculated according DeSilets formula

- a — different piezoelectric materials: 1 — quartz, 2 —  $\text{LiNbO}_3$ , 3 —  $\text{BaTiO}_3$ , 4 — PZT 5A
- b — different transducer diameters: 1 — 5 mm, 2 — 10 mm, 3 — 15 mm, 4 — 20 mm
- c — a different number of layers: 1 — without a layer, 2 — one layer, 3 — two layers

tance characteristics and on the reflected pulses. To neglect the influence of other probe parameters, the length of the cable, the PZT material, one matching layer calculated according DeSILETS [7], the back loading, the parallel inductance compensating a clamped capacitance  $C_0$ , are assumed to be the same.

In Fig. 4 the influence of the length of short ( $\Phi_c = 0.02$  or  $0.05$ ) cables matched to the probe impedance ( $R'_c = 1$ ) on the circuit parameters is shown. As one can see, changes of admittances, transfer functions and reflected pulses in comparison with the values for a probe without a cable can be neglected, although for a longer cable ( $\Phi_c = 0.05$  corresponds, for example, to a 3 m cable for 5 MHz or 1.5 MHz for 10 MHz) the changes of the admittance and the transfer function are noticeable.

If the probe impedance is large (i.e.  $R'_c = 0.05$ ) the cable can be treated as a capacitance and should be compensated by a parallel inductance larger than for a probe without a cable (Fig. 5). Comparing the results for such a compensated

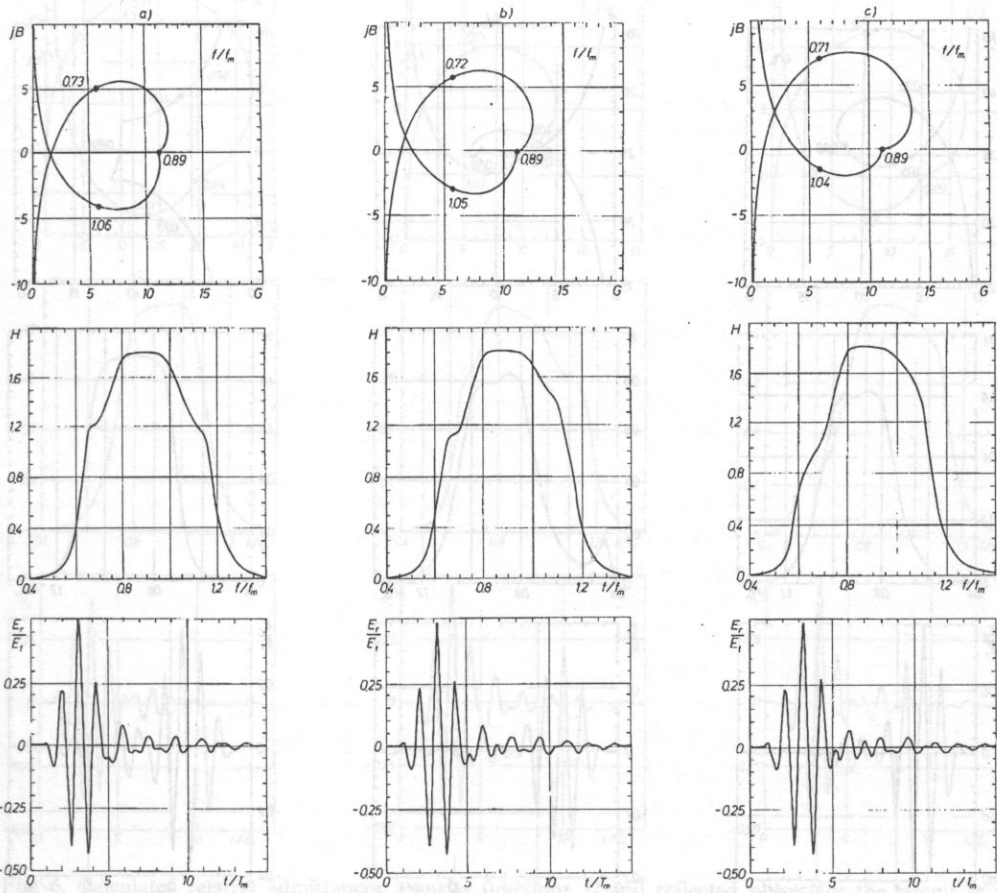


Fig. 4. Calculated relative admittances for PZT transducers radiated into water ( $k_t=0.5$ ,  $R_b=0.044$ ) through a matching layer ( $R_{o1}=0.125$ ,  $n=0.25$ ), without a back load ( $R_a=0$ ), with a parallel inductance ( $m=0.865$ ), their transfer functions  $H$  and reflected pulses ( $R'_t=0.01$ ,  $R'_r=10$ , a transmitting pulse is a half-period of sine of 0.89 frequency)

a — without a cable

with cables matched to the probe impedance ( $R'_c=1$ ) of a different length: b —  $\Phi_c=0.02$ , c —  $\Phi_c=0.05$ .

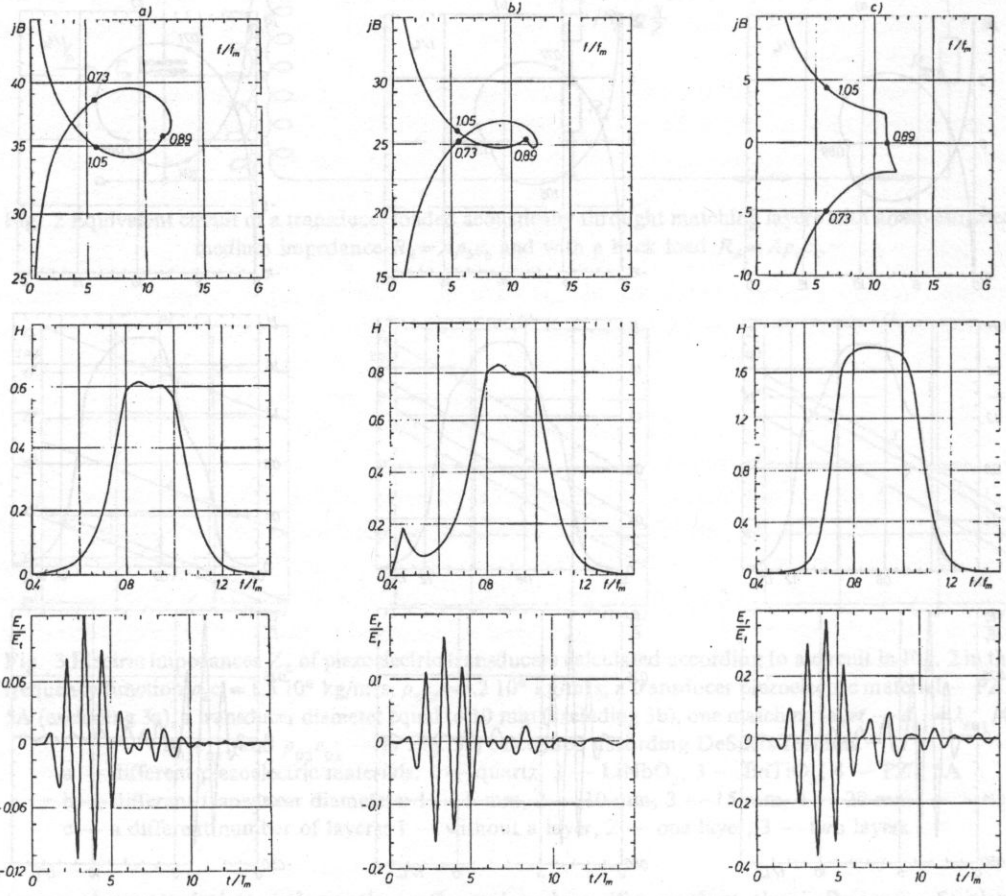


Fig. 5. Calculated relative admittances, transfer functions  $H$  and reflected pulses for the circuit as in Fig. 4, with a cable of a characteristic resistance less than a probe impedance ( $\Phi_c=0.02$ ,  $R'_c=0.05$ ) with different parallel inductances: a -  $m=0$  (without a coil), b -  $m=0.865$ , c -  $m=1.59$ .

In Fig. 4 the influence of the length of short ( $\Phi_c = 0.02$ ) on the change of admittances, transfer functions and reflected pulses at computation with the values for a probe without a cable can be neglected, although for a longer cable ( $\Phi_c = 0.05$  corresponds, for example, to a 3 m cable for 5 MHz or 1.5 MHz for 10 MHz) the changes of the admittances and the transfer functions are noticeable.

If the probe impedance is large (i.e.,  $R'_c=0.05$ ) the cable can be treated as a capacitance and should be compensated by a parallel inductance larger than for a probe without a cable (Fig. 5). Comparing the results for such a compensated



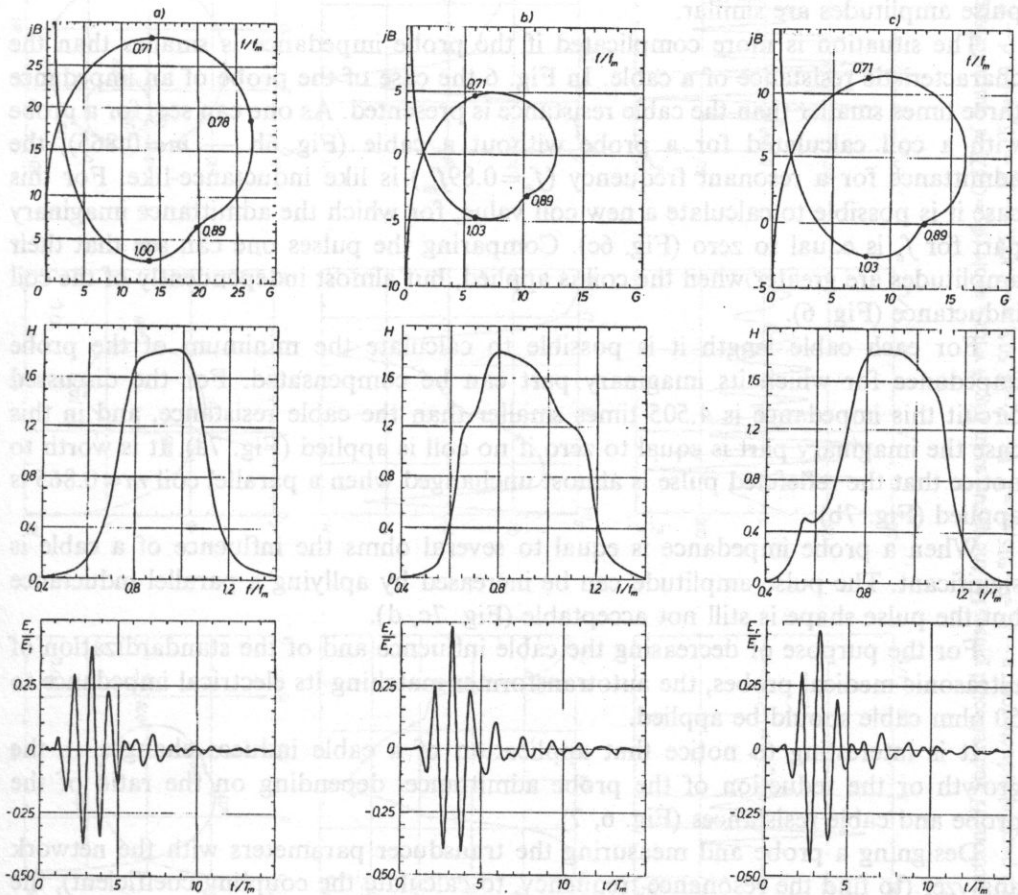


Fig. 6. Calculated relative admittances, transfer functions  $H$  and reflected pulses for the circuit as in Fig. 4, with a cable of a characteristic resistance greater than a probe impedance ( $\Phi_c = 0.02$ ,  $R'_c = 3$ ) with different parallel inductances: a —  $m = 0$  (without a coil), b —  $m = 0.865$ , c —  $m = 0.689$ .

probe with the results for a probe without any cable (Figs. 5c and 4a), one can see noticeable differences in admittances, transfer functions and pulse shapes, but the pulse amplitudes are similar.

The situation is more complicated if the probe impedance is smaller than the characteristic resistance of a cable. In Fig. 6 the case of the probe of an impedance three times smaller than the cable resistance is presented. As one can see, for a probe with a coil calculated for a probe without a cable (Fig. 6b —  $m=0.865$ ), the admittance for a resonant frequency ( $f_e=0.89f_m$ ) is like inductance-like. For this case it is possible to calculate a new coil value, for which the admittance imaginary part for  $f_e$  is equal to zero (Fig. 6c). Comparing the pulses one can see that their amplitudes are greater when the coil is applied, but almost independently of the coil inductance (Fig. 6).

For each cable length it is possible to calculate the minimum of the probe impedance for which its imaginary part can be compensated. For the discussed circuit this impedance is 4.505 times smaller than the cable resistance, and in this case the imaginary part is equal to zero if no coil is applied (Fig. 7a). It is worth to notice that the reflected pulse is almost unchanged when a parallel coil  $m=0.865$  is applied (Fig. 7b).

When a probe impedance is equal to several ohms the influence of a cable is significant. The pulse amplitude can be increased by applying a parallel inductance but the pulse shape is still not acceptable (Fig. 7c, d).

For the purpose of decreasing the cable influence and of the standardization of ultrasonic medical probes, the autotransformer matching its electrical impedance to 50 ohm cable should be applied.

It is interesting to notice that application of a cable induces changes — the growth or the reduction of the probe admittance, depending on the ratio of the probe and cable resistances (Fig. 6, 7).

Designing a probe and measuring the transducer parameters with the network analyzer (to find the resonance frequency, to calculate the coupling coefficient), the influence of the wire connectors on the probe parameters should be taken into account. Although the connectors are very short they should be treated as a long line of the characteristic impedance equal to 300 ohms. This influence is of course dependent on the probe impedance which is a function of the transducer loading (a back load, matching layers, investigated medium). In Figs. 8a the calculated admittances of the PZT transducer of 20 mm dia, 10 MHz, loaded symmetrically with a perspex (applied usually to measure the transducer parameters) are shown. The electrical resonance and quadrant frequencies are remarkably changed when connectors are used. It means that on the basis of admittance measurements of low ohm (large diameters, high frequencies) transducers finding the electrical resonance frequency and coupling coefficient  $k_t$ , [1], [6] is impossible.

In Fig. 8b the admittances of the same transducer with one matching layer (used, for instance, for the eye examinations) with and without wire connectors are shown. The changes of admittance due to the connectors are different than for the probe

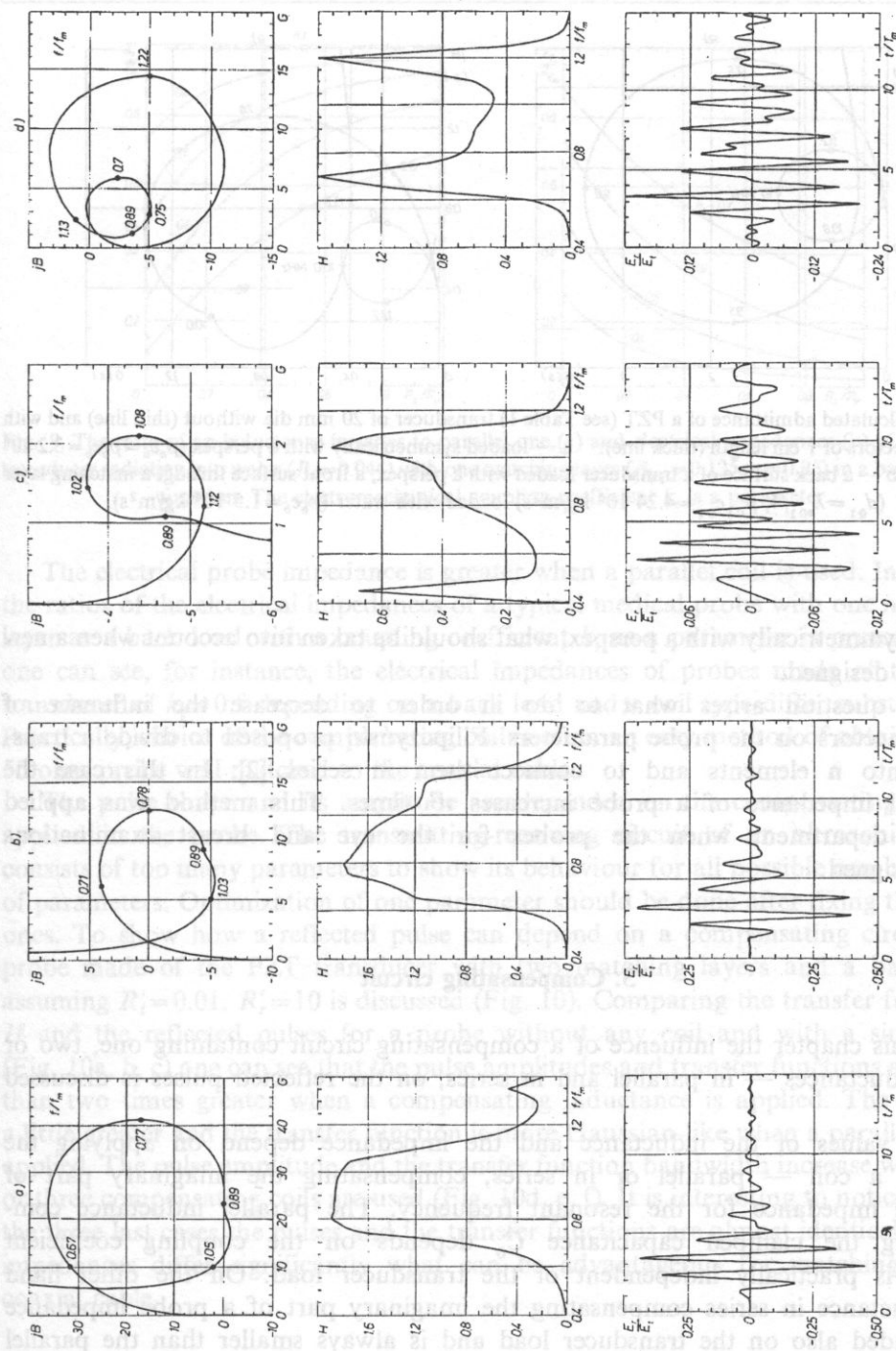


Fig. 7. Calculated relative admittances, transfer functions  $H$  and reflected pulses for the circuit as in Fig. 4 with a cable ( $\Phi_c = 0.02$ ) of characteristic resistance much greater than a probe impedance, without and with a parallel inductance: a —  $R'_c = 4.505, m = 0$  b —  $R'_c = 4.505, m = 0.865, c - R'_c = 2.5, m = 0$  d —  $R'_c = 2.5, m = 0.865$ .

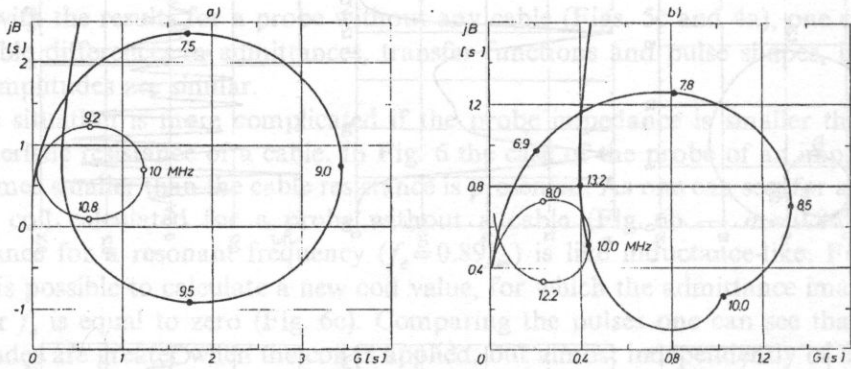


Fig. 8. Calculated admittance of a PZT (see Table 1) transducer of 20 mm dia without (thin line) and with wire connectors of 1 cm length (thick line): a — loaded symmetrically with a perspex ( $\rho_a c_a = \rho_b c_b = 3.2 \cdot 10^6$  kg/m<sup>2</sup>s) b — a back surface of a transducer loaded with a perspex, a front surface through a matching layer ( $d_{01} = \lambda_{e01}/4$ ,  $\rho_{01} c_{01} = 4.24 \cdot 10^6$  kg/m<sup>2</sup>s) loaded with water ( $\rho_b c_b = 1.5 \cdot 10^6$  kg/m<sup>2</sup>s).

loaded symmetrically with a perspex, what should be taken into account when a new probe is designed.

The question arises what to do in order to decrease the influence of the connectors on the probe parameters. Filipczyński proposed to divide a transducer into  $n$  elements and to connect them in series [2]. In this case the electrical impedance of a probe increases  $n^2$  times. This method was applied in our department when the probes for the eye and breast examinations were designed.

### 3. Compensating circuit

In this chapter the influence of a compensating circuit containing one, two or three inductances — in parallel and in series, on the reflected pulses is discussed (Fig. 1).

The values of the inductance and the impedance depend on applying the type of a coil — parallel or in series, compensating the imaginary part of a probe impedance for the resonant frequency. The parallel inductance compensating the clamped capacitance  $C_0$  depends on the coupling coefficient  $k_r$ , but is practically independent of the transducer load. On the other hand the inductance in series compensating the imaginary part of a probe impedance is depended also on the transducer load and is always smaller than the parallel one (Fig. 9a).

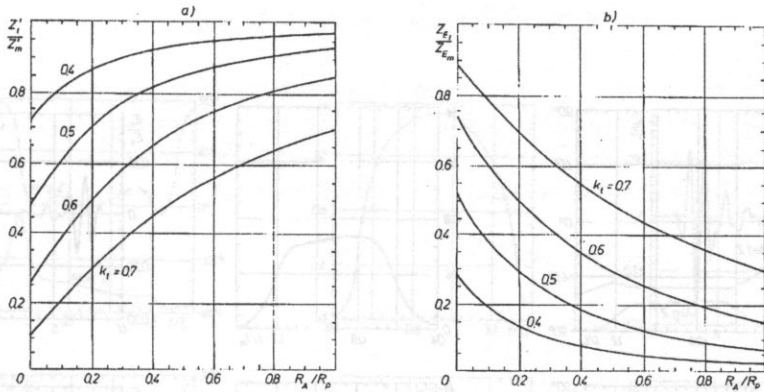
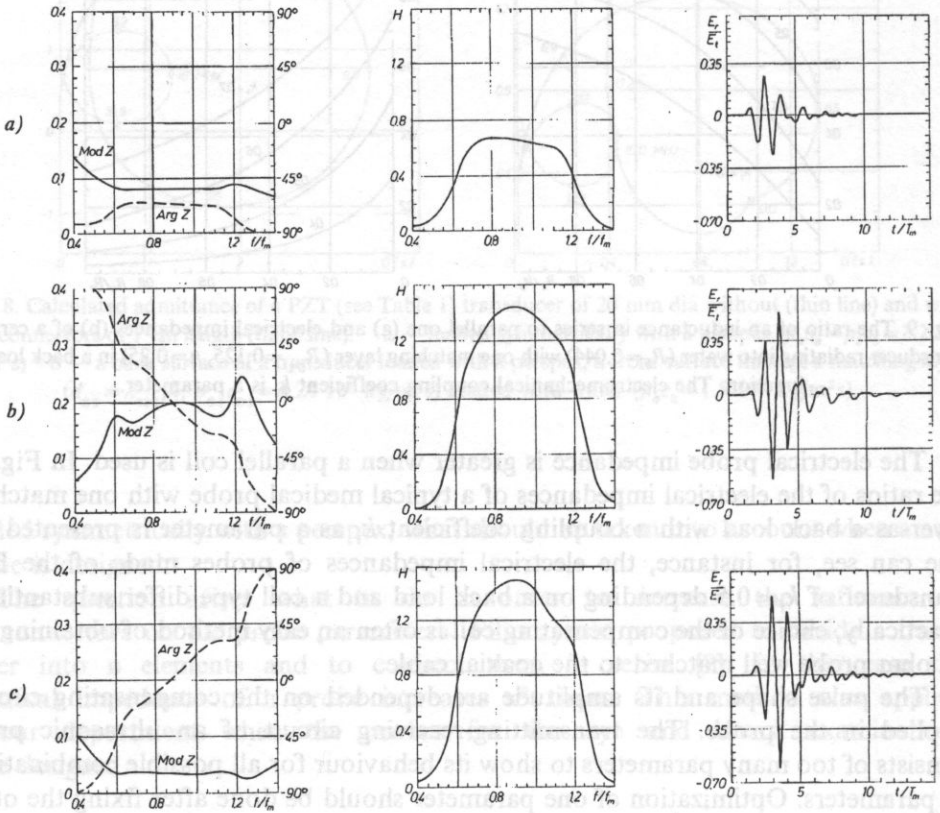


Fig. 9. The ratio of an inductance in series to parallel one (a) and electrical impedances (b) of a ceramic transducer radiating into water ( $R_b = 0.044$ ) with one matching layer ( $R_{01} = 0.125$ ,  $n = 0.25$ ) in a back load  $R_a$  function. The electromechanical coupling coefficient  $k_t$  is a parameter.

The electrical probe impedance is greater when a parallel coil is used. In Fig. 9b the ratios of the electrical impedances of a typical medical probe with one matching layer as a back load with a coupling coefficient  $k_t$  as a parameter is presented. As one can see, for instance, the electrical impedances of probes made of the PZT transducer of  $k_t = 0.5$  depending on a back load and a coil type differ substantially. Practically, choice of the compensating coil is often an easy method of obtaining the 50 ohm probe well matched to the coaxial cable.

The pulse shape and its amplitude are depended on the compensating circuits applied in the probe. The transmitting-receiving circuit of an ultrasonic probe consists of too many parameters to show its behaviour for all possible combinations of parameters. Optimization of one parameter should be done after fixing the other ones. To show how a reflected pulse can depend on a compensating circuit, the probe made of the PZT transducer with two matching layers and a back load assuming  $R'_i = 0.01$ ,  $R'_r = 10$  is discussed (Fig. 10). Comparing the transfer functions  $H$  and the reflected pulses for a probe without any coil and with a single one (Fig. 10a, b, c) one can see that the pulse amplitudes and transfer functions are more than two times greater when a compensating inductance is applied. The pulse is a little greater and the transfer function is more Gaussian-like when a parallel coil is applied. The pulse amplitude and the transfer function bandwidth increase when two or three compensating coils are used (Fig. 10d, e, f). It is interesting to notice that in the three last cases the pulses and the transfer functions are almost identical but the impedances differ significantly what can be advantageous for matching to the coaxial cable.



ones. To show how a reflected pulse can depend on a compensating circuit, the probe made of the PZT transducer with two matching layers and a back load assuming  $R_1^* = 0.01$ ,  $R_2^* = 10$  is discussed (Fig. 10). Comparing the transfer functions and the reflected pulses for a probe without any coil and with a single one (Fig. 10a, b) one can see that the pulse magnitudes and transfer functions are more than two times greater when a compensating inductance is applied. The pulse is a little greater and the transfer function is more Gaussian-like when a parallel coil is applied. The pulse amplitude and the transfer function bandwidth increase when two or three compensating coils are used (Fig. 10d, e). It is interesting to notice that in the three last cases the pulses and the transfer functions are almost identical but the inductances differ significantly, what can be advantageous for matching to the central coil.

It is also interesting to see that the inductance in the compensating series in connection with the parallel inductance is always and is always smaller than the parallel inductance (Fig. 9a).

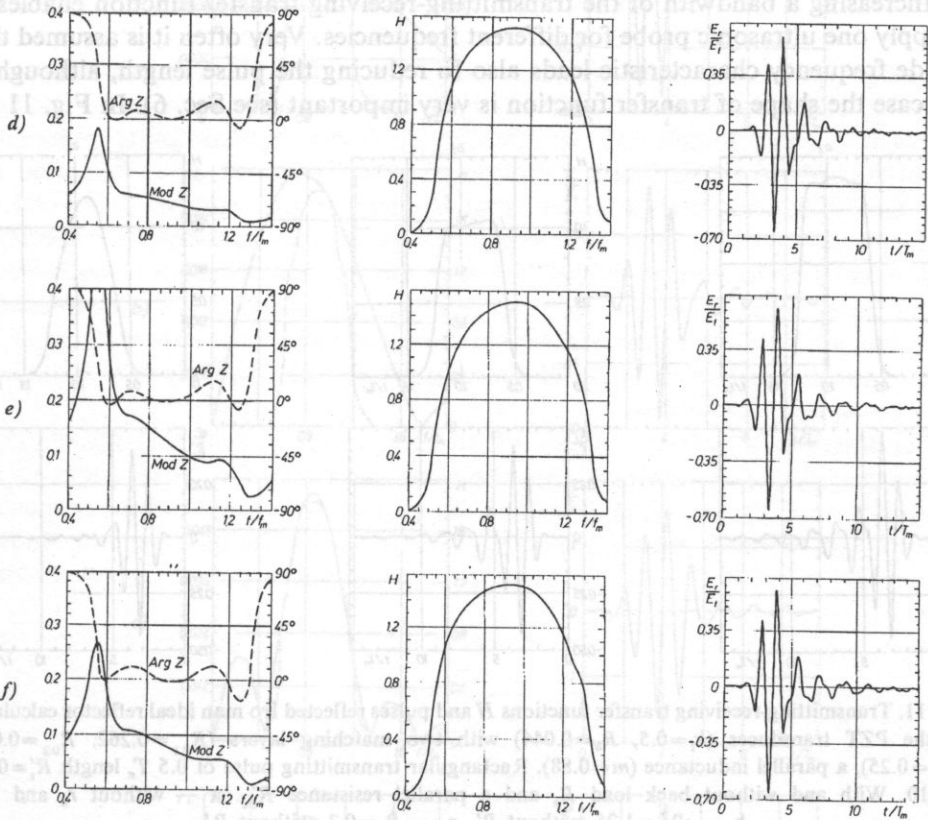


Fig. 10. Calculated relative electrical impedances  $Z$ , transmitting-receiving transfer functions  $H$  and pulses reflected from an ideal reflector in water for a PZT transducer ( $k_t=0.5$ ,  $R_b=0.044$ ) with two matching layers ( $R_{01}=0.262$ ,  $R_{02}=0.069$ ,  $n=p=0.25$ ) and a back load ( $R_a=0.15$ ). Rectangular transmitting pulse of  $0.5 T_e$  length ( $T_e=1/f_e$ ),  $R'_t=0.01$ ,  $R'_r=10$ . Different compensating circuits: a — without any inductance, b — parallel inductance  $m=0.883$  (without  $L_1$  and  $L_2$ ), c — inductance in series  $L_1=1.027$  (without  $m$  and  $L_2$ ), d —  $L_1=0.89$ ,  $m=0.925$  (without  $L_2$ ), e —  $m=0.712$ ,  $L_2=1.154$  (without  $L_1$ ), f —  $L_1=L_2=0.655$ ,  $m=0.834$ .

#### 4. Parallel resistance, back loading

Increasing a bandwidth of the transmitting-receiving transfer function enables us to apply one ultrasonic probe for different frequencies. Very often it is assumed that a wide frequency characteristic leads also to reducing the pulse length, although in this case the shape of transfer function is very important (see Sec. 6). In Fig. 11 the

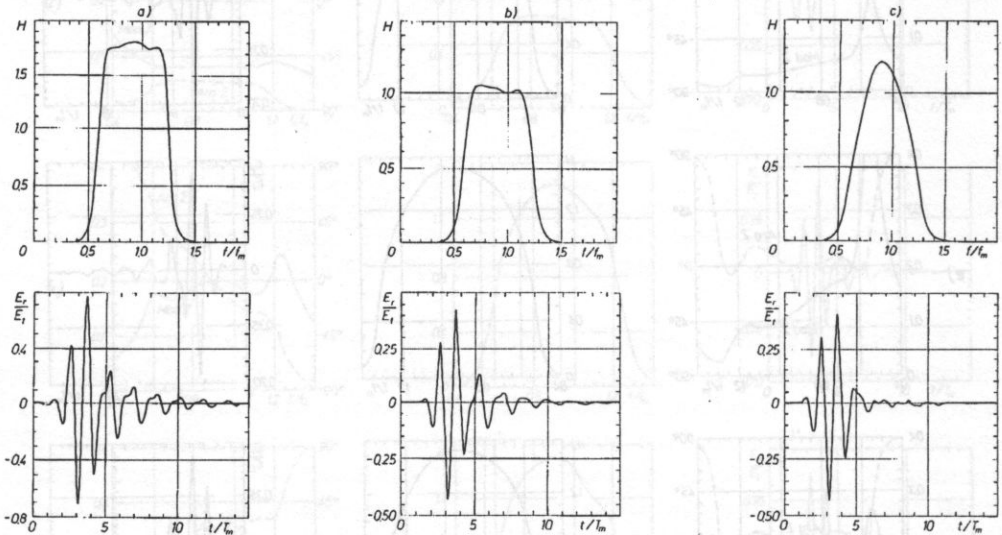


Fig. 11. Transmitting-receiving transfer functions  $H$  and pulses reflected from an ideal reflector calculated for the PZT transducer ( $k_t=0.5$ ,  $R_b=0.044$ ) with two matching layers ( $R_{01}=0.262$ ,  $R_{02}=0.069$ ,  $n=p=0.25$ ), a parallel inductance ( $m=0.88$ ). Rectangular transmitting pulse of  $0.5 T_a$  length  $R'_a=0.01$ ,  $R'_r=10$ . With and without back load  $R_a$  and a parallel resistance  $R'_{be}$ . a — without  $R_a$  and  $R'_{be}$ , b —  $R'_{be}=1.25$ , without  $R'_a$ , c —  $R_a=0.3$ , without  $R'_{be}$ .

transmitting-receiving transfer functions and reflected pulses for probes made of the PZT material with two matching layers, with and without a back load and with and without a parallel resistance are shown. Comparing the results one can see that the shorter pulse is obtained when a back surface of the transducer is loaded by  $R_a$ , which was chosen to give the same pulse amplitude as a circuit with a parallel resistance  $R_{be}$ . For this case the transfer function is Gaussian-like however its bandwidth is even narrower. It means that for shortening of the pulse the better way is to load a back surface of the transducer than to apply a parallel resistance.

#### 5. Transmitting pulse

The reflected pulse depends not only on the transmitting one, but also on the probe bandwidth. Therefore the length of the transmitting pulse should be chosen after taking into consideration the probe characteristics. In this section, as an



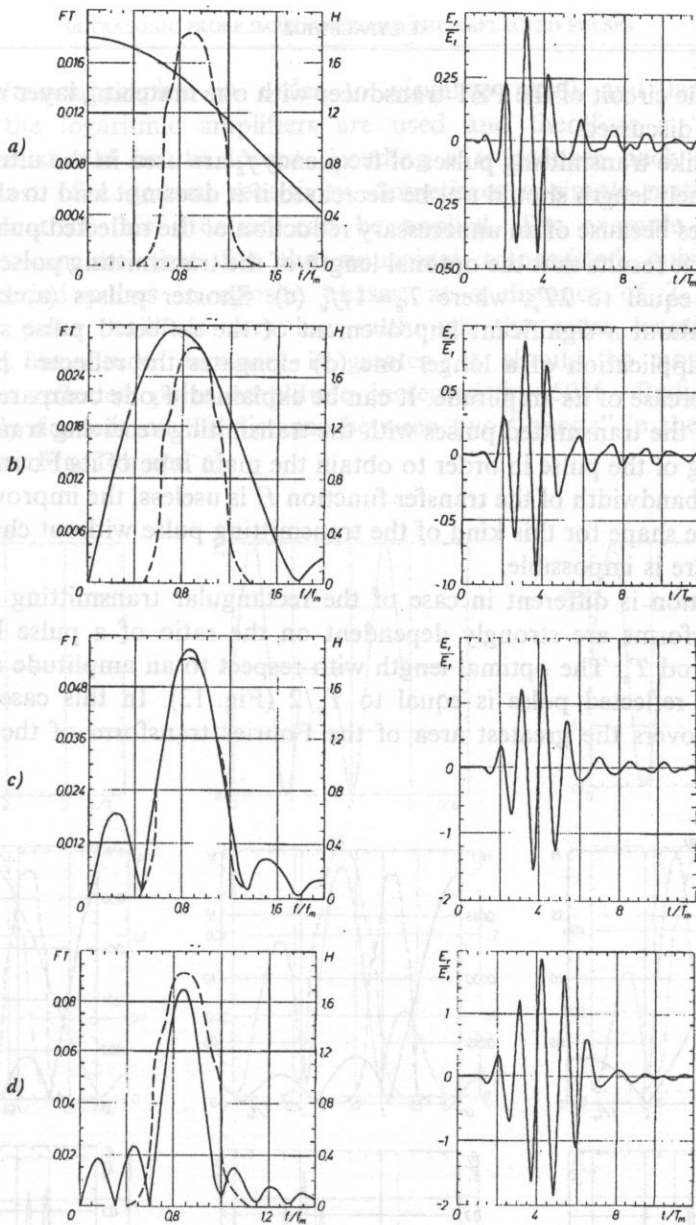


Fig. 12. Fourier transforms FT of burst transmitting pulses of a frequency  $f_0$  (compared with transmitting-receiving transfer function  $H$  — dashed line) and reflected pulses calculated for a PZT transducer ( $k_t=0.5$ ,  $R_b=0.044$ ) with one matching layer ( $R_{01}=0.125$ ,  $n=0.25$ ), without backing ( $R_a=0$ ), with a parallel inductance ( $m=0.887$ ). Different burst lengths,  $R'_t=0.01$ ,  $R'_r=10$ : a —  $T_e/2$ , b —  $1T_e$ , c —  $2T_e$ , d —  $3T_e$ , where  $T_e=1/f_0$ .

illustration, the circuit of the PZT transducer with one matching layer and a parallel inductance is discussed.

The burstlike transmitting pulses of frequency  $f_e$  are used in the ultrasonography very often. Their length should not be decreased if it does not lead to shortening the reflected pulses because of an unnecessary reduction of the reflected pulse amplitude. From Fig. 12 it results that the optimal length of the transmitting pulse for this kind of probes is equal to  $2T_e$ , where  $T_e = 1/f_e$  (c). Shorter pulses (a, b) reduce the amplitude without a significant improvement of the reflected pulse shape; on the other hand, application of a longer one (d) elongates the reflected pulse without significant increase of its amplitude. It can be explained if one compares the Fourier transforms of the transmitted pulses with the transmitting-receiving transfer function  $H$ . Shortening of the pulse in order to obtain the main lobe of its Fourier transform wider than a bandwidth of the transfer function  $H$  is useless, the improvement of the reflected pulse shape for this kind of the transmitting pulse without changing of the probe structure is impossible.

The situation is different in case of the rectangular transmitting pulses. Their Fourier transforms are strongly dependent on the ratio of a pulse length to the vibration period  $T_e$ . The optimal length with respect to an amplitude as well as the shape of the reflected pulse is equal to  $T_e/2$  (Fig. 13). In this case the transfer function  $H$  covers the greatest area of the Fourier transform of the transmitting pulse.

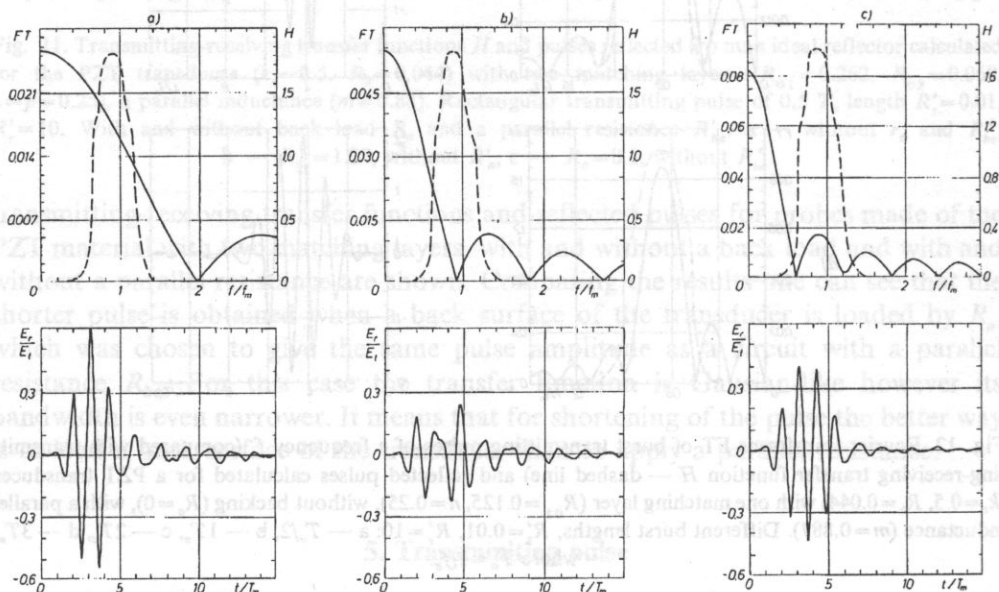


Fig. 13. Fourier transforms FT of rectangular transmitting pulses (compared with transfer function  $H$ —dashed line) and reflected pulses calculated for the transducer like in Fig. 12. A different transmitting pulse lengths: a —  $0.5T_e$ , b —  $1T_e$ , c —  $1.5T_e$ .

In the ultrasonography, in order to visualize small and large echos in one picture the logarithmic amplifiers are used and therefore a "tail" of the reflected pulse should be the lowest. Loading a transducer back surface helps but at the cost of a general sensitivity. Sometimes a simple method enabling an improvement of this situation can be applied. The example is shown in Fig. 14. One can see that for the sinusoidal transmitted pulse containing two single period pulses in opposite phases, at a distance of  $T_e/2$  (Fig. 14b) the reflected pulse "tail" is very low, although the pulse length (calculated for the 10% amplitude decrease) is greater. It should be noticed that in that case the reflected pulse amplitude increased by 50%. Reduction of the "tail" strongly depends on the distance between two "bursts" in the transmitting pulse (compare Fig. 14b and c).

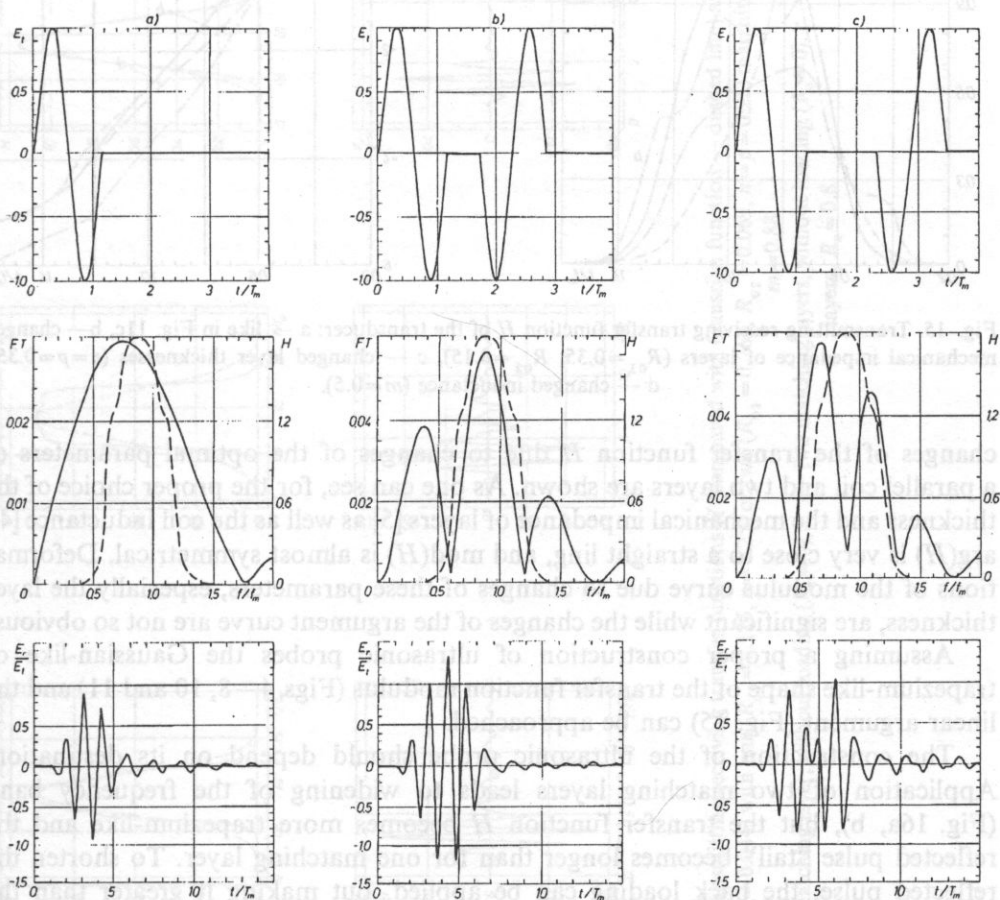


Fig. 14. Transmitting pulses (consisting of bursts of frequency  $f_e$  in opposite phases), their Fourier transforms FT (compared with transfer function  $H$  — dashed line) and reflected pulses calculated for the transducer like in Fig. 12. A different distance  $d_b$  between bursts: a — a single burst, b —  $d_b = T_e/2$ , c —  $d_b = T_e$ .

## 6. Influence of the transmitting-receiving transfer functions on reflected pulses

In general, the authors describing the ultrasonic probe behaviour do not discuss the influence of the shape and the argument of the transfer function  $H$  on the reflected pulses. This problem requires a special study, nevertheless some aspects of this question important from the designing point of view is presented. In Fig. 15 the

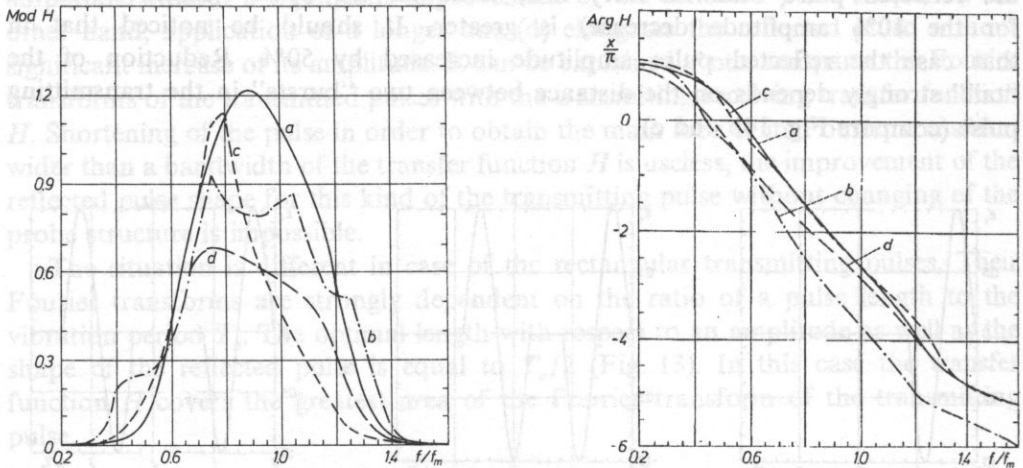


Fig. 15. Transmitting-receiving transfer function  $H$  of the transducer: a — like in Fig. 11c, b — changed mechanical impedance of layers ( $R_{01}=0.35$ ,  $R_{02}=0.15$ ), c — changed layer thicknesses ( $n=p=0.35$ ), d — changed inductance ( $m=0.5$ ).

changes of the transfer function  $H$  due to changes of the optimal parameters of a parallel coil and two layers are shown. As one can see, for the proper choice of the thickness and the mechanical impedance of layers [5] as well as the coil inductance [4],  $\text{arg}(H)$  is very close to a straight line, and  $\text{mod}(H)$  is almost symmetrical. Deformations of the modulus curve due to changes of these parameters, especially the layer thickness, are significant while the changes of the argument curve are not so obvious.

Assuming a proper construction of ultrasonic probes the Gaussian-like or trapezium-like shape of the transfer function modulus (Figs 4–8, 10 and 11) and the linear argument (Fig. 15) can be approached.

The construction of the ultrasonic probe should depend on its destination. Application of two matching layers leads to widening of the frequency band (Fig. 16a, b), but the transfer function  $H$  becomes more trapezium-like and the reflected pulse “tail” becomes longer than for one matching layer. To shorten the reflected pulse, the back loading can be applied, but making it greater than the optimal value worsens the pulse shape (Fig. 16c, d). As one can see in Fig. 16, the optimal pulse shape is obtained when transfer function  $H$  is close to the Gaussian one.

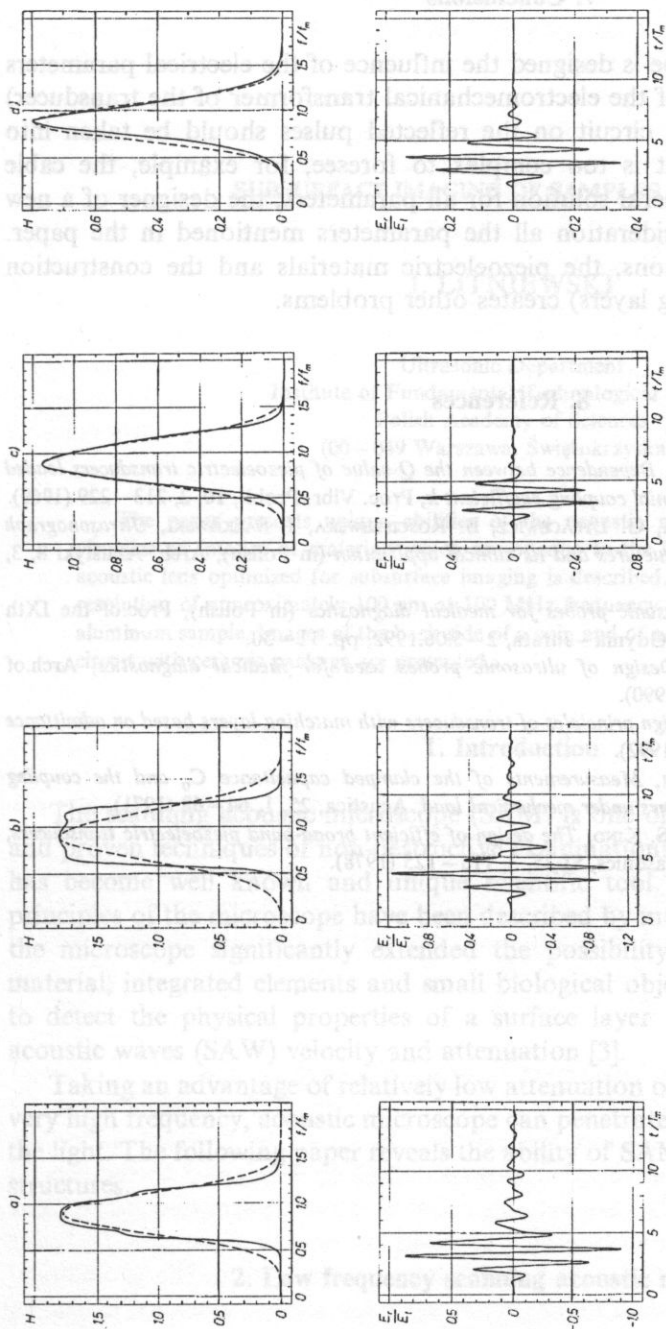


Fig. 16. Transmitting-receiving transfer functions  $H$  (compared with Gaussian function — dashed line) and reflected pulses calculated for the PZT transducer ( $k_t = 0.5, R_b = 0.044$ ) with one ( $R_{01} = 0.125, n = 0.25$ ) or two ( $R_{01} = 0.125, n = 0.25, R_{02} = 0.262, n = 0.069$ ) matching layers for a different back load. Parallel inductance layers,  $R_s = 0.8$ .  $m = 0.88$

## 7. Conclusions

When the ultrasonic probe is designed the influence of the electrical parameters (lying on the electrical side of the electromechanical transformer of the transducer) of the transmitting-receiving circuit on the reflected pulses should be taken into account. Because this circuit is too complex to foresee, for example, the cable influence and to find the general solution for all parameters, the designer of a new probe should take into consideration all the parameters mentioned in the paper. Each change of the dimensions, the piezoelectric materials and the construction possibilities (i.e. the matching layers) creates other problems.

## 8. References

- [1] L. FILIPCZYŃSKI, G. ŁYPACEWICZ, *Dependence between the Q-value of piezoelectric transducers loaded acoustically and the electromechanical coupling coefficient k*, Proc. Vibr. Probl., **10**, 2, 213–229 (1969).
- [2] L. FILIPCZYŃSKI, D. KOMITOWSKI, G. ŁYPACEWICZ, B. ROŚCISZEWSKA, J. SĄLKOWSKI, *Ultrasonograph UO-3 for visualization of eye structures and its clinical application* (in Polish), Arch. Akustyki **8**, 3, 265–282 (1973).
- [3] G. ŁYPACEWICZ, *Design of ultrasonic probes for medical diagnostics* (in Polish), Proc. of the IXth Symposium on Hydroacoustics, Gdynia—Jurata, 2–5.06.1992, pp. 11–30.
- [4] G. ŁYPACEWICZ, E. DURIASZ, *Design of ultrasonic probes used for medical diagnostics*, Arch. of Acoustics, **15**, 3–4, 137–159 (1990).
- [5] G. ŁYPACEWICZ, E. DURIASZ, *Design principles of transducers with matching layers based on admittance measurements*, **17**, 1, 117–131 (1992).
- [6] G. ŁYPACEWICZ, L. FILIPCZYŃSKI, *Measurements of the clamped capacitance  $C_0$  and the coupling coefficient  $k_t$  of ceramic transducers under mechanical load*, Acustica, **25**, 1, 64–68 (1971).
- [7] C.S. DE SILETS, J.D. FRASER, G.S. KINO, *The design of efficient broad-band piezoelectric transducers*, IEEE Trans. on Sonics and Ultrasonics, SI-25, 3, 115–125 (1978).

**SUBSURFACE IMAGING OF SAMPLES WITH SAM****J. LITNIEWSKI**

Ultrasonic Department  
Institute of Fundamental Technological Research  
Polish Academy of Sciences  
(00-049 Warszawa, Świętokrzyska 21)

The paper presents unique abilities of the acoustic microscope to penetrate and visualize an interior of materials which are opaque to the light. The construction of an acoustic lens optimized for subsurface imaging is described. The lens enables to achieve resolution of approximately 100  $\mu\text{m}$  at 100 MHz frequency when visualize an interior of aluminum sample. Images of the back side of a coin and of a die attach bond of integrated circuit with ceramic package are presented.

**1. Introduction**

The scanning acoustic microscope (SAM) is one of the most rapidly developing and proven techniques of non-destructive examinations of hard and soft material. It has become well known and unique scientific tool. The physical and technical principles of the microscope have been described by many authors [1, 2]. The use of the microscope significantly extended the possibility of imaging the surface of material, integrated elements and small biological objects. The microscope enables to detect the physical properties of a surface layer by measurements of surface acoustic waves (SAW) velocity and attenuation [3].

Taking an advantage of relatively low attenuation of the ultrasonic waves even at very high frequency, acoustic microscope can penetrate materials that are opaque to the light. The following paper reveals the ability of SAM to visualize unseen internal structures.

**2. Low frequency scanning acoustic microscope**

We have build a scanning acoustic reflecting microscope. The system enables to obtain high quality amplitude and phase images with special resolution 30  $\mu\text{m}$ , 10  $\mu\text{m}$  and 5  $\mu\text{m}$  operating at 35 MHz, 100 MHz and 200 MHz frequency respectively.

When the system operates in visualization option two modes of imaging are possible, C-scan and B-scan. In the C-scan mode the back scattered ultrasound collected by the lens and detected by the transducer is time gated such that only scatter from the focal plane are accepted. The amplitude or phase of the signal is stored while the transducer moves over the sample point by point to produce two dimensional image (Fig. 1). Depending on the focus position, the C-mode allows to visualize the surface or an interior of the sample. The image reflects acoustic properties of the material at the plain perpendicular to the acoustic beam axis.

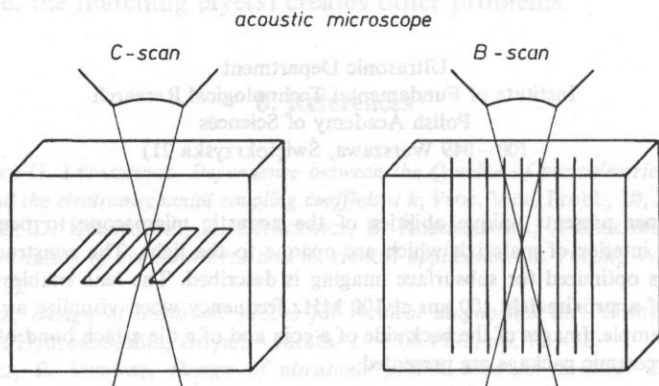


Fig. 1. Two modes of microscopic visualization, C-scan and B-scan.

The B-scan mode is similar to the data acquisition in ultrasonography. The back scatter signal at each transducer position is used to produce a line of information in the image. Therefore, only one dimensional scanning is required to obtain two dimensional image (Fig. 1). B-scan mode visualize internal structures of material. The image corresponds to the cross-section of the sample, parallel to the acoustic beam axis.

### 3. The lens for subsurface imaging of a hard sample

Imaging of the interior requires the acoustic beam to be focused under the surface of the sample. In an acoustic microscope the lens is coupled to the sample with a fluid, usually water. The converging acoustic wave transmitted by the lens must penetrate highly refractive interface between water and a sample. In water acoustic waves can be easily focused in a diffraction limited spot. The geometrical aberration is so small that it can be neglected even for a large aperture lenses. In solid materials with a high velocity of acoustic waves, the aberration spreads widely the focal area. The proper choice of a lens aperture limits the degradation of a focus introduced by geometrical aberration.



There are some other reasons which justify the use of small aperture lenses for subsurface imaging. For high angles of convergence the waves can not penetrate the water-sample interface. The high amplitude signal of the waves specularly reflected from the surface masks low amplitude signal coming from the interior. Additionally, waves incident on an interface at critical angles excite a Leaky Surface Waves (LSW) in a surface of the specimen. The LSW in turn excite waves in the coupling fluid at the critical angles. These waves are detected by the transducer and they disturb the signals received from the inside of the sample. The small aperture lenses preclude LSW generation.

The aim of this work was the construction of the acoustic microscope lens appropriate for optimized subsurface imaging. There was assumed that the microscope operating at 100 MHz frequency should visualize internal structures situated 3 mm under the surface of material with the velocity of longitudinal waves equaled to 6000 m/s.

The simple geometrical analysis of the acoustic system consist of the lens, coupling fluid and a plane sample allows to determine the size of the lens aperture minimizing the aberration and diffraction effects [4].

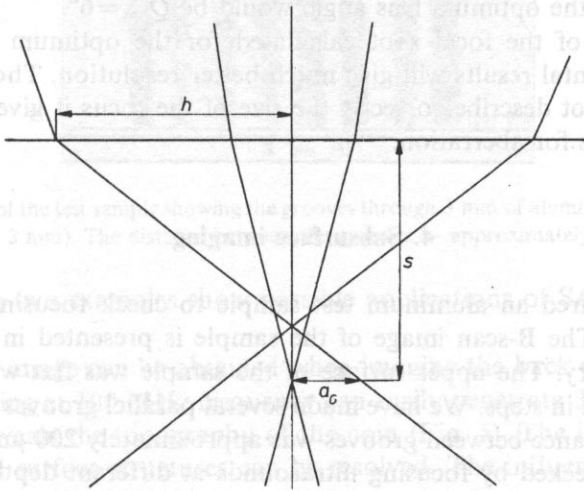


Fig. 2. Rays focusing below the surface of a solid sample, refraction of the interface and an aberration effect.

Using the notation of Fig. 2 one can find that the minimum geometrical aberration is:

$$a = a_G/2 = \frac{h^3 \left( \frac{1}{n} - 1 \right)^2}{4s^2}, \quad (3.1)$$

where  $n$  is a refractive index at the water/sample interface.

Diffraction spreads the focal spot into the Airy disc which first minimum can be found at the distance from the axis

$$d = \frac{1.22 \lambda s}{2h}, \quad (3.2)$$

$\lambda$  — wavelength in the solid sample.

The total size of the focal spot may be written as

$$a_t = (a^2 + d^2)^{1/2}. \quad (3.3)$$

It can be found that a minimum of  $a_t$  occurs for

$$h/s = (\lambda/s)^{1/4} \frac{1}{(1-n)^{1/2}}, \quad (3.4)$$

what gives an optimum lens angle

$$Q_{\text{opt}} = \sin^{-1} [n \sin \{ \tan^{-1} (h/s) \}]. \quad (3.5)$$

For the sample made of the material with  $n=0.25$  and for the focusing 3 mm below the surface the optimum lens angle would be  $Q_{\text{opt}}=6^\circ$ .

The total size of the focal spot calculated for the optimum lens amounts to 800  $\mu\text{m}$ . Experimental results will give much better resolution. Though the geometrical analysis do not describe correctly the size of the focus it gives good results in optimizing the lens for aberration.

#### 4. Subsurface imaging

We have prepared an aluminum test sample to check focusing abilities of the constructed lens. The B-scan image of the sample is presented in Fig. 3 giving an idea of its geometry. The upper surface of the sample was flat while the opposite surface was shaped in steps. We have made several parallel grooves on the surface of each step. The distance between grooves was approximately 200  $\mu\text{m}$ . The resolution of the lens was checked by focusing ultrasounds at different depth and visualizing the grooves.

The best C-scan image was obtained for focusing at 3 mm under the surface (Fig. 4). The grooves are easily resolved what proves that the lens resolution is of the order of 100  $\mu\text{m}$  (one and half wavelength in aluminum). The resolving power of the microscope is much higher than predicted by geometrical calculations. In calculations it is assumed that a plane uniform amplitude wave is focused by the lens. In the microscope the lens is situated in the transition zone between the far and near field of the transducer. Thus the lens is illuminated with a gaussian beam. Additionally at the lens/water and water/sample interfaces an amplitude of the waves corresponding to high angles of convergence is farther reduced. The natural apodization occurs and the waves are focused much better than the geometrical calculations predict.



Fig. 3. B-scan image of a test sample (image dimensions 12.8 mm  $\times$  4.2 mm).

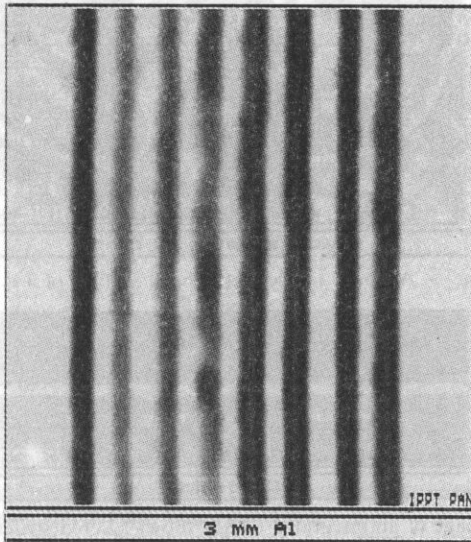


Fig. 4. C-scan image of the test sample showing the grooves through 3 mm of aluminum (image dimensions 3 mm  $\times$  3 mm). The distance between the grooves — approximately 200  $\mu$ m.

The following two examples show possible applications of SAM for subsurface imaging.

A spectacular image can be obtained when imaging the back side of a coin. The microscope working at 100 MHz frequency can easily penetrate 3 mm of aluminum and the image reveals the topography of the coin (Fig. 5). The image is of a good quality and small surface structures can be resolved. The influence of a coin front surface on image is of a minor importance.

The second example comes from micro electronics. In the integrated circuit package the heat must be dissipated to stabilize the electrical behavior of the semiconductor. The poor quality of the die attach bond can be detected with ultrasounds. The bright areas in the microscope image correspond to the high acoustic reflectivity due to the lack of bonding between the die and ceramic.

B-scan acoustomicroscopic image shows layered structures of integrated circuit (Fig. 6). The ceramic substrata, lead frame and die attach bond can be resolved in the acoustic cross-section of the chip (E-prom memory).

Fig. 7 shows C-scan image of an interior of the same integrated circuit. The time gate and the focus were located at the die attach bond, approximately 2 mm below

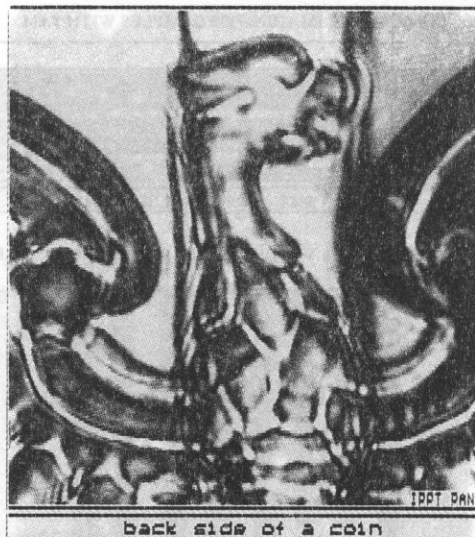


Fig. 5. Acoustic image of the back surface of a coin.

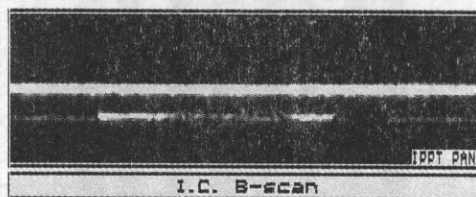


Fig. 6. B-scan image of an integrated circuit shows layered structure of a the chip.

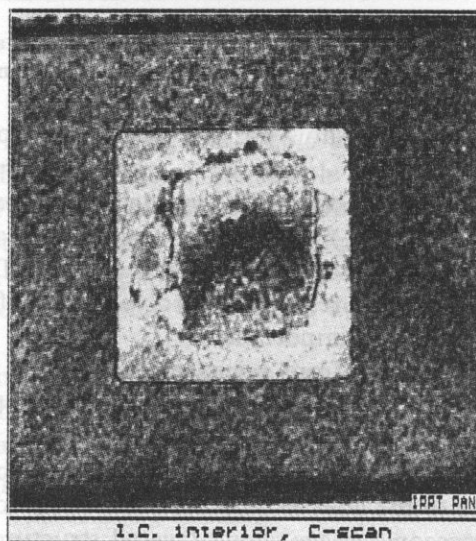


Fig. 7. An interior of an integrated circuit. The C-scan image shows a die attach bond inside the ceramic package (approximately 2 mm below the front surface).

the ceramic base. The central part of the bond image is black. This area indicates a good bonding. Ultrasonic waves penetrates the interface almost without any back reflections creating a black area in the image.

## 5. Conclusions

Scanning acoustic microscope can visualize an interior of the samples made of a hard material. It is possible to achieve resolution of the order of a single wavelength. Low aperture lenses must be used to avoid spreading of the focus because of the aberration and generation of LSW which can disturb subsurface image. At 100 MHz frequency depth of several millimeters can be achieved and visualized.

## References

- [1] C.F. QUATE, A. ATALAR and H.K. WICKRAMASINGHE. *Acoustic microscopy with mechanical scanning: a review*, Proc. IEEE 67, 1092–114 (1979).
- [2] G.A.D. BRIGGS, *An introduction to scanning acoustic microscopy*, Royal Society Handbook, 12, Oxford University Press, Oxford 1985.
- [3] J. LITNIEWSKI, *Acoustic microscope signal for defocusing conditions — application to biological image interpretation*, Ph. D. thesis, IFTR PAS, Warszawa 1990.
- [4] E. HECHT, *Optics*, Addison-Wesley, Reading, Massachusetts 1987.

## OPTIMIZATION OF TWO MATCHING LAYERS FOR THE WIDE-BAND TRANSDUCER

Z. WESOŁOWSKI

Institute of Fundamental Technological Research  
Polish Academy of Sciences  
(00-049 Warszawa, Świętokrzyska 21)

Two homogeneous elastic layers are situated between two homogeneous elastic materials. If the harmonic wave propagates in the direction perpendicular to the layers, then the reflection coefficient depends on the elastic constants of the layers, their thickness and frequency. If, instead of the monochromatic wave, the pulse is propagating, then the reflection coefficient depends on the frequency spectrum. The pulse in the form of two or four periods of the sine curve is considered. It is decomposed into a sum, of harmonic, monochromatic waves. In calculations the pulse was assumed to be a sum of 22 harmonic waves of different frequencies. The reflection coefficient for this sum was determined. The reflection coefficient possesses several minima. Only two of them are technically interesting. For one of them the thicknesses of the two layers are of the same order.

### 1. Monochromatic acoustic wave

Consider the case, when two homogeneous elastic layers are situated between two homogeneous elastic materials. The wave is produced in the first homogeneous material, propagates across the two layers and enters the second homogeneous material. One part of the energy of the incident wave is reflected. The reflection coefficient  $\beta$  is a function of thicknesses, densities and elastic constant of the layers. If  $\beta=0$ , the system is perfectly transparent, if  $\beta=1$  the system is perfectly insulating. For two homogeneous materials given in advance, the elastic layers joining them may be chosen to minimize or maximize the reflection coefficient. Instead of two layers, a larger number of them may be used. The equations quoted in this chapter allow us to perform calculations for an arbitrary number of layers. However, for most practical acoustic applications, already one or two layers are sufficient.

From the mathematical point of view more interesting is the optimization of the transition zone between two materials, if the propagation speed and the density are continuous functions of the distance  $x$ ,  $c=c(x)$ ,  $\rho=\rho(x)$ . It is easy to write the governing equations, and to calculate the reflection coefficient  $\beta$  for  $c(x)$ ,  $\rho(x)$  given in advance. In very numerous situations the appropriate analytical formula may be

obtained, cf, e.g [1]. It is impossible, however, to solve such problem exactly, since  $\beta$  can not be written as the functional of  $c(x)$ . This is due to the fact that the solutions of the ordinary differential equation can not be expressed by its coefficients.

Each of the four materials considered (two fixed half-spaces and two layers) is identified by the subscripts 0, 1, 2, 3 (Fig. 1). Thicknesses of the layers are denoted by  $h_1, h_2$ , respectively. The harmonic waves of frequency  $\omega$  propagate in the direction perpendicular to the layers. The displacement  $u$  in the  $k$ -th material consists of two harmonic waves, the first of amplitude  $A_k$  running to the right, and the second one of amplitude  $B_k$  running to the left.

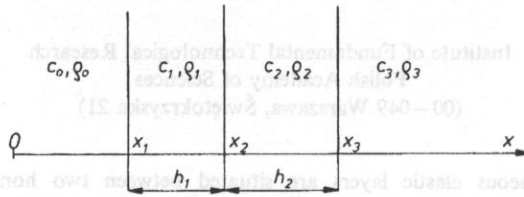


Fig. 1.

$$u = A_k \exp i\omega \left[ t - \frac{x - x_k}{c_k} \right] + B_k \exp i\omega \left[ t + \frac{x - x_k}{c_k} \right]. \tag{1.1}$$

At the boundaries between the layers both the displacement and the stress are continuous. It follows that the amplitudes  $A_k, B_k$  are connected by the matrix relations (cf. e.g. [1])

$$\begin{bmatrix} A_k \\ B_k \end{bmatrix} = M_k \begin{bmatrix} A_{k-1} \\ B_{k-1} \end{bmatrix}. \tag{1.2}$$

where

$$M_k = \frac{1}{2} \begin{bmatrix} (1 + \kappa_k) \exp(-i\alpha_k) & (1 - \kappa_k) \exp(i\alpha_k) \\ (1 - \kappa_k) \exp(-i\alpha_k) & (1 + \kappa_k) \exp(i\alpha_k) \end{bmatrix}. \tag{1.3}$$

$$\kappa_k = \frac{\rho_{k-1} c_{k-1}}{\rho_k c_k}, \quad \alpha_k = \omega \frac{h_{k-1}}{c_{k-1}}. \tag{1.4}$$

The transfer matrix  $M_k$  is non-singular, therefore its inverse  $M_k^{-1}$  always exists. Changing the formulae (1.2) for subsequent  $k=1, 2, 3$ , the amplitudes  $A_3, B_3$  may be expressed by the amplitude  $A_0, B_0$  and vice versa.

$$\begin{bmatrix} A_3 \\ B_3 \end{bmatrix} = M_3 M_2 M_1 \begin{bmatrix} A_0 \\ B_0 \end{bmatrix}, \quad \begin{bmatrix} A_0 \\ B_0 \end{bmatrix} = M_1^{-1} M_2^{-1} M_3^{-1} \begin{bmatrix} A_3 \\ B_3 \end{bmatrix}. \tag{1.5}$$

Two of four amplitudes may be taken at will. If we take  $B_3=0$  and prescribe the value of  $A_0$ , then  $A_0, A_3, B_3$  represent the amplitudes of the incident wave, the transmitted wave (both running to the right, Fig. 1) and the reflected wave (running

to the left). If we take  $A_0=0$ , then  $B_3, B_0, A_0$  represent the amplitudes of the incident and the reflected wave (both running to the left) and the reflected wave (running to the right).

Take  $A_0=0$  and consider the term proportional to  $B_3$  as the incident wave: and the terms proportional to  $A_3, B_0$  as the reflected and transmitted waves, respectively. The other possible choice ( $B_3=0$ ) leads to the same reflection coefficient, since a system of layers has no directional properties, [2].

In accord with the above relations, the following expressions for  $A_3, B_3$  are obtained

$$8A_3 = B_0 \exp(-\alpha_1)^* \quad (1.6)$$

$$*[(1-\kappa_1)(1+\kappa_2)(1+\kappa_3) \exp(+\alpha_2+\alpha_3) + (1-\kappa_1)(1-\kappa_2)(1-\kappa_3) \exp(+\alpha_2-\alpha_3) + (1+\kappa_1)(1-\kappa_1)(1+\kappa_3) \exp(-\alpha_2+\alpha_3) + (1+\kappa_1)(1+\kappa_2)(1-\kappa_3) \exp(-\alpha_2-\alpha_3)].$$

$$8B_3 = B_0 \exp(-\alpha_1)^* \quad (1.7)$$

$$*[(1-\kappa_1)(1+\kappa_2)(1-\kappa_3) \exp(+\alpha_2+\alpha_3) + (1-\kappa_1)(1-\kappa_2)(1+\kappa_3) \exp(+\alpha_2-\alpha_3) + (1+\kappa_1)(1-\kappa_2)(1-\kappa_3) \exp(-\alpha_2+\alpha_3) + (1+\kappa_1)(1+\kappa_2)(1+\kappa_3) \exp(-\alpha_2-\alpha_3)].$$

The right-hand sides of (1.6), (1.7) are complex numbers. Their squared moduli are given by the following expressions:

$$64 A_3 \bar{A}_3 = B_0 \bar{B}_0 [D_1^2 + D_2^2 + D_3^2 + D_4^2 + 2(D_1 D_3 + D_2 D_4) \cos 2\alpha_2 + 2(D_1 D_2 + D_3 D_4) \cos 2\alpha_3 + 2D_1 D_4 \cos(2\alpha_2 + 2\alpha_3) + 2D_2 D_3 \cos(2\alpha_2 - 2\alpha_3)]. \quad (1.8)$$

$$64 B_3 \bar{B}_3 = B_0 \bar{B}_0 [D_5^2 + D_6^2 + D_7^2 + D_8^2 + 2(D_5 D_7 + D_6 D_8) \cos 2\alpha_2 + 2(D_5 D_6 + D_7 D_8) \cos 2\alpha_3 + 2D_5 D_8 \cos(2\alpha_2 + 2\alpha_3) + 2D_6 D_7 \cos(2\alpha_2 - 2\alpha_3)]. \quad (1.9)$$

where the real parameters  $D_k$  depend on the speed ratios  $\kappa_k$  only,

$$\begin{aligned} D_1 &= (1-\kappa_1)(1+\kappa_1)(1+\kappa_3), & D_2 &= (1-\kappa_1)(1-\kappa_2)(1-\kappa_3), \\ D_3 &= (1+\kappa_1)(1-\kappa_2)(1+\kappa_3), & D_4 &= (1+\kappa_1)(1+\kappa_2)(1-\kappa_3), \\ D_5 &= (1-\kappa_1)(1+\kappa_2)(1-\kappa_3), & D_6 &= (1-\kappa_1)(1-\kappa_2)(1+\kappa_3), \\ D_7 &= (1+\kappa_1)(1-\kappa_2)(1-\kappa_3), & D_8 &= (1+\kappa_1)(1+\kappa_2)(1+\kappa_3). \end{aligned} \quad (1.10)$$

Energy flux  $q_3$  corresponding to the wave of amplitude  $A_3$  and speed  $c_3$  is proportional to the squared frequency

$$q_3 = \rho_3 c_3 \omega^2 A_3 \bar{A}_3. \quad (1.11)$$

This flux is a vector quantity possessing the direction of wave propagation. Analogous relations hold for the remaining waves of amplitudes  $A_0, B_0, A_1, \dots, B_3$ . The reflection coefficient equals the ratio of the energy flux of the reflected wave and the energy flux of the incident wave. Therefore

$$\beta = \frac{A_3 \bar{A}_3}{B_3 \bar{B}_3}. \quad (1.12)$$



Obviously  $0 < \beta < 1$ . The first inequality follows from (1.12), since both the numerator and denominator are positive. The second inequality follows from the energy conservation law (reflected energy cannot be larger than the incident energy).

Since (1.12) is essential for the further calculations, we write explicitly the complete formula for  $\beta$  resulting from substitution of (1.7)–(1.9) into (1.12). There is

$$\begin{aligned} \beta = & [D_1^2 + D_2^2 + D_3^2 + D_4^2 + 2(D_1D_3 + D_2D_4) \cos 2\alpha_2 \\ & + 2(D_1D_2 + D_3D_4) \cos 2\alpha_3 + 2D_1D_4 \cos(2\alpha_2 + 2\alpha_3) \\ & + 2D_2D_3 \cos(2\alpha_2 - 2\alpha_3)]^* \\ & * [D_5^2 + D_6^2 + D_7^2 + D_8^2 + 2(D_5D_7 + D_6D_8) \cos 2\alpha_2 \\ & + 2(D_5D_6 + D_7D_8) \cos 2\alpha_3 + 2D_5D_8 \cos(2\alpha_2 + 2\alpha_3) \\ & + 2D_6D_7 \cos(2\alpha_2 - 2\alpha_3)]^{-1} \end{aligned} \quad (1.13)$$

where  $D_K$  are defined by (1.10). Note that all parameters in the above equations are dimensionless.

The reflection coefficient  $\beta$  is a function of the frequency  $\omega$  propagation speeds  $c_1$  and  $c_2$  (speeds  $c_0$  and  $c_3$  are fixed) and thicknesses  $h_1, h_2$ ,  $\beta = \beta(\omega, c_1, c_2, h_1, h_2)$ .

In order to find for a fixed frequency  $\omega$  the minimum value of  $\beta$ , the partial derivatives of the function (1.13) with respect to  $c_1, c_2, h_1$  and  $h_2$  must be calculated and put equal to zero. Then the speeds  $c_1, c_2$ , thicknesses  $h_1$  and  $h_2$  and value of the minimum reflection coefficient  $\beta$  may be calculated. The corresponding system of trigonometric equations is very complex and no satisfactory analytic treatment of the equations may be expected.

In the much easier special case of one layer only there exists the following solution. Take the propagating speed in the matching layer equal to the geometric mean of the two other speeds. Take the layer thickness equal to a quarter of the wave length  $2\pi c_1/\omega$  in this layer,

$$c_1 = \sqrt{c_0 c_3}, \quad h_1 = c_1 \frac{\pi}{2\omega}, \quad h_2 = 0, \quad c_2 = \text{arbitrary} \quad (1.14)$$

From the relations (1.12), (1.13) it follows that for the above data

$$\beta_s = 0 \quad (1.15)$$

Note that this result was obtained only for a monochromatic wave. In the applications the situation is more involved, since the real pulse is never monochromatic. In [5] and [6] attempts were made to match the impedances for wide-band pulse using two different layers. In the next chapter such optimization will be provided for wide-band spectrum corresponding to two different short acoustic pulses.

## 2. Wide-band pulse

Consider the case, when the ultrasound wave passes from a material of high impedance into a material of low impedance. In the typical biological applications the impedances are 30 and 1.5, respectively, [4]. The incident wave reflects partially on the biological inhomogeneities. The reflected wave carries the information

concerning the structure of the examined object. The reflected wave may be properly detected if no other wave arrives simultaneously at the experimentator. Therefore, at the instant when the reflected wave arrives to the measuring device, the incident wave must be already terminated. This fact forces the experimentator to produce in medium 0 very short pulses, e.g. four perioses of the sine curve only. Typical pulse used in ultrasonics is

$$u(t) = \begin{cases} 0 & \text{for } t < 0, \\ \sin \omega_0 t & \text{for } 0 > t < N2\pi/\omega_0 \\ 0 & \text{for } t > N2\pi/\omega_0, \end{cases} \quad (2.1)$$

where  $\omega_0$  is a certain fixed frequency, and  $N$  natural number,  $N=1, 2, 3, 4, \dots$ . In order to save space, consider here only even values of  $N$ ,  $N=2n$ .

Time shift transforms the function (2.1) into the odd function of time

$$u(t) = \begin{cases} 0 & \text{for } t < -n2\pi/\omega_0, \\ \sin \omega_0 t & \text{for } -n2\pi/\omega_0 < t < n2\pi/\omega_0, \\ 0 & \text{for } t > n2\pi/\omega_0. \end{cases} \quad (2.2)$$

Since the medium is nondispersive, the pulse propagates with speed  $c_0$  in the medium 0 without change of the profile and duration (but in media 1, 2 and 3 it has another profile). The time-dependent displacement in medium 0 is therefore

$$u(x, t) = \begin{cases} 0 & \text{for } t < x/c_0 - 2\pi n/\omega_0, \\ \sin \omega_0 (t - x/c_0) & \text{for } x/c_0 - 2\pi n/\omega_0 < t < x/c_0 + 2\pi n/\omega_0 \\ 0 & \text{for } t > x/c_0 + 2\pi n/\omega_0. \end{cases} \quad (2.3)$$

This motion is not the monochromatic harmonic wave.

Apply the Fourier sine transform to the odd function  $f(t)$

$$f(t) = \int_0^{\infty} I(\omega) \sin \omega t d\omega, \quad I(\omega) = \frac{2}{\pi} \int_0^{\infty} f(t) \sin \omega t dt. \quad (2.4)$$

If  $N$  is odd, then  $u(t)$  after time shift is an even function of time, and the cosine Fourier transform must be applied. If  $N$  is not an integer, then the exponential Fourier transform must be applied. However, this case is not interesting, since such displacement is not a continuous function of time. The formula (2.4) allows us to represent the founction  $f(t)$  in form of a sum of harmonic waves.

For the function (2.2) the spectral intensity  $I(\omega)$  may be calculated from the formula

$$I(\omega) = \frac{2}{\pi} \int_0^{2\pi n/\omega_0} \sin \omega_0 t \sin \omega t dt. \quad (2.5)$$

The integration is elementary. Figure 2 a gives the intensity  $I(\omega)$  for  $N=4$  the pulse consisting of four perioses of the sine function.

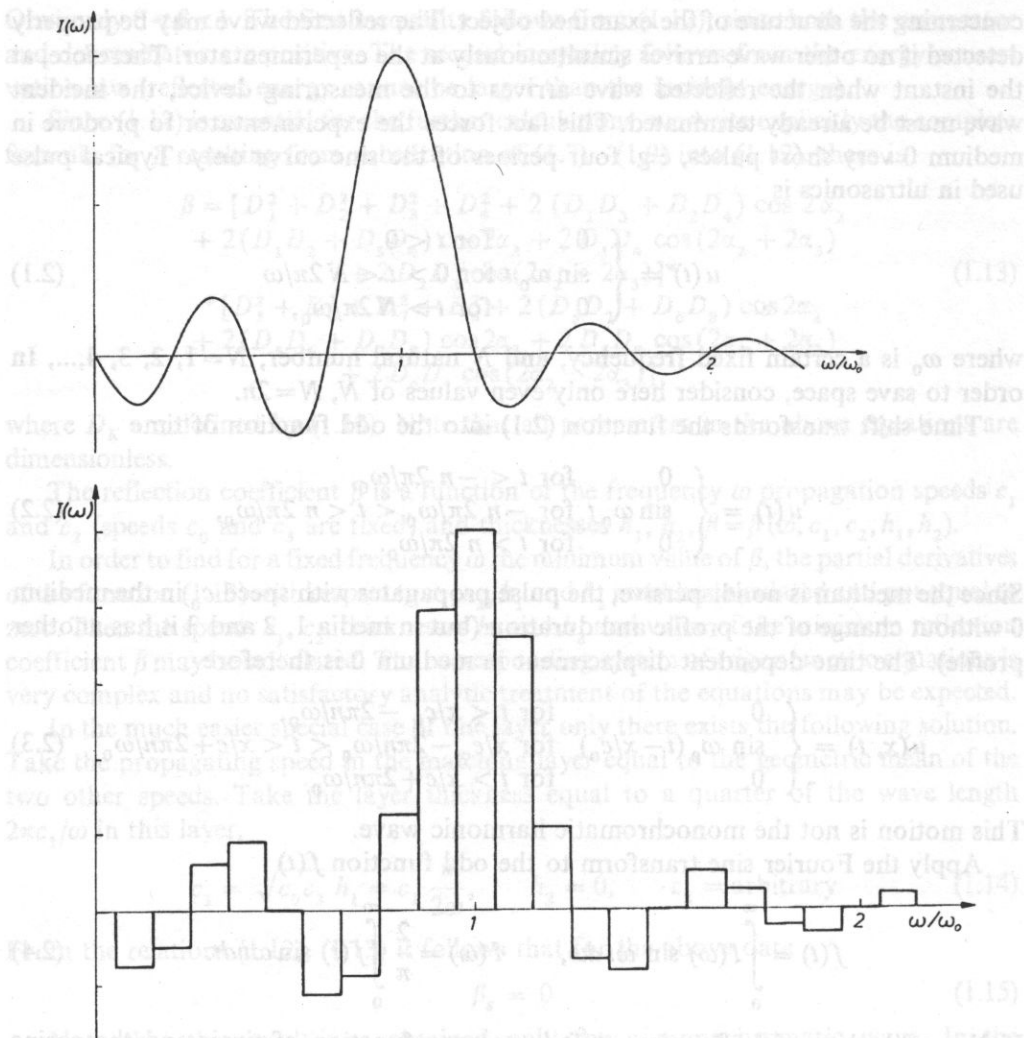


Fig. 2.

Consider first the case  $N=4$ ,  $n=2$ , represented in Fig. 2. With the accuracy sufficient for our purposes, the function  $f(t)$  may now be represented as a sum of 18 sinusoidal terms

$$\begin{aligned}
 f(t) = & - .60 \sin (.1\omega_0 t) - .38 \sin (.2\omega_0 t) + .41 \sin (.3\omega_0 t) + \\
 & + .71 \sin (.4\omega_0 t) - .94 \sin (.6\omega_0 t) - .73 \sin (.7\omega_0 t) + 1.03 \sin (.8\omega_0 t) + \\
 & + 3.18 \sin (.9\omega_0 t) + 4.00 \sin (\omega_0 t) + 2.89 \sin (1.1\omega_0 t) + .86 \sin (1.2\omega_0 t) + \\
 & - .55 \sin (1.3\omega_0 t) - .64 \sin (1.4\omega_0 t) + 4.0 \sin (1.6\omega_0 t) + .20 \sin (1.7\omega_0 t) + \\
 & - .17 \sin (1.8\omega_0 t) - .24 \sin (1.9\omega_0 t) + .16 \sin (2.1\omega_0 t),
 \end{aligned} \quad (2.6)$$

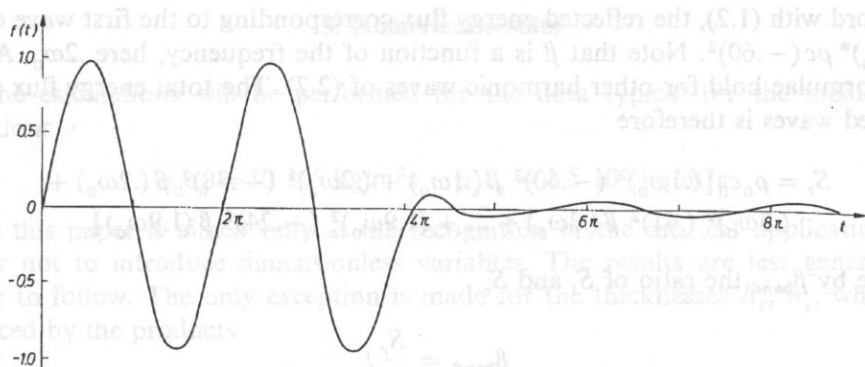


Fig. 3.

The above function corresponds to the intensity  $I(\omega)$  shown in Fig. 2b. It is the approximation of the smooth intensity shown in Fig. 2a. Obviously  $f(-t) = f(t)$ , as demands by (2.2). Figure 3 shows the function  $f(t)$  calculated from (2.4). Each of the harmonic motions of (2.6) results in the medium 0 in a harmonic monochromatic wave. The time-dependent displacement in medium 0 equals therefore the sum of 18 monochromatic waves

$$u(x, t) = -.60 \sin \{ .2\omega_0 (t - x/c_0) \} - .38 \sin \{ .2\omega_0 (t - x/c_0) \} \quad (2.7) \\ + .41 \sin \{ .3\omega_0 (t - x/c_0) \} + .71 \sin \{ .4\omega_0 (t - x/c_0) \} + \dots \\ -.17 \sin \{ 1.8\omega_0 (t - x/c_0) \} - .24 \sin \{ 1.9\omega_0 (t - x/c_0) \} + .16 \sin \{ 2.1\omega_0 (t - x/c) \},$$

Instead of the non-harmonic pulse (2.1), we face now the superposition of 18 harmonic waves of different frequencies  $.1\omega_0, .2\omega_0, .3\omega_0, \dots, 2.1\omega_0$  being the fractions of the center frequency  $\omega_0$ . The waves of frequency much larger than the center frequency  $\omega_0$  have very small amplitudes. For each such wave we may apply the formulae derived in the first chapter.

Since each of the separate waves of (2.7) propagates and reflects independently from the others, the energy flux is the sum of individual energy fluxes. Take first into account the first wave of (2.7), namely the wave  $-.60 \sin \{ .1\omega_0 (t - x/c_0) \}$  of frequency  $.1\omega_0$ . It carries the energy flux  $\rho_0 c_0 (.1\omega_0)^2 (-.60)^2$ . The energy flux is a function of time and space. The above formula should be understood as giving the average value for one period. In electrical engineering it corresponds to resistive load and the real power. The part corresponding to reactive load has zero mean value and is not taken into account. In acoustics it corresponds to the sound intensity. The second wave carries the energy flux  $\rho_0 c_0 (.2\omega_0)^2 (-.38)^2$ . Analogous energies are carried by the other waves. It follows that the total energy flux of all incident waves is given by the formula

$$S_i = \rho_0 c_0 [ (.1\omega_0)^2 (-.60)^2 + (.2\omega_0)^2 (-.38)^2 \quad (2.8) \\ + (.3\omega_0)^2 (.41)^2 + \dots + (1.9\omega_0)^2 (-.24)^2 ].$$

In accord with (1.2), the reflected energy flux corresponding to the first wave equals  $\beta(.1\omega_0)^* \rho c (-.60)^2$ . Note that  $\beta$  is a function of the frequency, here  $.2\omega_0$ . Analogous formulae hold for other harmonic waves of (2.7). The total energy flux of the reflected waves is therefore

$$S_r = \rho_0 c_0 [(.1\omega_0)^2 (-.60)^2 \beta(.1\omega_0) + (.2\omega_0)^2 (-.38)^2 \beta(.2\omega_0) + (.3\omega_0)^2 (.41)^2 \beta(.3\omega_0) + \dots + (1.9\omega_0)^2 (-.24)^2 \beta(1.9\omega_0)]. \quad (2.9)$$

Denote by  $\beta_{\text{band}}$  the ratio of  $S_r$  and  $S_i$ ,

$$\beta_{\text{band}} = \frac{S_r}{S_i}. \quad (2.10)$$

This is the effective reflection coefficient for the pulse (2.1)

In the next chapter we shall perform the calculations for the short pulse  $N=2$ , Fig. 4. The function  $I(\omega)$  is wider and has a lower maximum than that shown in Fig. 2a. The relation analogous to (2.5) corresponding to this pulse consists of 22 following terms:

$$\begin{aligned} f(t) = & -.07 \sin(.1\omega_0 t) - .63 \sin(.2\omega_0 t) - .66 \sin(.3\omega_0 t) + \quad (2.11) \\ & -.44 \sin(.4\omega_0 t) + .58 \sin(.6\omega_0 t) + 1.19 \sin(.7\omega_0 t) + 1.68 \sin(.8\omega_0 t) + \\ & + 1.97 \sin(.9\omega_0 t) + 2.00 \sin(\omega_0 t) + 1.78 \sin(1.1\omega_0 t) + 1.38 \sin(1.2\omega_0 t) + \\ & + .88 \sin(1.3\omega_0 t) + .39 \sin(1.4\omega_0 t) - .24 \sin(1.6\omega_0 t) - .32 \sin(1.7\omega_0 t) + \\ & -.27 \sin(1.8\omega_0 t) - .14 \sin(1.9\omega_0 t) + .11 \sin(2.1\omega_0 t) + .16 \sin(2.2\omega_0 t) + \\ & -.14 \sin(2.3\omega_0 t) + .08 \sin(2.4\omega_0 t). \end{aligned}$$

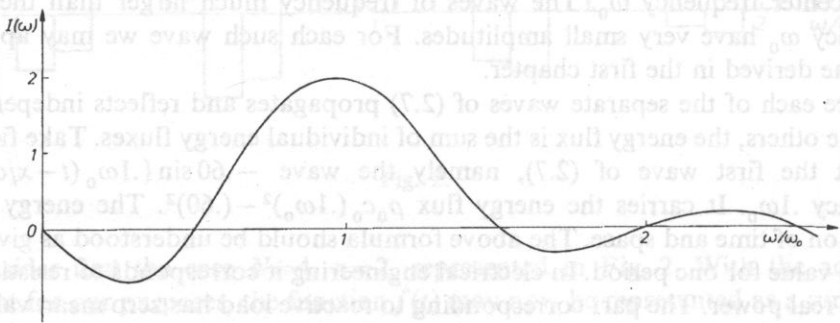


Fig. 4.

Numerical summation similar to that presented in Fig. 3 for (2.5) proves that the above formula provides sufficiently good approximation for the calculation of optimal matching layers.

### 3. Numerical results

The calculations will be performed for the data typical for the medical applications

$$\rho_0 c_0 = 30 \cdot 10^6 \text{ kg/m}^2\text{s}, \quad \rho_3 c_3 = 1.5 \cdot 10^6 \text{ kg/m}^2\text{s} \quad (3.1)$$

Since this paper is aimed only at the recognition of the medical applications, we prefer not to introduce dimensionless variables. The results are less general, but easier to follow. The only exception is made for the thicknesses  $h_1, h_2$ , which are replaced by the products

$$H_1 = \omega_0 h_1, \quad H_2 = \omega_0 h_2. \quad (3.2)$$

Let us start with the pulse consisting of four periods of the sine curve. The matching layer (1.14) is

$$(c_1)_S = 6.7082 \cdot 10^6 \text{ m/s}, \quad (H_1)_S = 10.532 \text{ m/s}. \quad (3.3)$$

If the wave is monochromatic of frequency  $\omega_0$ , then the reflection coefficient  $\beta_S$  for this wave equals zero. However, for the pulse represented in Fig. 3, the reflection coefficient for the layer (3.3) calculated from (2.7)–(2.9) is not zero,

$$\beta_S = .10931. \quad (3.4)$$

This is not a minimum even for one layer. A slightly better result may be obtained for other thicknesses and propagation speed,

$$(c_1)_m = 6.7091 \cdot 10^6 \text{ m/s}, \quad (H_1)_m = 10.34 \text{ m/s}, \quad \beta_m = .10695. \quad (3.5)$$

This is the wide-band minimum for one layer.

In order to find two layers leading to lower  $\beta$ , the numerical analysis of (2.9) was performed. There exist many minima, but only some of them are interesting. For

$$\begin{aligned} c_1 &= 12.7 \cdot 10^6 \text{ m/s}, & H_1 &= .172 \text{ m/s}, \\ c_2 &= 3.30 \cdot 10^6 \text{ m/s}, & H_2 &= .043 \text{ m/s}, \end{aligned} \quad (3.6)$$

there exists a minimum

$$\beta = .03023 \quad (3.7)$$

It is more than three times lower than  $\beta_S$ , as given by (3.4), or than  $\beta_m$ , as given by (3.5)

Essential for the possibility of manufacturing the two layers (3.5) is the knowledge of the neighbourhood of the minimum. If the values of  $\beta$  near the point (3.5) are high, then it would be rather difficult to achieve value of  $\beta$  close to (3.6). Figure 5 shows the map of points  $c_1, c_2$  for which  $.035 < \beta < .040$  provided  $H_1, H_2$  are fixed. The ovals are centered at (3.5). The length of the horizontal line represents propagation speed of  $10^6 \text{ m/s}$ .

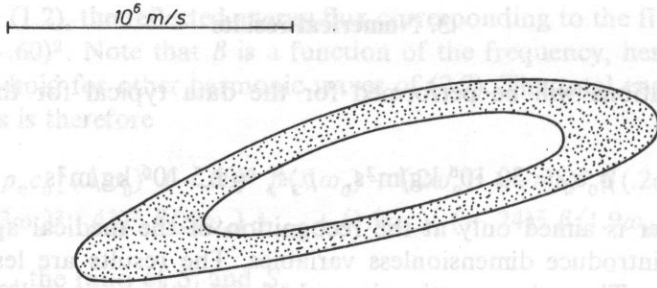


Fig. 5.

It is interesting to note there exists another minimum, situated far from the minimum (3.6)

$$\begin{aligned} c_1 &= 7.79 \cdot 10^6 \text{ m/s}, & H_1 &= .120 \text{ m/s}, \\ c_2 &= 2.04 \cdot 10^6 \text{ m/s}, & H_2 &= .159 \text{ m/s}. \end{aligned} \quad (3.8)$$

$$\beta = .07195. \quad (3.9)$$

This minimum is not so low as that given by (3.7). Note that the thicknesses of the layers are of the same order. In some situations this fact may simplify the manufacturing process. The reflection coefficient  $\beta$ ,  $.0775 < \beta < .0875$  occupies the area between the two ovals, Fig. 6. Inside the inner oval the reflection coefficient

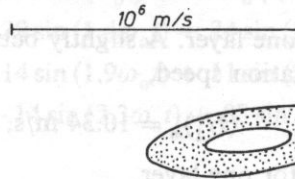


Fig. 6.

satisfies the inequality  $\beta < 0.7775$ . Both ovals are centered at (3.8), the horizontal line represents  $10^6$  m/s. Note that the minimum is wide, therefore no extra accuracy is needed for manufacturing the layers.

Two examples of technically uninteresting minima are

$$\begin{aligned} c_1 &= 11.24 \cdot 10^6 \text{ m/s}, & H_1 &= 50.86 \text{ m/s}, \\ c_2 &= 3.25 \cdot 10^6 \text{ m/s}, & H_2 &= 15.19 \text{ m/s}. \end{aligned}$$

$$\beta = .12676.$$

This minimum is local minimum of the reflection coefficient. Note that its value is larger than  $\beta_s$ , as given by (3.4). A very narrow minimum exists at

$$\begin{aligned} c_1 &= 6.70 \cdot 10^6 \text{ m/s}, & H_1 &= 10.20 \text{ m/s}, \\ c_2 &= 17.50 \cdot 10^6 \text{ m/s}, & H_2 &= .114 \text{ m/s}. \end{aligned}$$

$$\beta = .10726.$$

Pass now to the very short pulse consisting of two periods only,  $N=2$ ,  $n=1$ . In accord with the spectral decomposition Fig. 4, we base on the formula (2.11). The matching layer (1.14) coincides with that given by (3.3), since it is determined by the central frequency  $\omega_0$ , and is independent of the distribution of frequencies in the band. The wide-band pulse (2.11) reflecting on the layer (1.14) has the reflection coefficient

$$\beta_s = .21918. \quad (3.10)$$

The value of  $\beta$  is slightly smaller for the following single layer, namely

$$(c_1)_m = 6.710 \cdot 10^6 \text{ m/s}, \quad (H_1)_m = 9.914 \text{ m/s}, \quad \beta_m = .20546. \quad (3.11)$$

This is the wide-band minimum for one layer. Note that both (3.3) and (3.11) give layers slightly thicker than  $(H_1)_s$ , and propagation speeds slightly lower than  $(c_1)_s$

The formula (2.10) leads to the conclusion that at

$$\begin{aligned} c_1 &= 13.25 \cdot 10^6 \text{ m/s}, & H_1 &= .198 \text{ m/s}, \\ c_2 &= 3.37 \cdot 10^6 \text{ m/s}, & H_2 &= .0506 \text{ m/s}, \end{aligned} \quad (3.12)$$

there exists a minimum

$$\beta = .05961. \quad (3.13)$$

$10^6 \text{ m/s}$

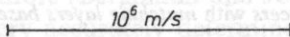
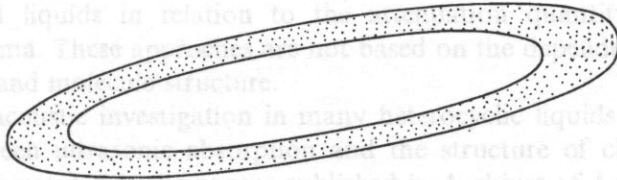



Fig. 7.

$10^6 \text{ m/s}$

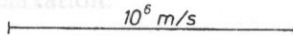
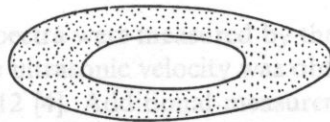



Fig. 8.



Figure 7 shows the map of values  $c_1, c_2$  corresponding to  $0.65 < \beta < 0.7$ . It is seen that the valley is rather wide. At the point

$$\begin{aligned} c_1 &= 8.36 \cdot 10^6 \text{ m/s}, & H_1 &= .125 \text{ m/s}, \\ c_2 &= 2.31 \cdot 10^6 \text{ m/s}, & H_2 &= .217 \text{ m/s}. \end{aligned} \quad (3.14)$$

there exist another minimum

$$\beta = .1770. \quad (3.15)$$

The valley corresponding to this minimum is rather narrow. The values  $.180 < \beta < .185$  are situated between the two ovals, Fig. 8. Note that the gain due to the second layer is larger for the short pulse.

### References

- [1] Z. WESOŁOWSKI, On the dynamics of the transition region between two homogeneous materials, *J. Tech. Phys.*, **32**, 2, 293–312 (1991).
- [2] Z. WESOŁOWSKI, Symmetry of dynamic properties of a set of elastic layers, *Arch. Mech.*, **39**, 261–267 (1987).
- [3] Z. WESOŁOWSKI, *On the transition zone between two homogeneous materials*, *Acta Mechanica* (in print).
- [4] C.S. DESILETS, J.D. FRASER, G.S. KINO, *The design of efficient broad-band piezoelectric transducers*, *IEEE Trans. Sonics and Ultrasonics*, SU-25, 113–125 (May 1978).
- [5] G. ŁYPACEWICZ, E. DURIASZ, *Design principles of transducers with matching layers based on admittance measurements*, *Arch. Acoustics*, **17**, 1, 117–131 (1992).
- [6] J. SOUQUET, P. DEFRANOUUD, J. DESBOIS, *Design of low-loss wide-band ultrasonic transducers for noninvasive medical application*, *IEEE Trans. Sonics and Ultrasonics*, SU-26, 75–81, March 1979.

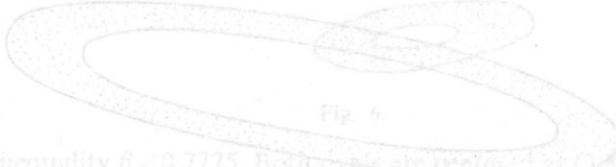


Fig. 6

satisfies the inequality  $\beta < 0.7775$ . Both ovals are centered at  $(0, 0)$ , the horizontal line represents  $10^6$  m/s. Note that the minimum is wide, therefore an extra accuracy is needed for manufacturing the layers.

Two examples of technically uninteresting minima are

$$\begin{aligned} c_1 &= 11.24 \cdot 10^6 \text{ m/s}, & H_1 &= 50.86 \text{ m/s}, \\ c_2 &= 3.25 \cdot 10^6 \text{ m/s}, & H_2 &= 15.19 \text{ m/s}. \end{aligned}$$

$$\beta = .12676.$$

This minimum is local minimum of the reflection coefficient. Note that its value is larger than  $\beta_{12}$  as given by (3.4). A very narrow minimum exists at

$$\begin{aligned} c_1 &= 2.0 \cdot 10^6 \text{ m/s}, & H_1 &= 10.20 \text{ m/s}, \\ c_2 &= 17.50 \cdot 10^6 \text{ m/s}, & H_2 &= .114 \text{ m/s}. \end{aligned}$$

$$\beta = 0.18716.$$

## INFLUENCE OF THE MOLECULAR STRUCTURE ON ACOUSTIC ABSORPTION IN THE GROUP OF SATURATED KETONES

B.B.J. LINDE AND A. ŚLIWIŃSKI

Institute of Experimental Physics  
University of Gdańsk  
(80-952 Gdańsk, Wita Stwosza 57)

The results of acoustic investigation into some heterocyclic liquids showed very close relation between ultrasonic absorption and structure of chemical molecules [1, 2, 3].

### 1. Introduction

Many authors (Bergmann and Jeansch, Parthasaraty, Rao, Lagemann, Schaaffs and Sette) very accurately determined relations between the velocity of ultrasonic waves and liquid molecules structure, but there are no systematic papers concerned with the relationship between the absorption and molecular structure. Three authors only have classified liquids in relation to the attenuation quantity: Pinkerton, Michajłow and Verma. These approaches are not based on the dependences between sound attenuation and molecule structure.

The results of acoustic investigation in many heterocyclic liquids showed very close relation between ultrasonic absorption and the structure of chemical compounds and it was presented in the papers published in Archives of Acoustics [2, 3].

On the basis of own investigation, concerning absorption in cyclic compounds with a carbonyl group, certain strict relation between acoustic absorption and the structure of molecule was also established. In this paper we tried to explain relation as a result of isomeric relaxation.

### 2. Experiment

The ultrasonic absorption spectra were measured by the ultrasonic pulse method from 10 to 180 MHz [4] and the ultrasonic velocity was obtained using an ultrasonic pulse-phase interferometer UI-12 [4]. Additional measurements of the viscosity by means of the ultrasound viscosimeter UNIPAN 505 A were performed in order to calculate the classical absorption coefficient. All acoustic measurements were perfor-

med in the temperature range from 253 to 313 K with the accuracy of 0.05 K. The temperature was stabilized by a U — 10 ultrathermostat.

The estimated errors of determining the absorption coefficient are contained in the range from 3.5 to 5%.

### 3. Results and discussion

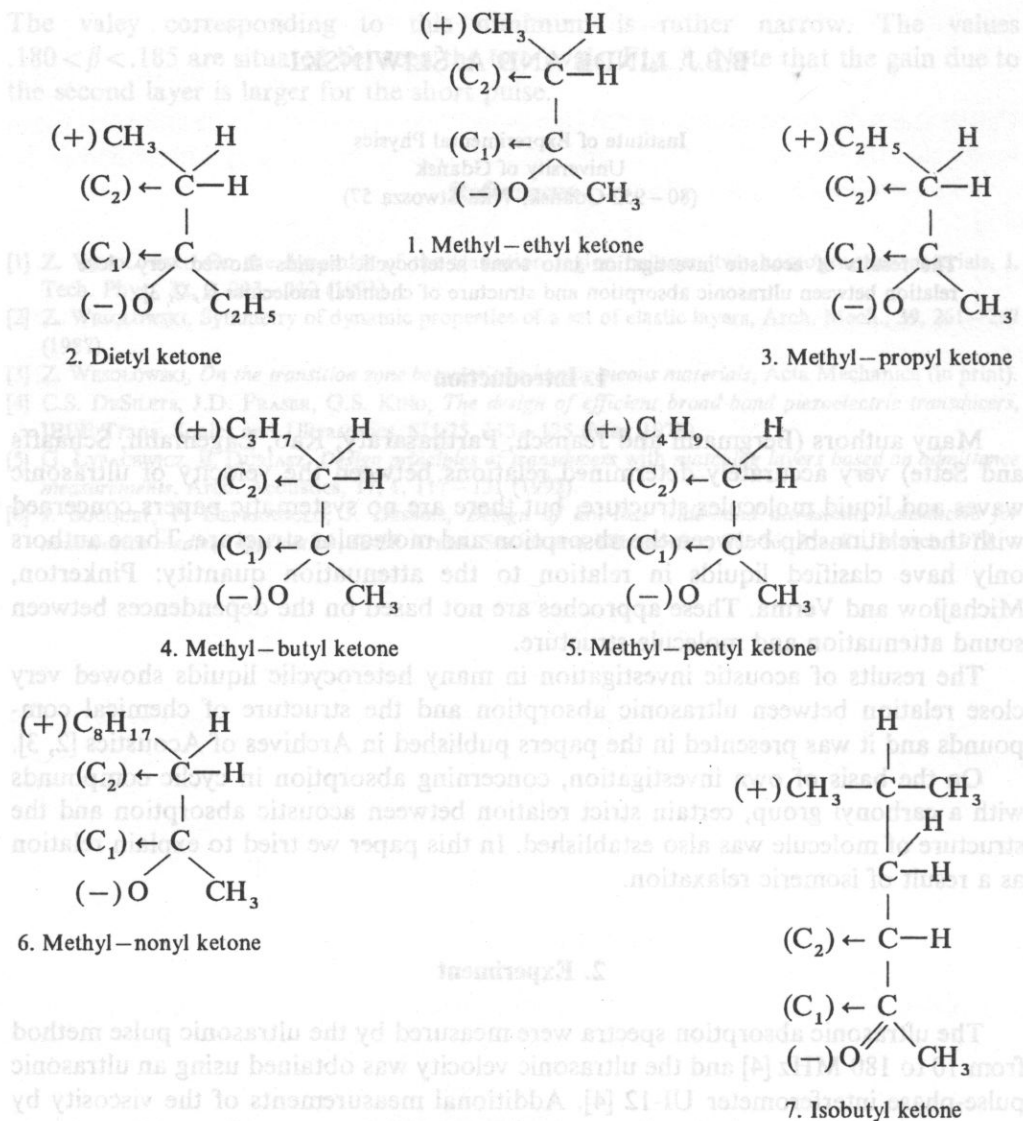


Fig. 1. Chemical structures of the measured ketones.

Seven different ketones have been subject to ultrasonic investigations, volume viscosity, classical absorption and thermal coefficients of absorption and ultrasonic velocity of the ketones have been calculated (Table 1 and 2)

$$\left(\frac{\alpha}{f^2}\right)_{kl} = \frac{8\pi^2\eta_s}{3\rho c^3} \quad \eta_v = \frac{4}{3}\eta_s \frac{\frac{\alpha}{f^2} - \left(\frac{\alpha}{f^2}\right)_{kl}}{\left(\frac{\alpha}{f^2}\right)_{kl}} \quad (3.1)$$

Table 1

Ketone	$\frac{\alpha}{f^2} 10^{-15} [s^2m^{-1}]$	$\frac{\Delta v}{\Delta T} [ms^{-1}K^{-1}]$	$\frac{\Delta\alpha}{f^2\Delta T} [s^2m^{-1}K^{-1}]$	$C [ms^{-1}]$
1	29,0	-5,4	-0,2	1193,6
2	31,9	-	-	1235,5
3	33,0	-3,97	-0,25	1238,1
4	35,4	-	-	1248,5
5	41,6	-4,22	-0,41	1284,4
6	66,0	-2,1	-1,06	1379,6
7	68,2	-	-	1211,4

No relaxation region in all the liquids considered in the measured frequency range exists. The dependence of ultrasonic absorption on the frequency can be described by a linear relation

$$y = ax + b \quad \text{with } a = 0 \quad (3.2)$$

However, the calculated classical absorption coefficients and volume viscosities (Table 2) suggest that in all compounds the relaxation process should exist [5, 6, 7]. The experimental absorption coefficients are several times higher than the classical ones, and shear viscosity of the ketones are 3 to 8 times lower than the volume viscosity (Table 2).

It is evident that the relaxation times of these processes in the liquids are shorter than  $10^{-9}$  s.

In this group of compounds the relationship between the ultrasonic absorption and the structure of molecules is visible. The absorption increases with increasing the

Table 2

$\left(\frac{\alpha}{f^2}\right) \times 10^{15} [s^2m^{-1}]$	Methyl-propyl ketone	Methyl-pentyl ketone
	33.0	41.6
$\left(\frac{\alpha}{f^2}\right)_{kl} \times 10^{15} [s^2m^{-1}]$	10.5	5.2
$\rho \times 10^3 [kG m^{-3}]$	0.809	0.815
$\eta_s \times 10^{-2} [P]$	0.62	1.23
$\eta_v \times 10^{-2} [P]$	1.77	9.28
$\frac{\eta_v}{\eta_s}$	2.8	7.6

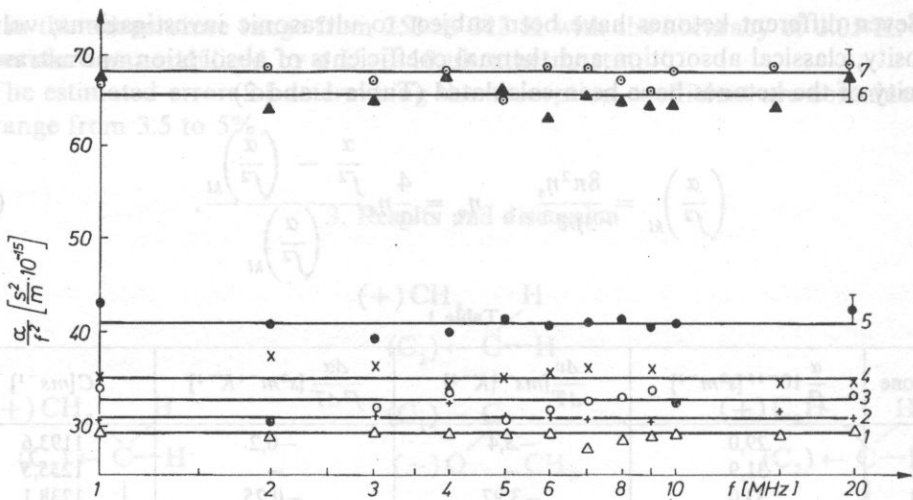


Fig. 2. Ultrasonic attenuation in the group of ketones absorption at 293 K. The numbering of the curves is the same as in Fig. 1.

chain-length of the ketones. This relation is opposite to that observed in heterocyclic compounds (Fig. 2).

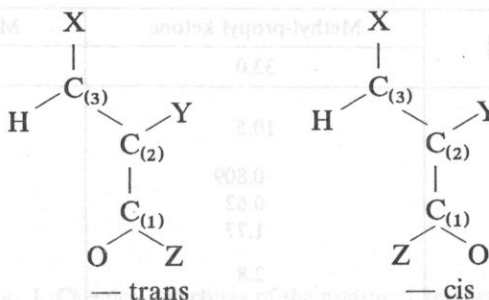
It is not possible to explain the relation in the same way. It means that the absorption is not caused by Kneser processes, and that the Herzfeld formula

$$\left(\frac{\alpha}{f^2}\right)_{\text{rel}} = \frac{\alpha}{f^2} - \left(\frac{\alpha}{f^2}\right)_{\text{kl}} = \frac{2\pi^2\tau}{c} \frac{C_i(C_p - C_v)}{C_p C_v} = A \quad (3.3)$$

is not useful in that case.

The calculated thermal coefficients of absorption are negative (Table 1), what suggests that the rotational isomerism is responsible for the absorption [6, 8], and for such compounds as it was predicted by YOUNG and PETRAUSKAS [9], the contributions of absorption due to shear viscosity, heat conduction etc. are negligible when compared to the absorption due to rotation of molecules.

In saturated ketones



there are no electrical forces and charge-conjugation between  $\pi$ -electrons of double bonds, then rotational barrier around the  $C_{(1)}-C_{(2)}$  bond is not high. Acoustic absorption is then small and relaxation time shorter than that in unsaturated ketones. The relaxation region is possible in higher frequency range or at lower temperature.

In such compounds as ketones there are effects of electrical attraction between the partially negatively charged oxygen and the partially positively charged  $C_{(3)}$ . In these compounds the cis-conformation is favoured. The exchange of methyl group for propyl-, etc. grows the quantity of protons (positive charge) close to  $C_{(3)}$  and should strengthen the conjugation of the  $C_{(1)}-C_{(2)}$  bond and hence increase the rotational barrier and acoustic absorption as well what has appeared in the experiment.

#### 4. Conclusion

All the relations founded in saturated ketones are similar for unsaturated ones [6], but because the conjugation is absent, in saturated ketones, the relaxation time is much shorter and the absorption lower for frequency range. These relations for saturated compounds do not manifest so clearly thus it is much more difficult to notice their presence.

#### References

- [1] B. LINDE, M. KOSMOL and A. ŚLIWIŃSKI, *Determination of the influence of liquid molecule structure on acoustic absorption quantity*, Archives of Acoustics, **11**, 4, 353–383 (1986).
- [2] B. LINDE, and A. ŚLIWIŃSKI, *Ultrasound absorption dependence on molecular structure of benzene-similar compounds*, Proc. of the XXIV Congress of the Polish Physical Society, 102–103 Toruń 1979.
- [3] B. LINDE and A. ŚLIWIŃSKI, *Methyl group influence on ultrasound absorption in benzene-similar liquids*, Proc. of the XXIV OSA 439–442, Wrocław 1979.
- [4] J. WEHR, *Pomiary prędkości i tłumienia fal ultradźwiękowych*, PWN, Warszawa 1972.
- [5] A.J. MATHESON, *Molecular acoustics*, Wiley-Interscience, London–Toronto 1971.
- [6] W. MASON, *Physical acoustics*, vol. VII part A, Academic Press, New York–London 1965.
- [7] V.F. NOZDRIEV, *Molekularnaya akustika*, Izd. Vyshaya Shkola, Moskva 1974.
- [8] M.S. DE GROT, *Ultrasonic relaxation due to rotational isomerism*, N.V. Drukkorij V/H J.J. Groen, Leiden 1958.
- [9] S.K.KOR and A.K. SRIVATSAVA, *Ultrasonic absorption due to rotational isomerism*, Acustica, **49**, 1, 84–86 (1981).

## DETERMINATION OF DYNAMIC PROPERTIES OF SINTERED COPPER POWDER FROM ULTRASONIC MEASUREMENTS

J. LEWANDOWSKI

Institute of Fundamental Technological Research  
Polish Academy of Sciences  
(00-049 Warszawa, Świętokrzyska 21)

The overall (effective) dynamic properties of sintered copper powder with air-saturated pores at moderate porosities are deduced from suitable ultrasonic measurements carried out at low porosities in the long-wavelength approximation. The effective dynamic properties of the two-phase composite at low and moderate porosities are analysed computationally, the properties of the pure matrix material being in the first step determined by extrapolation from suitable ultrasonic measurements carried out at low porosities, and by employing the Berryman's self-consistent single scattering theory. The presented results confirm the ultrasonic measurements to be extremely useful in estimating the influence of the volume concentration and shape of the inclusions on the overall dynamic properties of porous two-phase composites at porosities from a wide range of porosity.

**KEYWORDS:** ultrasonics, porous composite, inclusion shape

### 1. Introduction

One of the main objectives of material science of random composites is the formulation of stress-deformation relations that govern the mechanical response of a material under specific environmental conditions (loading). In the approximation of the linear elasticity theory, these relations can be written when the effective Lamé constant are known. Therefore, predicting the effective Lamé constants of macroscopically isotropic composites is of great engineering importance. The subsequent considerations are confined to this case and concerned with bulk samples of an isotropic two-phase solid. The inclusions are of the form of ellipsoidal pores with the same shape, and random size and orientation, the pores being air saturated or evacuated.

This paper grew out of the analysis, which the author performed to prepare the paper [1] for publication. In Ref. [1], for the sake of brevity the emphasis in the presentation of the results of analysis is laid on the propagation properties of sintered copper powder rather than on the overall dynamic properties. Due to the

limitation in the desired size of this volume, it was decided that the concluding sections of the text concerned with the investigations of the dynamic properties should be presented as a supplementary article.

Because of the great engineering importance of the problem, there are numerous works devoted to the ultrasonic technique as a tool for the determination of the effective dynamic moduli of sintered metal powders. Therefore, it seems to be reasonable to point out the main reason which, in our opinion, justifies presenting the subsequent study as another paper concerned with the problem mentioned above.

According to the simple two-phase model, which is commonly used for the prediction of the elastic behaviour of a sintered metal powder, such a material is regarded as consisting of a solid matrix with the properties of a pure metal, in which inclusions are dispersed in the form of voids. Therefore, in such approach the matrix phase is treated in the linear acoustic approximation as a perfectly elastic material with the real elastic moduli of the pure lossless metal. In this model, the matrix subdomains are regarded to be filled by a material which is free from both inelasticity (dissipation properties) and scattering centres. The apparent sensitivity of the velocity and attenuation of ultrasonic waves propagating through such a medium, to the changes in the inclusion shape is discussed and analysed for non-spherical inclusions, to some more or less limited extent, in such papers as [1-6].

The assumptions of the simple two-phase model are in contradiction to the really existing inelasticity in the matrix phases of the sintered metal powders, the inelasticity being mainly due to the lattice defects, impurities and some distributions of residual local stresses and imperfect adhesion between adjacent metal grains. These randomly occurring flaws contribute to highly variable scattering and dissipation properties of the matrix material and causes that the observed components of the Hooke's tensor are complex.

This paper presents an attempt of applying a more complicated model of two-phase media proposed by the author in the paper [1] to the determination of the effective dynamic moduli of sintered metal powders. In this model, the complex elastic moduli of the matrix phase of the composite under study are to be determined from ultrasonic measurement of the propagation velocity and attenuation of ultrasonic waves in two samples of the composite, the samples being characterized by different and small volume concentrations of the inclusions. In the present work, the influence of the pore shape on the effective dynamic moduli of the composite is examined computationally with the aid of an algorithm supplied by the self-consistent scattering approach of BERRYMAN [4].

## 2. Formulation of the problem

As it was mentioned, the subsequent considerations are concerned with bulk samples of an isotropic two-phase (porous) solid of the form of sintered metal powder. The matrix material is composed of a large number of metal (copper) grains



of random size, shape and orientation, the adjacent grains being joined together more or less closely (perfectly) by adhesion due to the sintering process under high hydrostatic press. The imperfection of the adhesion between adjacent grains and the other matrix material flaws as well as the size and orientation of the pores with the same ellipsoidal shape are also assumed to be random, the pores being air-saturated or evacuated. Under these assumptions, the matrix material may also be regarded as an isotropic solid material, although its elastic moduli differ from those of the polycrystalline metal, and are to be determined experimentally from ultrasonic measurets in a manner mentioned above.

In the remainder of this paper, the standard abbreviations are used for the quantities involved in the description of the propagation of ultrasonic waves and the material parameters of the constituents of the heterogeneous material under study. Thus  $\omega$  and  $t$  denote the angular frequency and time, respectively,  $\rho$  stands for the density,  $C_{ijkl}$   $i, j, k, l=1, 2, 3$  denote the components of a Hooke's tensor  $K$  and  $\mu$  are the bulk and shear modulus, respectively, of an elastic isotropic solid.  $\lambda$  denotes the Lamé constant which is related to the moduli  $K$  and  $\mu$  by the following formula:

$$\lambda = K - \frac{2}{3}\mu. \quad (2.1)$$

The effective material parameters of the isotropic two-phase solid as a whole and all the other quantities referred to this material are labelled by asterisks, i.e.  $\rho^*$  denotes the effective density,  $K^*$ ,  $\mu^*$  and  $\kappa^*$  denote the effective elastic moduli of the heterogeneous solid. Similarly, throughout the paper all the abbreviations with the sub- or superscripts  $m$  and  $i$  denote quantities referred to the isotropic material of the matrix and inclusion, respectively. Similarly as in [1], the ultrasonic waves propagating through the two-phase medium are assumed to be plane linearly polarized waves, which can be described by the following formulae:

$$u(r, t)^* = \mathbf{e}_q B_{pq}^* \exp(-i K_{pq}^* \mathbf{e}_p \mathbf{r}) \exp(i\omega t), \quad (2.2)$$

where

$$K_{pq}^* = (\omega/v_{pq}^*) - i\alpha_{pq}^*, \quad p, q = 1, 2, 3, \quad (2.3)$$

$B_{pq}^*$  stands for the amplitude of the wave,  $\mathbf{e}_p$  and  $\mathbf{e}_q$  are the unit vectors in the directions of the  $Ox_p$  and  $Ox_q$  reference axes of a Cartesian coordinate system fixed in the sample, respectively. Formulae (2.2), (2.3) describe an attenuated plane wave being polarized in the direction  $\mathbf{e}_q$  and propagating in the direction  $\mathbf{e}_p$  with the velocity  $v_{pq}^*$  and amplitude attenuation coefficient  $\alpha_{pq}^*$ , henceforth referred to as attenuation coefficient.

Let us suppose that the velocity and attenuation coefficient are measured on ultrasonic pulses propagating through a single bulk sample of the two-phase composite under study, the pulses being generated by a transducer oscillating with the frequency  $\omega$  normally or transversly to the coupling surface. On the strength of the definition of the bulk volume, the vlume of the sample is large enough to include

a large number of inhomogeneities of each type occurring in the heterogeneous solid. Then it seems to be reasonable to suppose that the measured velocity and attenuation coefficient of the ultrasonic pulses are equal to the propagation velocity  $v_{pq}^*$  and attenuation coefficient  $\alpha_{pq}^*$  of the respective ultrasonic wave appearing in formulae (2.3)

If

$$v_{pq}^* = 1/Z^{*(a)}, \quad \alpha_{pq}^* = -\omega Z^{*(b)}, \quad Z^* = [\rho^*/C(\omega)_{pqpq}^*]^{1/2} \quad (2.4)$$

then the expression given by formulae (2.2), (2.3) is a solution to the following equation of motion for the effective homogeneous (equivalent) medium:

$$C(\omega)_{ijkl}^* u^*(r, t)_{kjl} + \omega^2 \rho^* u^*(r, t)_i = 0. \quad (2.5)$$

Throughout the paper, the real and imaginary parts of complex quantities are denoted by the superscripts (a) and (b), respectively. If the effective response of the bulk sample of the composite is a plane attenuated wave given by formulae (2.2)–(2.4), then the equivalent homogeneous solid is characterized by the density  $\rho^*$  and components of the complex Hooke's tensor,

$$C(\omega)_{jklm}^* = C(\omega)_{jklm}^{*(a)} + iC(\omega)_{jklm}^{*(b)}, \quad (2.6)$$

which can be calculated from the macroscopic propagation parameters  $v_{pq}^*$  and  $\alpha_{pq}^*$  of the wave, by making use of the following formulae:

$$C(\omega)_{pqpq}^*{}^{(a)} = B(1 - z^2), \quad C(\omega)_{pqpq}^*{}^{(b)} = 2Bz, \quad (2.7)$$

where

$$B = (v_{pq}^*)^2 \rho^* (1 + z^2)^{-2}, \quad z = (\alpha_{pq}^*/\omega) v_{pq}^*.$$

Formulae (2.7) are obtained by solving Eqs. (2.4) with respect to  $C(\omega)_{pqpq}^*{}^{(a)}$  and  $C(\omega)_{pqpq}^*{}^{(b)}$ ,  $p, q=1, 2, 3$ . Formulae (2.7) enable the effective complex moduli  $C(\omega)_{pqpq}^*{}^{(a)}$  and  $C(\omega)_{pqpq}^*{}^{(b)}$  to be determined from the measurements of the macroscopic parameters of the ultrasonic wave propagation,  $v_{pq}^*$  and  $\alpha_{pq}^*$ , in the composite bulk sample under examination. Thus Eqs. (2.2)–(2.7) suggest an experimental method of performing the task of establishing the structure and frequency dependences of the propagation and effective material parameters of two-phase media with non-spherical inclusions. More strictly speaking, in accordance with (2.4), the dependence of the effective material parameters on the volume concentrations of the matrix and inclusion phases  $c_m$  and  $c_i$ , respectively, and on size, shape and orientations of the inclusions as well as on the frequency can be determined empirically from ultrasonic measurements, after preparing the respective bulk samples. This task is regarded as the main problem of this paper.

Equations (2.5) together with formulae (2.4) show how the overall macroscopic response of the composite material to dynamic loading of a transducer oscillating with the frequency  $\omega$ , normally or transversely to the coupling surface, is determined by the effective material parameters. In view of that the dynamic effective material parameters are the essential parameters determining the utility of heterogeneous

materials in engineering applications. For this reason, every method which enables us to establish the structure and frequency dependence of these parameters is of great importance.

In contrast to the simplicity of the above macroscopic relationships, which suggest the experimental assessment of the structure and frequency dependences of the propagation and material parameters of two-phase media, in theoretical attempts of finding these dependences, problems of great complexity are always involved. The dynamics of the multi-phase media with non-spherical inclusions is so complicated that, for a wide range of the volume concentrations  $c_i$  of the inclusions, we would be content with performing a computational analysis of the problem of the propagation of ultrasonic waves in such media. The computational investigations, some results of which are presented in Ref. [1] and in the next section of this paper, enable us to establish the desired dependences. Similarly as in paper [1], in performing such numerical analysis we make use of the self-consistent approach proposed by BERRYMAN [4] for analysing  $N$ -phase media,  $N$  being a natural number. According to the Berryman's approach, the self-consistent effective (equivalent) medium is determined by requiring the net scattered, long-wavelength displacement field to vanish on the average.

On employing the results of MAL and KNOPOFF [8] as well as of WU [9] in the way that was presented in Ref. [1], BERRYMAN [4] arrived at an algorithm for computational investigation of mechanical properties of  $N$ -phase media with ellipsoidal inclusions. Considering the two-phase media with ellipsoidal inclusions, the Berryman's concept yields the algorithm (2.8) given below which is employed in our computational analysis

$$K^* = (c_i K_i P^{*i}) / (c_i P^{*i} + c_m P^{*m}), \quad (2.8)$$

$$\mu^* = (c_i \mu_i Q^{*i} + c_m \mu_m Q^{*m}) / (c_i Q^{*i} + c_m Q^{*m}).$$

The quantities  $P^*$  and  $Q^*$  can be expressed in terms of Wu's [9] tensor  $T$  in the following general form [4]:

$$P^* = \frac{1}{3} T_{ppqq}^*, \quad Q^* = \frac{1}{5} (T_{pqpq}^* - \frac{1}{3} T_{ppqq}^*), \quad (2.9)$$

where the formulae  $P$ ,  $Q$  and  $T$  derived by Wu [9] are also listed in the Appendix of [4]. These formulae will not be rewritten here.  $P^*$ ,  $Q^*$  and  $T^*$  denote expressions obtained from the formulae for  $P$ ,  $Q$  and  $T$ , after replacing the matrix material parameters by the respective parameters of the effective equivalent homogenous medium (material of type — \*)

Among those data which are required by computational methods are the material parameters of the matrix phase. The material parameters of the matrix phase (sintered metal grains) are to be determined from ultrasonic measurements. To point out this concept let us notice that equation (2.5), together with formulae (2.2)–(2.4), define the overall effective response of a bulk sample made of the

matrix material to the dynamic loading of the transducer, after replacing each of the asterisk by superscripts  $m$ . If the hypothesis of the possibility of finding the homogeneous equivalent medium is reasonable and the effective response of the bulk sample of the matrix material is a plane attenuated wave given by formulae (2.2)–(2.4), after replacing the superscripts  $*$  by  $m$ , the equivalent matrix material, henceforth called shortly matrix phase, is characterized by the density  $\rho^m$  and the components of the complex Hooke's tensor.

To determine the matrix phase elastic moduli  $K^m$  and  $\mu^m$ , we employ a sequence of values of  $K^*$  and  $\mu^*$  (deduced from measurement of the values of  $v_{pq}^*$  and  $\alpha_{pq}^*$ ) for two distinct porosities, say  $c_{i1}$  and  $c_{i2}$ , both the porosities belonging to the range of low porosity. In this porosity range, it is to be expected that the effective elastic moduli of the sintered metal powder become linear functions of porosity as the latter approaches sufficiently small values  $c_{i1}$  and  $c_{i2}$ , and, consequently a linear extrapolation of these quantities beyond the limits  $c_{i1} \leq c_2 \leq c_{i2}$  is possible. Carrying out such an extrapolation for the limiting case  $c_i = 0$ , we obtain an estimation of the values of the matrix elastic moduli,  $K^m$  and  $\mu^m$ . It can be done by using the following formulae given by author in Ref. [1]:

$$\begin{aligned} K^m &= K_1^* - c_{i1} (K_1^* - K_2^*) / (c_{i1} - c_{i2}) \\ \mu^m &= \mu_1^* - c_{i1} (\mu_1^* - \mu_2^*) / (c_{i1} - c_{i2}), \end{aligned} \quad (2.10)$$

where the symbol  $F_\varepsilon^*$ ,  $\varepsilon = 1, 2$ , denotes the value of the effective quantity  $F^*$  ( $F^*$  stands for  $K^*$  and  $\mu^*$ ) at the porosity  $c_{i\varepsilon}$ .

### 3. Numerical results

Numerical calculations were performed for frequency  $f = \omega / (2\pi) = 4Mc/\text{sec}$ . The following values were taken as the material parameters of the composite (sintered copper powder) under analysis [1]:  $\rho^m = 8.92 \text{ g/cm}^3$ ,  $\rho^i = 0.001347 \text{ g/cm}^3$ ,  $K_m^{(a)} = 1.41268 \cdot 10^{11} \text{ Pa}$ ,  $K_m^{(b)} = 1.2159 \cdot 10^9 \text{ Pa}$ ,  $\mu_m^{(a)} = 4.878 \cdot 10^{10} \text{ Pa}$ ,  $\mu_m^{(b)} = 4.78857 \cdot 10^7 \text{ Pa}$ ,  $K_i^{(a)} = 1.595 \cdot 10^5 \text{ Pa}$ ,  $K_i^{(b)} = 0$ ,  $\mu_i^{(a)} = 0$ ,  $\mu_i^{(b)} = \omega \eta / \rho^i$ , where  $\eta$  denotes the dynamic viscosity of air ( $\eta_i = 1.8 \cdot 10^{-4} \text{ Poise}$ ). The values of  $K_m^{(a)}$ ,  $K_m^{(b)}$ ,  $\mu_m^{(a)}$  and  $\mu_m^{(b)}$  were calculated from the linear extrapolation of formulae (2.10) and (2.7), by using the following results of our own experiments:  $c_{i1} = 0.0068$ ,  $c_{i2} = 0.0176$ ,  $c_{L1} = 4758 \text{ m/sec}$ ,  $c_{T1} = 2325 \text{ m/sec}$ ,  $\alpha_{L1} = 19.52 \text{ m}^{-1}$ ,  $\alpha_{T1} = 7.97 \text{ m}^{-1}$ ,  $c_{L2} = 4677 \text{ m/sec}$ ,  $c_{T2} = 2304 \text{ m/sec}$ ,  $\alpha_{L2} = 24.78 \text{ m}^{-1}$ ,  $\alpha_{T2} = 12.25 \text{ m}^{-1}$ . Some results of the numerical calculations are presented in Figs. 1–8. These results visualize how, at the loading frequency  $f = 4 \text{ Mc/sec}$ , the dynamic elastic moduli (Lamé constants)  $K^*$  and  $\mu^*$  of the sintered copper powder depend on the volume concentration of the ellipsoidal inclusions, their shape and size. The calculations were carried out for both prolate ( $a > b = c$ ) and oblate ( $a = b > c$ ), air-saturated spheroids under the assumption that the shape of each pore in the bulk sample under examination is to be characterized by the same value of the shape

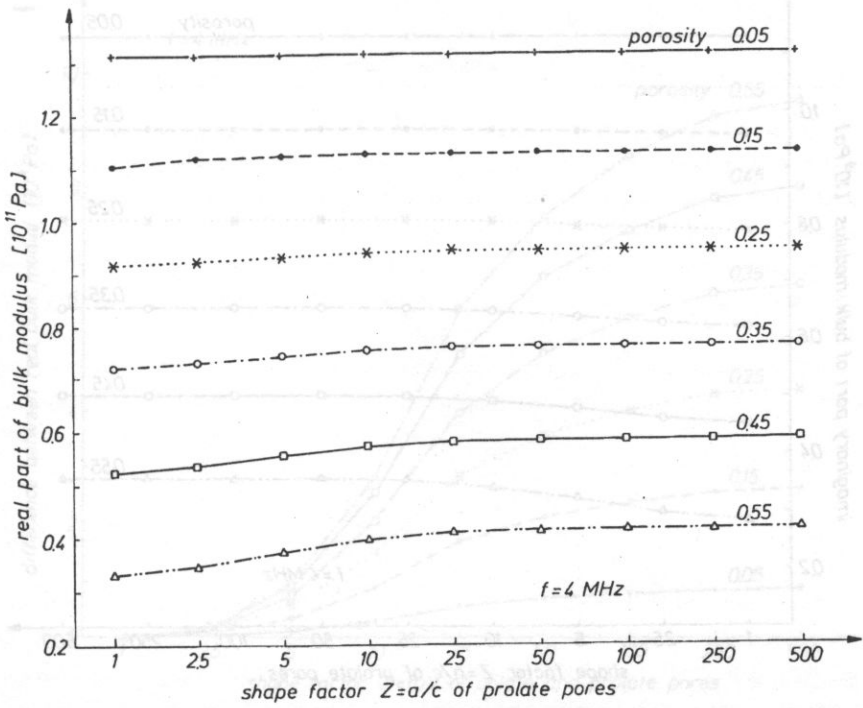


Fig. 1. Real part of bulk modulus of sintered copper powder as a function of the porosity and shape factor  $Z = a/c$  of the air-saturated prolate pores.

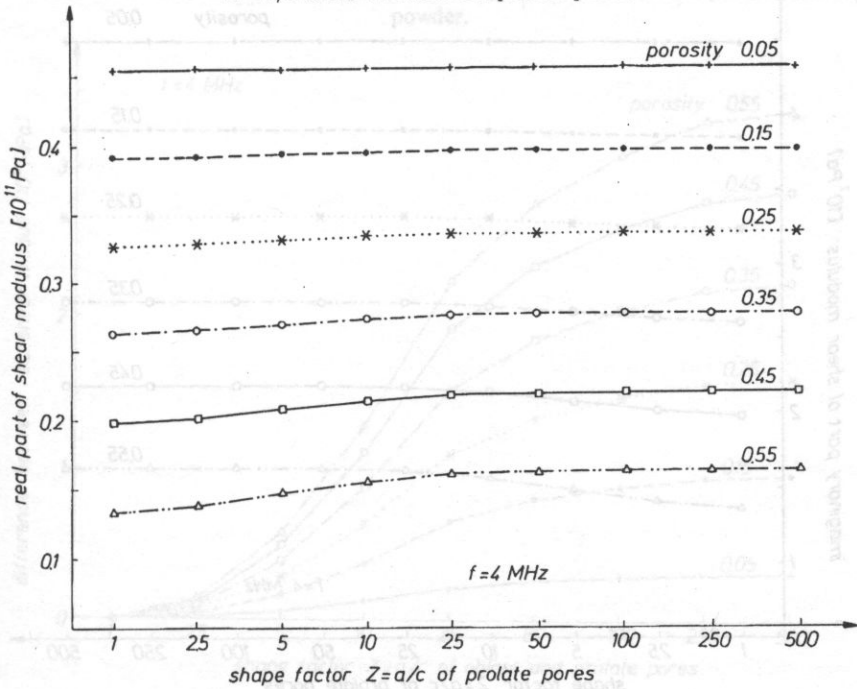


Fig. 2. Real part of shear modulus of sintered copper powder as a function of the porosity and shape factor  $Z = a/c$  of the air-saturated prolate pores.

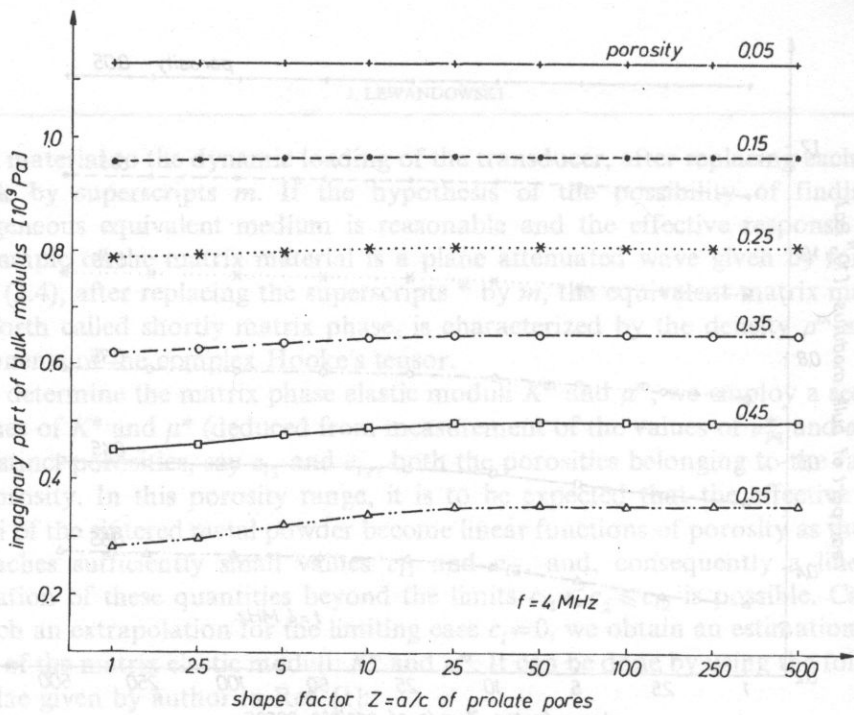


Fig. 3. Imaginary part of bulk modulus of sintered copper powder as a function of the porosity and shape factor  $Z = a/c$  of the air-saturated prolate pores.

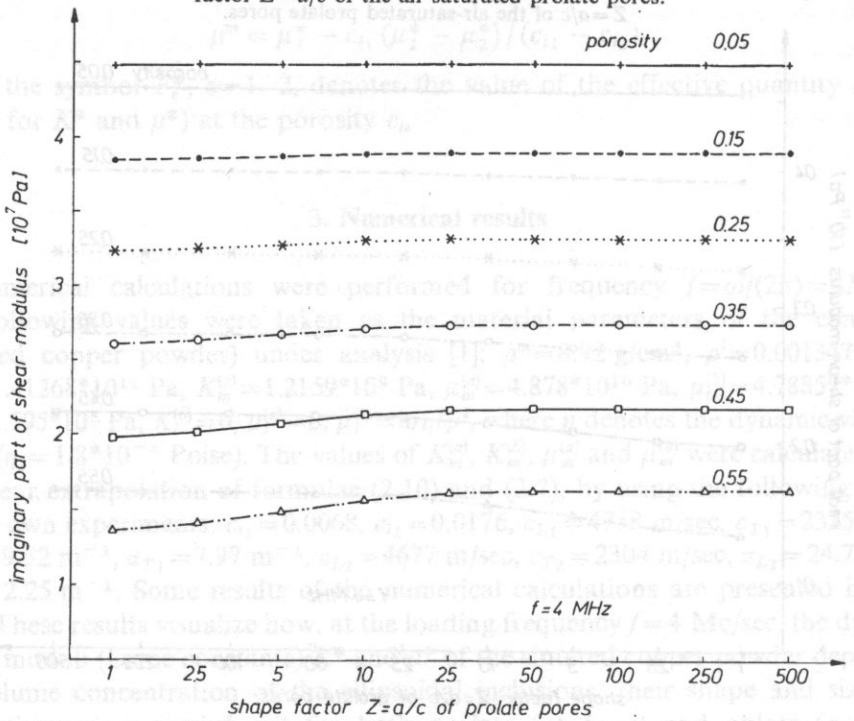


Fig. 4. Imaginary part of shear modulus of sintered copper powder as a function of the porosity and shape factor  $Z = a/c$  of the air-saturated prolate pores.

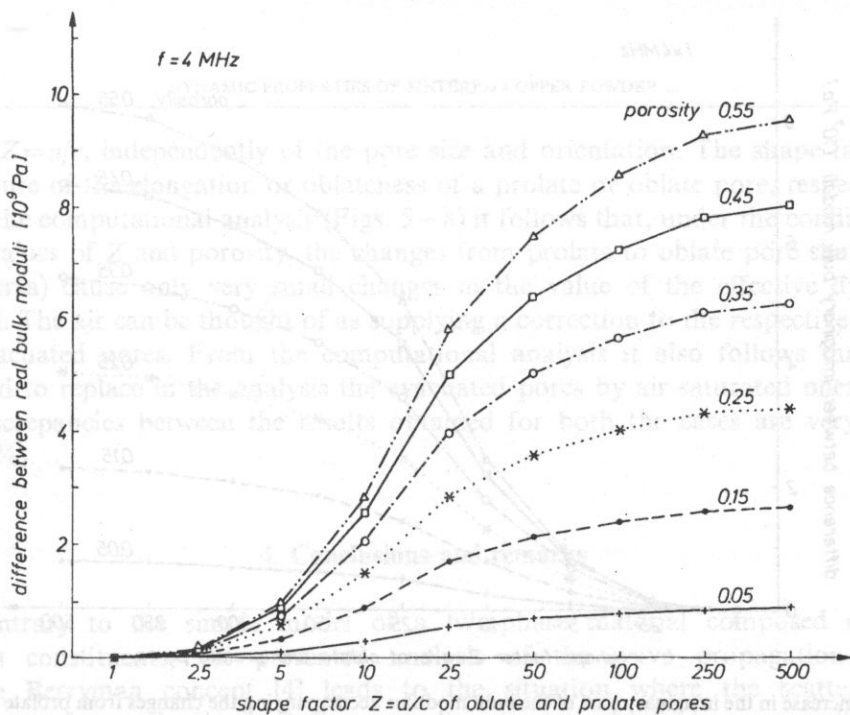


Fig. 5. Increase in the real part of the bulk modulus accompanying the changes from prolate to oblate pore shapes as a function of the porosity and shape factor  $Z = a/c$  of the air-saturated pores in sintered copper powder.

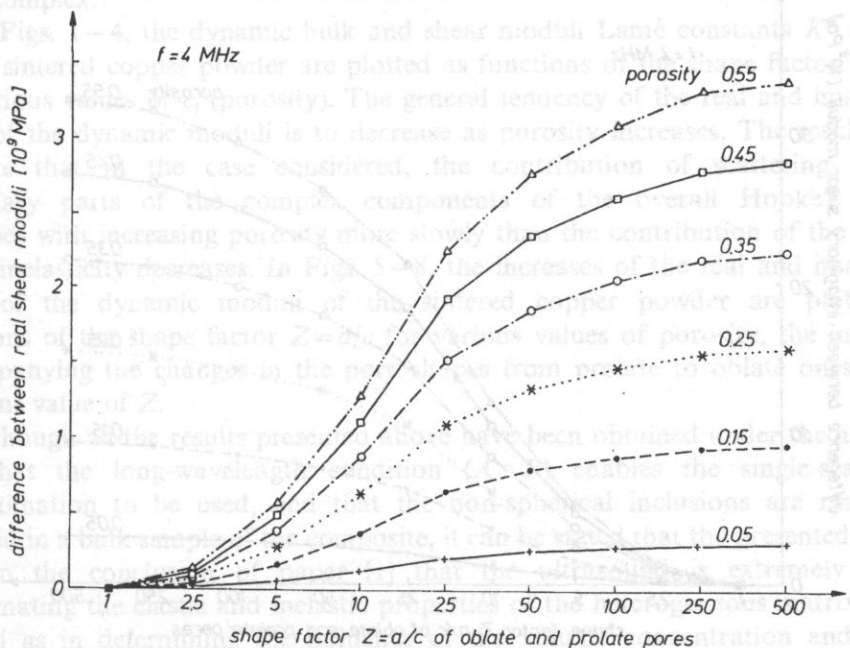


Fig. 6. Increase in the real part of the shear modulus accompanying the changes from prolate to oblate pore shapes as a function of the porosity and shape factor  $Z = a/c$  of the air-saturated pores in sintered copper powder.

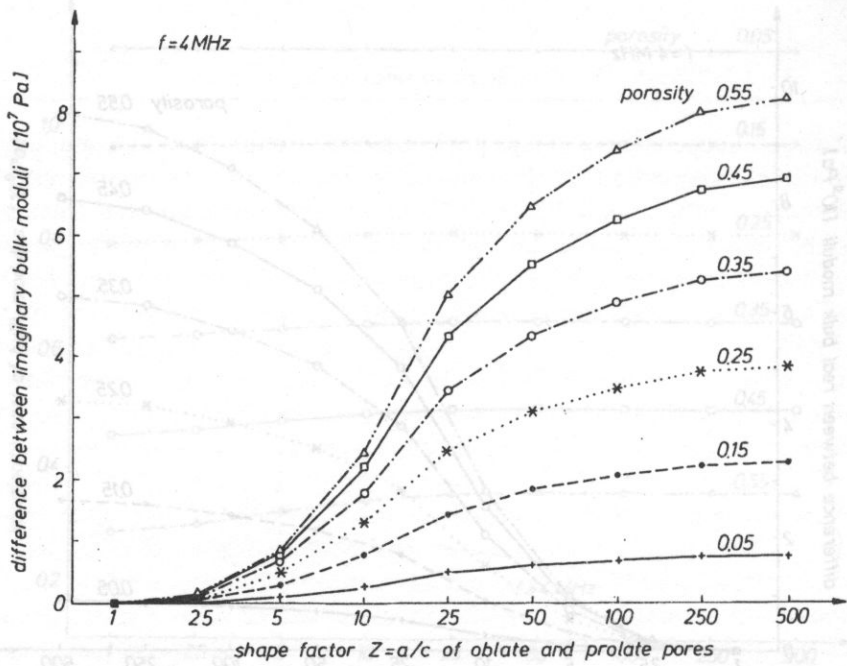


Fig. 7. Increase in the imaginary part of the bulk modulus accompanying the changes from prolate to oblate pore shapes as a function of the porosity and shape factor  $Z = a/c$  of the air-saturated pores in sintered copper powder.

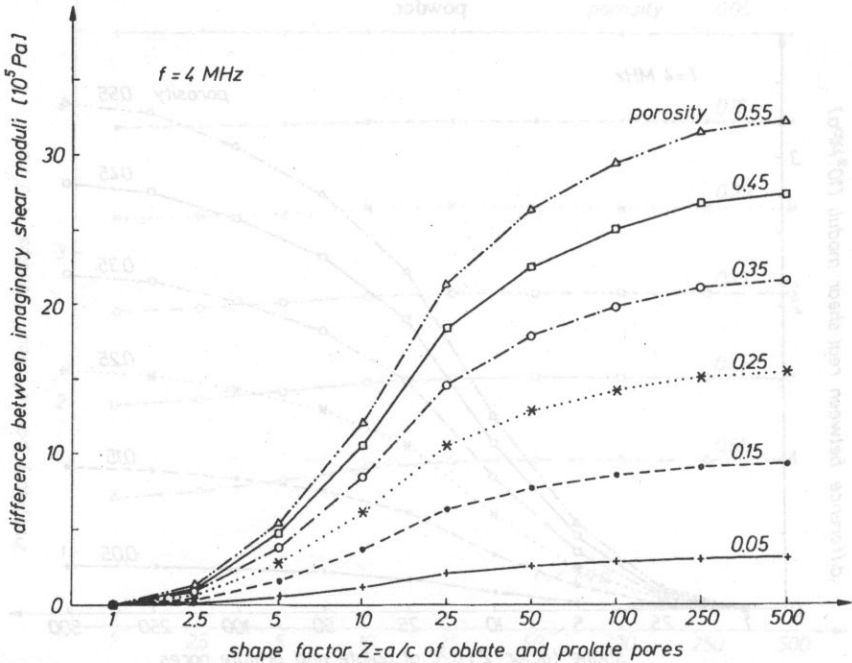


Fig. 8. Increase in the imaginary part of the shear modulus accompanying the changes from prolate to oblate, pore shapes as a function of the porosity and shape factor  $Z = a/c$  of the air saturated pores in sintered copper powder.



factor  $Z=a/c$ , independently of the pore size and orientation. The shape factor is a measure of the elongation or oblateness of a prolate or oblate pore, respectively. From the computational analysis (Figs. 5–8) it follows that, under the condition of fixed values of  $Z$  and porosity, the changes from prolate to oblate pore shapes (or vice versa) cause only very small changes in the value of the effective dynamic moduli. The air can be thought of as supplying a correction to the respective results for evacuated pores. From the computational analysis it also follows that it is justified to replace in the analysis the evacuated pores by air-saturated ones, since the discrepancies between the results obtained for both the cases are very small ( $<1.5\%$ ).

#### 4. Conclusions and remarks

Contrary to the simple model of a two-phase material composed of two lossless constituents, the presented analysis of the wave propagation based on the Berryman concept [4] leads to the situation where the scattering is not the only mechanism of the overall attenuation of the composite, but in lasticity of the materials of the phases themselves contribute also to this effect. It occurs since the elastic moduli of the both phases are assumed to be complex.

In Figs. 1–4, the dynamic bulk and shear moduli Lamé constants  $K^*$  and  $\mu^*$  of the sintered copper powder are plotted as functions of the shape factor  $Z=a/c$  for various values of  $c_i$  (porosity). The general tendency of the real and imaginary parts of the dynamic moduli is to decrease as porosity increases. The results also indicate that in the case considered, the contribution of scattering to the imaginary parts of the complex components of the overall Hooke's tensor increases with increasing porosity more slowly than the contribution of the matrix phase inelasticity decreases. In Figs. 5–8, the increases of the real and imaginary parts of the dynamic moduli of the sintered copper powder are plotted as functions of the shape factor  $Z=a/c$  for various values of porosity, the increases accompanying the changes in the pore shapes from prolate to oblate ones under constant value of  $Z$ .

Although all the results presented above have been obtained under the assumption that the long-wavelength condition ( $\lambda \gg D$ ) enables the single-scattering approximation to be used, and that the non-spherical inclusions are randomly oriented in a bulk sample of the composite, it can be stated that the presented results confirm the conclusion of paper [1] that the ultrasound is extremely useful in estimating the elastic and inelastic properties of the heterogeneous matrix phase as well as in determining the influence of the volume concentration and shape of the inclusions on the overall dynamic properties of the multi-phase composite under study.

## References

- [1] J. LEWANDOWSKI, *Acoustic and dynamic properties of two-phase media with non-spherical inclusions*, Ultrasonics (in press).
- [2] W. KREHER, J. RANACHOWSKI and F. REJMUND, *Ultrasonic waves in porous ceramics with non-spherical holes*, Ultrasonics, 70–74 (1977).
- [3] J.G. BERRYMAN, *Theory of elastic properties of composite materials*, Appl. Phys. Lett., 35, 856–858 (1979).
- [4] J.G. BERRYMAN, *Long-wavelength propagation in composite elastic media II. Ellipsoidal inclusions*, J.Soc.Am., 68, 6, 1820–1831 (1980).
- [5] A.N. NORRIS, *Effects of pore shapes on low frequency wave speeds in porous media*; in: *Nondestructive evaluation* [Eds.] Thomson, D.O. and D.E. Cinenti vol. 5 Plenum Publ. Co. 1986 pp. 1609–1615.
- [6] J. LEWANDOWSKI, *Acoustic waves in solids with random cavities, I: Effective macroscopic parameters*, Acta Mechanica, 68, 1–19 (1987).
- [7] E. KRÖNER, *Statistical continuum mechanics*, Lecture notes, Springer, Berlin–Heidelberg–New York 1971.
- [8] A.K. MAL, L. KNOPOFF, J. Inst. Math. Its Appl., 3, 376 (1967).
- [9] T.T. WU, *The effect of inclusion shape on the elastic moduli of a two-phase material*, Int. J. Solids Structure, 2, 1–8 (1966).

## THE INSTRUMENTATION FOR MEASUREMENTS OF EVOKED OTOACOUSTIC EMISSIONS

Z. RANACHOWSKI

Institute of Fundamental Technological Research  
Polish Academy of Sciences  
(00-49 Warszawa, ul. Świątokrzyska 21)

Evoked Otoacoustic Emissions (EOAEs) are studied by the use of the recently built EOAEs processor. For this purpose 101 dentist students underwent screening earphone audiometry and electrostimulation high-frequency tests and were tested with use of the EOAEs processor. Three different parameters were evaluated from the recorded waveforms. Great inter- and intraindividual differences within the recordings were observed. The problems concerning the probe fitting are also discussed.

### 1. Introduction

The first description of the measurement of EOAEs was reported by D.T. KEMP in 1979 [1] and, since then, it has been studied by many investigators. Otoacoustic emissions are a release of audiofrequency energy into the ear canal from the cochlea, transmitted through the ossicular chain and tympanum and are considered as an energy leakage from the cochlear travelling wave. The physical source of the audiofrequencies mentioned above are the outer hair cells, situated in the cochlea. The observations of cochlear mechanics show that the healthy cochlea vibrates far more at the specific frequencies, in response to stimulation, than a disordered cochlea. The full understanding of cochlear functions in the hearing process still has not been achieved. However, the outer hair cells are supposed to be a part of active biomechanical feedback intended to sharpen up the tuning and enhance the sensitivity of the cochlea to the sound excitations [2].

Otoacoustic emissions would seem therefore to be a tool for examining certain functional aspects of the cochlea, as for example:

- a screening hearing test in neonates [3],
- confirmation of peripheral auditory impairment in children [4],
- differential diagnosis of endocochlear and retrocochlear types of hearing loss [5].

Spontaneous or unstimulated otoacoustic emissions (SOAEs) are pure tones of about 20 dB SPL found in the quiet ear canal in 25 to 60% of healthy ears [6]. They can be modulated by pressure on the tympanum. However, the particular internal cochlear feedback conditions needed to sustain spontaneous emissions are not always present. Therefore, SOAEs have found till now limited clinical application.

EOAEs recordings are usually obtained by averaging the acoustical signal measured by a miniature microphone. The averaging process is synchronised to the presentation of a repeated transient stimulus, usually a click or a tone burst. The stimulus is generated by a miniature earphone. Both the microphone and the earphone are placed in a small probe sealed in the auditory meatus. The probe is equipped with tabular waveguides to obtain the optimal matching to the acoustic impedance of the meatus. An additional pipe is placed between the waveguides to appease the pressure increase during the probe fitting procedure. The construction details for the otoacoustic probe and the block diagram of the EOAEs recording system are shown in Fig. 1.

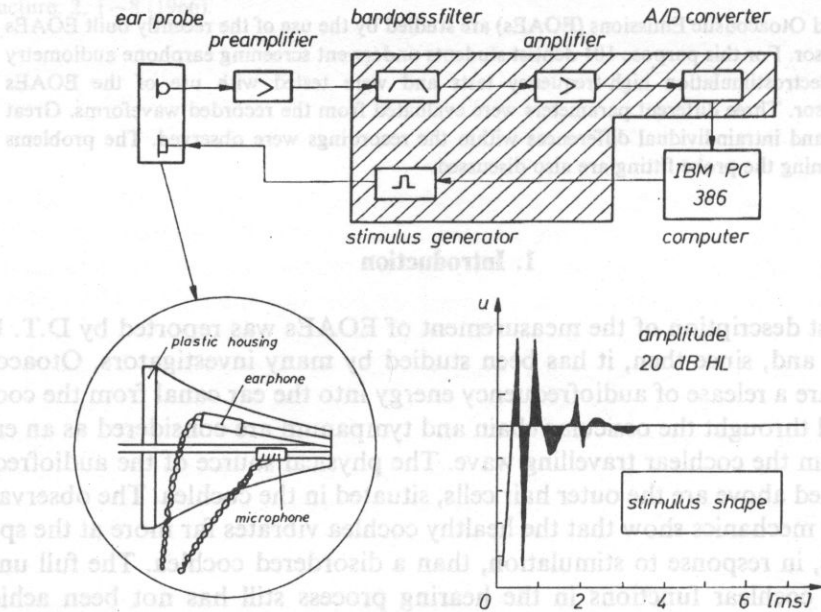


Fig. 1. Block diagram of the EOAEs Analyser and the construction details of the EOAEs probe.

The intensity of EOAEs is generally less than 20 db SPL [7]. This is smaller than the level of electrical noise generated within the microphone and, as well as physiological and ambient noise, picked up by the microphone. The total noise level usually exceeds the level of a few microvolts when the signal level is about one microvolt RMS. The use of a low noise preamplifier and an audio-bandpass filter is necessary but insufficient. To improve the poor signal to the noise ratio

(ca. — 20 dB) the averaging process is used. Every response to the stimulus of about 20 ms duration is transformed into a digital form by means of fast A/D converter, and stored in the computer memory as a single „time window”. The „time window” starts a few ms after the stimulus because the initial period is contaminated by the acoustic oscillations which inevitably follow the stimulus emitted in the limited cavity. For the consisted EOAE waveform and Gaussian noise averaging process of consequent sweeps improves the signal to noise ratio (SNR) factor equal to the square root of the sweep number. In practice the number of about 1000 sweeps yielding 29 dB SNR improvement is used.

Otoacoustic emissions exhibit nonlinearity both in the time and frequency domain. This means that output level is not proportional to the input, and that the components of a complex input interact with each other. The results of clinical EOAE test are often contaminated by the oscillations caused by the echoes of the stimulus in the meatus. The intensity of the echos depends of the fitting of the probe. The effect of EOAE nonlinearity in the time domain allows to reduce the influence of the oscillations. According to the procedure proposed by BRAY and KEMP [7], the EOAE waveforms are averaged when stimulated with a nonlinear differential block, shown in Fig. 2. Every

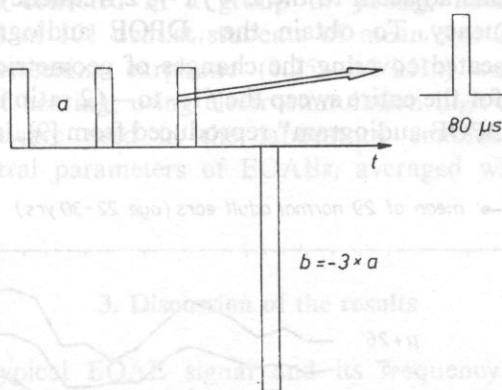


Fig. 2. The signal block used in differential nonlinear stimulation technique.

fourth component of the nonlinear stimulus is inverted and three times greater amplitude than three other components of the stimulus. The acoustic responses to all linearly behaving systems i.e. nonphysiological responses are cancelled by the summation of all the stimulus components. Only the saturated part of the physiological emission signal is passed to the further processing units. In practice, only half of the saturated EOAE remains due to its partial cancellation. Signal-to-noise ratio is therefore worse when compared to the Basic EOAEs Echo Technique. In clinical conditions the small loss of the SNR is rarely significant, and the advantages of the method overcome its drawbacks.

Distortion-product otoacoustic emissions are continuous signals that appear at some combination of harmonic tone stimulation, considering the nonlinearity in the frequency domain of the cochlea mentioned above. The first DPOEs measurements

were reported by D.T. KEMP in 1979. In practical applications [9] the two-tone stimulation method is used. That kind of stimulation leads to interaction between the two travelling waves in the cochlea, creating several distortion products (DP). For the tones labelled  $f_1$  and  $f_2$ , the  $2 \times f_1 - f_2$  DP is believed to be generated at the place being the point of maximal interactions between the two travelling waves. The instrumentation for recording the DPOEs is more complicated than that used for echo techniques. The ear probe equipped with two earphones is fed by two generators transmitting  $f_1$  and  $f_2$ .

The pure tone waveforms are synthesised by the computer. The duration of the emission of the chosen tone combination is about 4 seconds. The microphone placed in the ear probe detects the DPOE signal. The processing procedure of this signal consists of:

- high- and lowpass filtering 100–8000 Hz.
- averaging in the time domain,
- evaluating the  $2 \times f_1 - f_2$  component by means of Fast Fourier Transform (FFT),
- evaluating the level of the background noise as the average of the magnitudes of four FFT components adjacent to the  $2 \times f_1 - f_2$  frequency two above and two below the main frequency. To obtain the „DPOE audiogram” the procedure described above is repeated covering the changes of geometric mean is realised in a 1/4 octave step, and for the entire sweep the  $f_1 - f_2$  ratio is held at the value of 1.2. The example of „DPOE audiogram” reproduced from [9], is presented in Fig. 3.

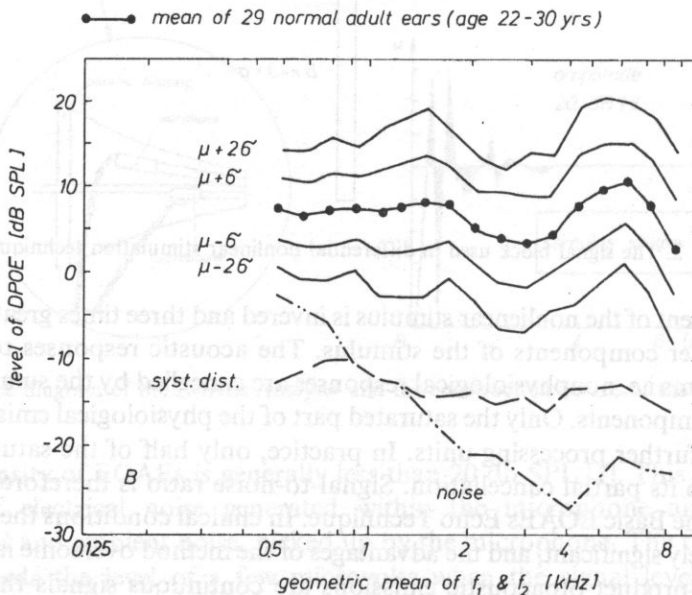


Fig. 3. An example of distortion-product otoacoustic emission audiogram ( $\mu$  and  $\delta$  — mean and standard deviation from all the ears examined) [9].

## 2. Experimental

The investigation of EOAEs in Laboratory of Audiology, ENT Clinic, Dentist Dep. in Warsaw Medical Academy started in 1990 (9, 10, 11, 12] under direction of Prof. W. BOCHENEK. Basic click-evoked echo technique using the instrumentation shown in Fig. 1 is applied. The EOAEs processor is equipped with three probes of different sizes of our design, and one original probe offered by D.T. KEMP [13]. Three stimulus, types may be generated under control of the computer: positive click, negative click and modulated sine burst.

The recorded signal is amplified in the separate low-noise. Fet-driven preamplifier and in the main filter and amplifier section. The total gain is adjustable in the range of 60–100 dB. The lower frequency limit is set to 5000 Hz and the upper to 12 kHz. To record the signal in the computer memory, a fast 8-bit, 40 kHz analog to digital converter is used. This allows to represent a EOAEs signal of 18 ms duration as 720 bytes long waveform and enables us to obtain a 100 Hz resolution for Fast Fourier Transformation.

Recordings were collected in a group of young, normal hearing persons. The group consisted of 101 dentist students of mean age 23.1. They underwent routine otoscopy, screening earphone (0.25–8.0 kHz) audiometry and check of the upper limit of hearing, using electrostimulation high-frequency audiometry (SEHFA). The software used in the laboratory enabled the comparison of amplitude and spectral parameters of EOAEs, averaged within a certain group of subjects.

## 3. Discussion of the results

In Fig. 4 the typical EOAE signal and its frequency spectrum is shown. The upper curves are the results of two consequent series of 1024 sweeps. Below the crosspower spectrum of two sweep series (the dashed bars) and the power of the noise, obtained by subtracting the two sweep series (the black bars) is presented. The spectral line representing the maximal power component was in the investigated group a subject of significant variation within the range of 0.9 to 2.8 kHz. The correlation between the upper limit of hearing and the spectral maximum power component has not been defined because of the variations mentioned above. After collecting more data will be possible to verify the theory that there is a correlation between the spectral maximum power component of EOAE and the patient's age, described in [14].

The average delay between the onset of the click and the maximal amplitude of the EOAE was about 7 milliseconds. There were some cases of registration of longer delays (ca 10% increase), accompanying the presence of slight ear impairments.

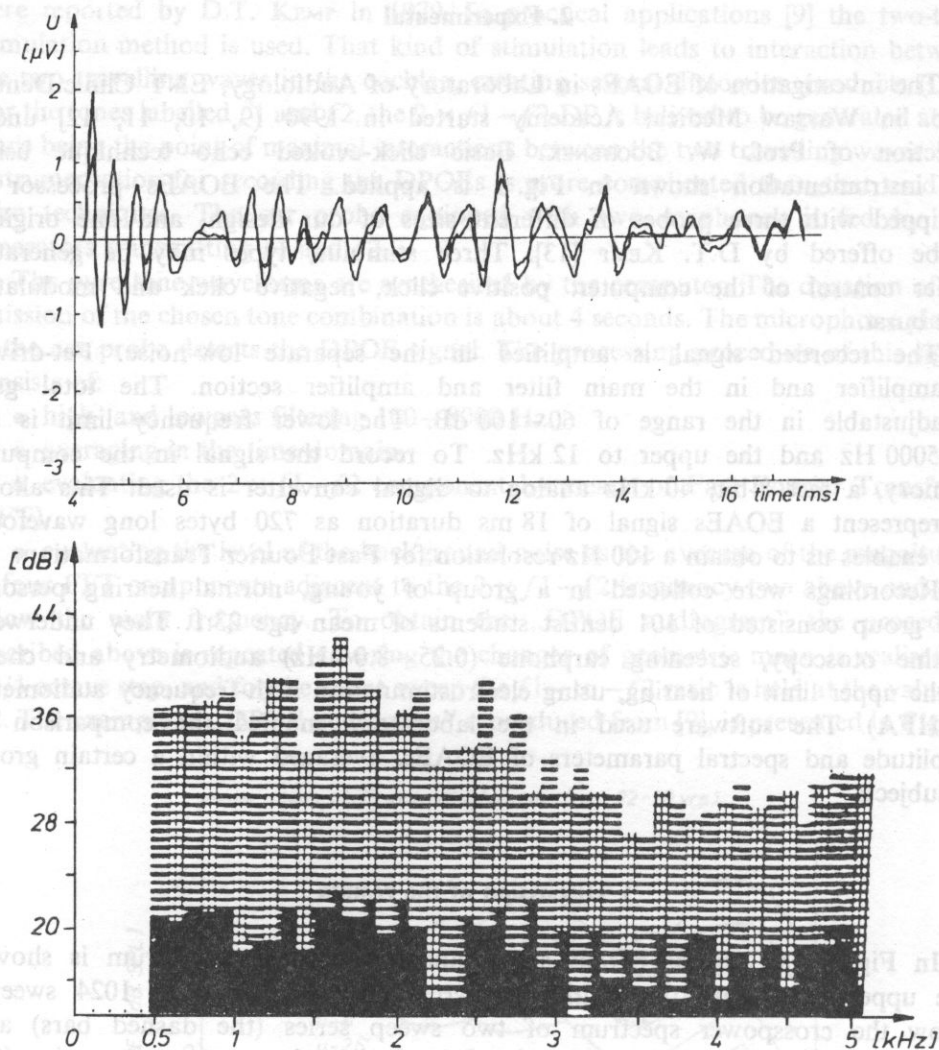


Fig. 4. The typical EOAE signal and its frequency spectrum (below).

The variations in the average EOAE amplitude level achieved 15%. The factor of a great influence the quality of the EOAEs recording was the probe fitting and the patient noise. Figure 5 is an example of the recording with the poor fitting and the noises caused by loud breathing. The initial part of the sweep (5–8 ms) is highly contaminated by the oscillations of the click in the ear canal. The latter part of the signal (9–17 ms) exhibits considerable differences between the signal level during the first and the second averaging process. The presence of EOAEs is therefore impossible to detect here.



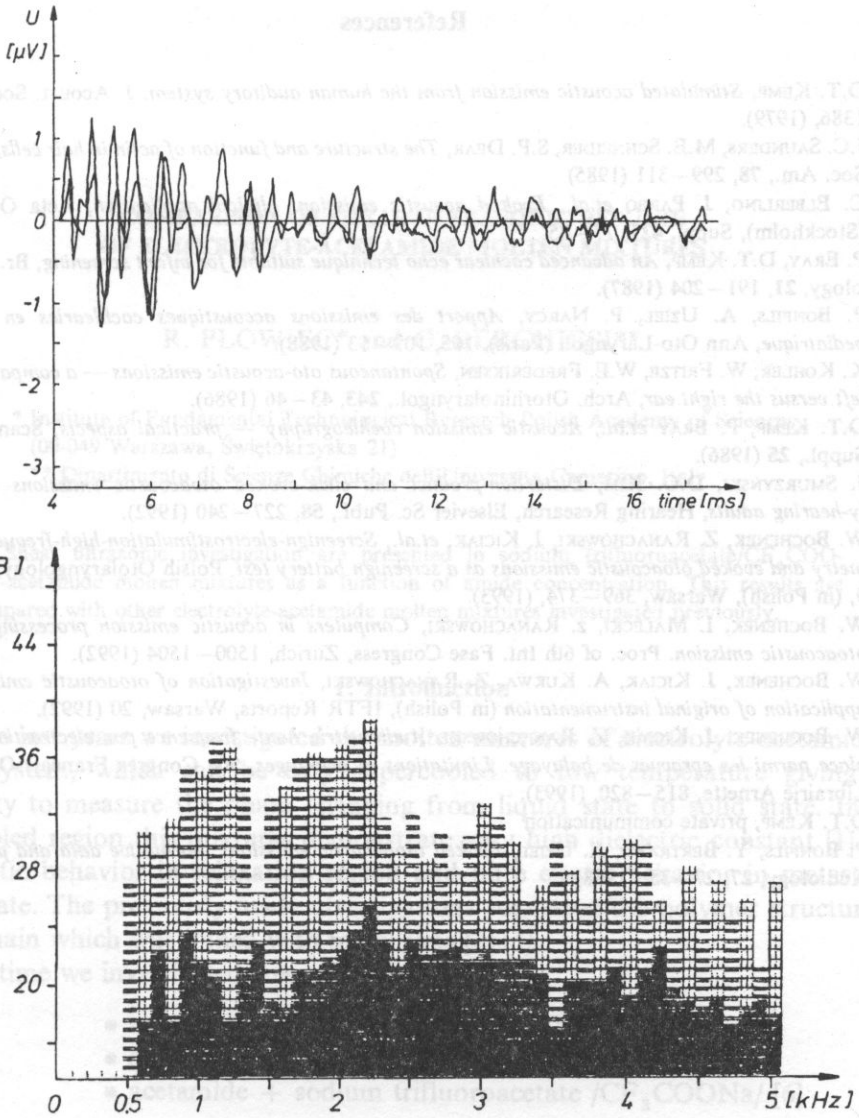


Fig. 5. An example of EOA signal and its frequency spectrum (below). The probe fitting and the loudly breathing cause more significant noise contents (the black bars below) than those shown in Fig. 4.

Further modifications of the instrumentation should improve the procedure of recording the EOA signals. The aim is to optimize the rejection of artefacts caused by the click reflections in the meatus, using the Differential Nonlinear Stimulation Technique.

• density measurements as a function of temperature

## References

- [1] D.T. KEMP, *Stimulated acoustic emission from the human auditory system*. J. Acoust. Soc. Am., **64**, 1386, (1979).
- [2] J.C. SAUNDERS, M.E. SCHNEIDER, S.P. DEAR, *The structure and function of actin in hair cells*, J. Acoust. Soc. Am., **78**, 299–311 (1985).
- [3] C. ELBERLING, J. PARBO *et al.*, *Evoked acoustic emission: clinical application*, Acta Otolaryngol. (Stockholm), Suppl. **421**, 77–85.
- [4] P. ERAY, D.T. KEMP, *An advanced cochlear echo technique suitable for infant screening*, Br. Journal of Audiology, **21**, 191–204 (1987).
- [5] P. BONFILS, A. UZIEL, P. NARCY, *Apport des émissions acoustiques cochleaires en audiologie pédiatrique*, Ann Oto-Laryngol. (Paris). **105**, 109–13 (1988).
- [6] K. KOHLER, W. FRITZE, W.E. FREDERIKSEN, *Spontaneous oto-acoustic emissions — a comparison of the left versus the right ear*, Arch. Otorhinolaryngol., **243**, 43–46 (1986).
- [7] D.T. KEMP, P. BRAY *et al.*, *Acoustic emission cochleography — practical aspects*, Scand. Audiol. Suppl., **25** (1986).
- [8] J. SMURZYŃSKI, D.O. KIM, *Distortion-product and click-evoked otoacoustic emissions of normally-hearing adults*, Hearing Research, Elsevier Sc. Publ., **58**, 227–240 (1992).
- [9] W. BOCHENEK, Z. RANACHOWSKI, J. KICIAK, *et al.*, *Screening-electrostimulation-high-frequency audiometry and evoked otoacoustic emissions as a screening battery test*, Polsih Otolaryngology, **24**, suppl. 9, (in Polish), Warsaw, 369–374, (1993).
- [10] W. BOCHENEK, I. MALECKI, Z. RANACHOWSKI, *Computers in acoustic emission processing including otoacoustic emission*. Proc. of 6th Int. Fase Congress, Zurich, 1500–1504 (1992).
- [11] W. BOCHENEK, J. KICIAK, A. KUKWA, Z. RANACHOWSKI, *Investigation of otoacoustic emissions with application of original instrumentation* (in Polish), IFTR Reports, Warsaw, 20 (1992).
- [12] W. BOCHENEK, J. KICIAK, Z. RANACHOWSKI, *Audiometrie haute fréquence par electrostimulation sa place parmi les épreuves de balayage. Limitations et avantages*, 90e Congres Francais ORL, Paris. Librairie Arnette, 815–820, (1993).
- [13] D.T. KEMP, private communication
- [14] P. BONFILS, Y. BERTRAND, A. UZIEL, *Evoked otoacoustic emissions: normative data and presbycusis*, Audiology, **27**, 27–35. (1988).

## COMPARISON OF SHEAR ULTRASONIC RESULTS OF ELECTROLYTE-ACETAMIDE MOLTEN MIXTURES

R. PŁOWIEC\* and G. BERTCHIESI\*\*

\* Institute of Fundamental Technological Research Polish Academy of Sciences  
(00-049 Warszawa, Świątokrzyska 21)

\*\* Dipartimento di Scienze Chimiche dell'Universita Camerino, Italy

Shear ultrasonic investigation are presented in sodium trifluoroacetate/ $\text{CF}_3\text{COO-Na}$ -acetamide molten mixtures as a function of amide concentration. This results are compared with other electrolyte-acetamide molten mixtures investigated previously.

### 1. Introduction

In the last years we investigated the molten mixtures of electrolyte-acetamide in binary system, which can be easy supercooled to low temperature giving the possibility to measure the phase changing from liquid state to solid state. In the supercooled region this mixtures demonstrate very high dielectric constant [1] and viscoelastic behavior in relaxation region and pure elastic behavior in metastable glassy state. The previously made investigations suggested the polymer structure of amide chain which was joined with metal ions [2] [3].

Last time we investigated tree mixtures:

- acetamide + sodium thiocyanate / $\text{NaSCN}$ / [2]
- acetamide + calcium nitrate / $\text{Ca}(\text{NO}_3)_2$ / [3]
- acetamide + sodium trifluoroacetate / $\text{CF}_3\text{COONa}$ / [6]

To know what is the influence of acetamide concentration on polymer chain creation and the influence on the range of relaxation processes the last mixture was investigated as a function of amide concentration. Tree different concentration was prepared for measurements: a) 8.06 mol/kg b) 11.98 mol/kg and c) 19.48 mol/kg.

### 2 Measurements

To determine the range of relaxation processes of these mixtures we performed the measurements as follows:

- density measurements as a function of temperature

- steady flow viscosity as a function of temperature
- ultrasonic shear impedance measurements as a function of frequency and temperature
- ultrasonic measurements of shear elasticity in metastable glassy state as a function of temperature and frequency.

For density measurements the vibrating densitometer of PAAR (Austria) was used. The measurements were made in temperature range 10–60°C. The results may be fitted by linear equation

$$\rho = a + bT,$$

where  $\rho$  is in kg/m<sup>3</sup> and  $T$  — temperature in Kelvin. For the 8.06 mol/kg solution  $a = 1693.05$ ,  $b = 1.060$ , for 11.98 mol/kg solution  $a = 1789.86$ ,  $b = 1.098$  and for 19.48 mol/kg solution  $a = 1927.21$ ,  $b = 1.188$ .

For steady flow viscosity measurements the Hoesppler viscometer was used. As an example the results for 8.06 mol/kg amide concentration are shown on Fig. 1.

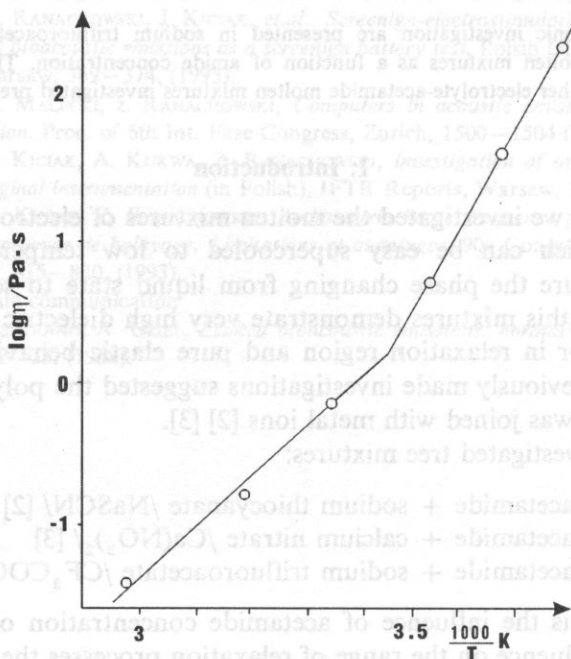


Fig. 1. The changes of viscosity for 8.06 mole/kg solution as a function of temperature.

For shear ultrasonic measurements the MATEC (USA) set was used. The normal incidence technique and the superposition method was applied in measurements [4] on frequency 10.30 and 90 MHz. The special attention was paid on dry atmosphere during the measurements, specially in low temperatures because of influence of humidity on the shear impedance value. The results of ultrasonic

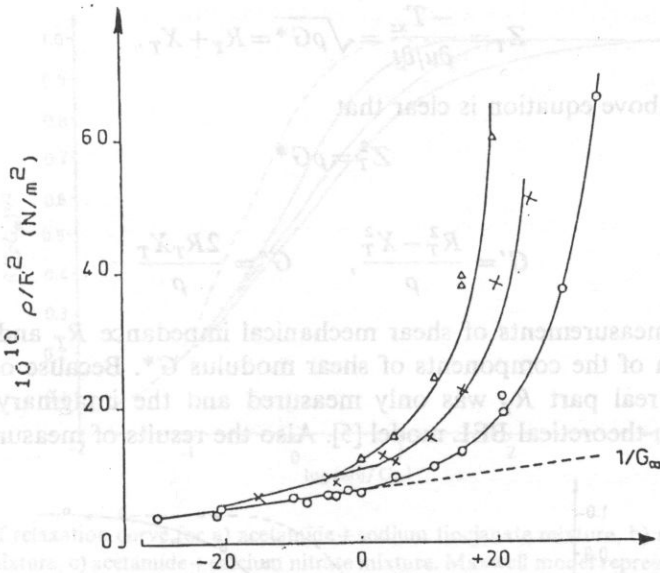


Fig. 2. The run of  $\rho/R^2$  as a function of temperature and frequency for the 8.06 mole/kg solution. ( $\Delta=10$  MHz,  $x=30$  MHz,  $o=90$  MHz).

measurements of shear elasticity in metastable glassy state are shown on Fig. 2 as an example for 8.06 mol/kg solution and are given by equation

$$1/G_{\infty} \text{ (N/m}^2\text{)} = 2.83 \cdot 10^{-10} + 1.575 \cdot 10^{-11} (T - T_g),$$

where  $T_g$  is the glass transition temperature and is equal 240 K for 8.06 mole/kg solution.

### 3. Theory

If the element of liquid of density  $\rho$  is shearing in the plane  $xy$  with the transversal motion  $u$  as a result of the shear stress  $T_{xz}$  the motion equation is

$$\rho dx dy dz = \frac{\partial T_{xz}}{\partial z^2} dx dy dz.$$

When the shear wave is propagated in  $z$  direction then

$$\rho \frac{\partial^2 u}{\partial t^2} = G^* \frac{\partial^2 u}{\partial z^2},$$

where the complex shear modulus  $G^* = G' + j G''$

The mechanical impedance is the magnitude which characterize the mixture to be measured under shearing stress. It is defined as a ratio of shearing stress  $T$  to the acoustic velocity  $(\partial u / \partial t)$

$$Z_T = \frac{-T_{xz}}{\partial u / \partial t} = \sqrt{\rho G^*} = R_T + X_T.$$

From the above equation is clear that

$$Z_T^2 = \rho G^*$$

and

$$G' = \frac{R_T^2 - X_T^2}{\rho}, \quad G'' = \frac{2R_T X_T}{\rho}$$

Then, the measurements of shear mechanical impedance  $R_T$  and  $X_T$  permit to determine both of the components of shear modulus  $G^*$ . Because of the technical limitation the real part  $R_T$  was only measured and the imaginary part  $X_T$  was calculated from theoretical BEL model [5]. Also the results of measurements, which

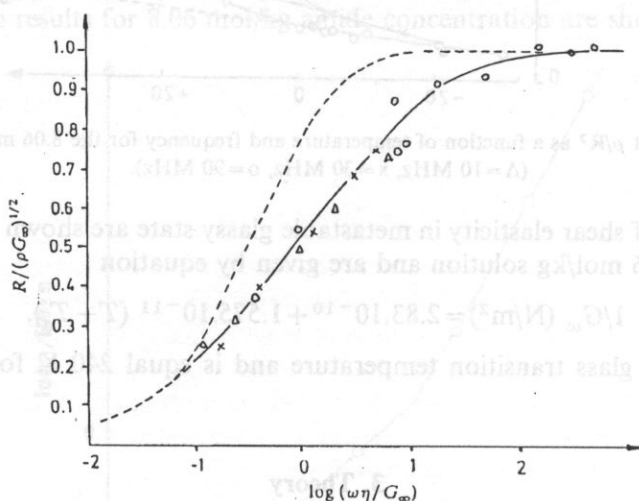


Fig. 3. The relaxation curve for acetamide + sodium trifluoroacetate solution in normalised scale. ( $\Delta = 10$  MHz,  $\times = 30$  MHz,  $\circ = 90$  MHz).

show both Fig. 3 and 4 are presented in normalized scale, it means that the real part of impedance  $R_T$  is related to the highest impedance in glassy state  $Z_T = \sqrt{\rho G_\infty}$  (and the frequency used in measurements is related to the Maxwell relaxation frequency or relaxation time ( $\tau_m = \eta_0 / G_\infty$ )).

#### 4. Results and discussion

The run of relaxation curve as a function of frequency (in normalized scale) for amide concentration 8.06 is shown on Fig. 3. The points are the results measured on frequency 10, 30 and 90 MHz. The continuous line presents the theoretical BEL model of relaxation with the parameter  $\beta = 0.5$  and  $K = 0.66$  in the equation

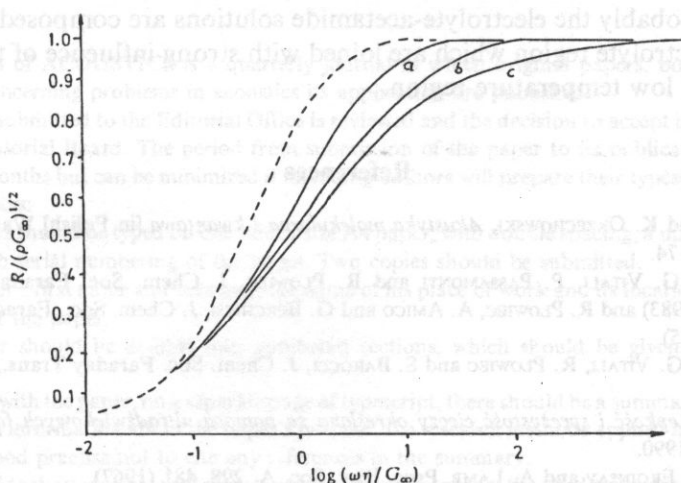


Fig. 4. The run of relaxation curve for a) acetamide+sodium thiocyanate mixture, b) acetamide+sodium trifluoroacetate mixture, c) acetamide+calcium nitrate mixture. Maxwell model represents the dotted line.

$$\frac{1}{G^*} = \frac{1}{G_\infty} + \frac{1}{j\omega\eta} + \frac{2K}{G_\infty(j\omega\tau_m)^\beta}$$

The dotted line on Fig. 3 present the Maxwell model with one relaxation time ( $K=0$ ). The scattering of results is caused by high hygroscopic of the investigated mixtures, specially in low temperature range.

We must say that the run of the relaxation curve for the 11.98 and 19.48 solution was exactly the same ( $\beta=0.5$ ,  $K=0.66$ ), it means that the concentration of amide have no influence on the relaxation processes in this mixtures.

There is another question for electrolyte-acetamide molten mixtures that the run of relaxation curves is close to the theoretical BEL model ( $\beta=0.5$ ,  $K=1$ ) which was created rather for the simple liquid [5], and it is difficult to say that the investigated mixtures the simple liquids are.

On Fig 4 you can see the relaxation curves of the last investigated electrolyte-acetamide molten mixtures i.e. of acetamide + NaSCN (a), acetamide +  $\text{CF}_3\text{COONa}$  (b) and acetamide +  $\text{Ca}(\text{NO}_3)_2$ . The range of relaxation times for curve (a) ( $\beta=0.5$ ,  $K=0.875$ ) and curve (b) ( $\beta=0.5$ ,  $K=0.66$ ) are even more narrow then BEL model curve which exactly follow the results of mixture (c) ( $\beta=0.5$ ,  $K=1$ ).

## 5. Conclusion

The measurements of electrolyte-acetamide solution with shear ultrasonic waves in relaxation region made clear that there is any influence of the amide concentration on the character of relaxation curve. This fact, the run of the relaxation curve close to the theoretical BEL model curve, dielectric [1] and NMR [6] results may

suggests that probably the electrolyte-acetamide solutions are composed of acetamide region and electrolyte region which are joined with strong influence of the metal ions tightly only in low temperature region.

### References

- [1] R. PŁOWIEC and K. ORZECZOWSKI, *Akustyka molekularna i kwantowa* [in Polish] Warszawa 1992 vol. 13, pp. 167–174.
- [2] G. BERTHESI, G. VITALI, P. PASSAMONTI and R. PŁOWIEC, *J. Chem. Soc. Faraday Trans.*, **79**, 2, 1257–1263 (1983) and R. PŁOWIEC, A. AMICO and G. BERTHESI, *J. Chem. Soc., Faraday Trans.*, **81**, 2, 217–224 (1985).
- [3] G. BERTHESI, G. VITALI, R. PŁOWIEC and S. BAROCCI, *J. Chem. Soc. Faraday Trans.*, **85**, 2, 635–641 (1989).
- [4] R. PŁOWIEC, *Lepkość i sprężystość cieczy określana za pomocą ultradźwiękowych fal ścinania*, Warszawa, PWN 1990.
- [5] A. BARLOW, J. ERGINSAY and A. LAMB, *Proc. Roy. Soc. A*, **298**, 481 (1967).
- [6] G. BERTHESI, M. DE ANGELIS, G. RAFAIANI and G. VITALI, *J. of Molecular Liquids*, **51**, 11–38 (1992).